impressive increase, it still falls drastically short of the prediction made by the Hall–Petch equation. Additionally, there are published data that indicate a "negative Hall–Petch effect" at the finest grain size ($d < 30$ nm), indicating that a softening mechanism is at work. Some researchers believe that it is entirely possible that at such small grain levels, the concept of a moving dislocation or dislocation pileup is no longer applicable and other mechanisms, such as grain boundary sliding, diffusion, etc., are at work.

Arguments have been made that in the upper nanocrystalline range ($50\text{ nm} < d < 100\text{ nm}$), dislocation-related activities similar to those seen with microcrystalline metals dominate while in the lower nanocrystalline range ($d < 50$ nm) dislocation activity (formation and movement) decreases significantly. Stresses needed to activate dislocation sources are extremely high at such small grain sizes. Some in situ HRTEM studies have been performed that support this argument. Finally, the strengthening and deformation mechanisms of nanocrystalline materials are not yet well understood, and more theoretical and experimental research is needed. In the next chapter, the ductility and toughness characteristics of these materials will be discussed.

6.11 SUMMARY

Metals and alloys are processed into different shapes by various manufacturing methods. Some of the most important industrial processes are casting, rolling, extruding, wire drawing, forging, and deep drawing.

When a uniaxial stress is applied to a long metal bar, the metal deforms elastically at first and then plastically, causing permanent deformation. For many engineering designs, the engineer is interested in the 0.2 percent offset yield strength, ultimate tensile strength, and elongation (ductility) of a metal or alloy. These quantities are obtained from the engineering stress-strain diagram originating from a tensile test. The hardness of a metal may also be of engineering importance. Commonly used hardness scales in industry are Rockwell B and C and Brinell (BHN).

Grain size has a direct impact on the properties of a metal. Metals with fine grain size are stronger and have more uniform properties. The strength of metal is related to its grain size through an empirical relationship called the Hall–Petch equation. Metals with grain size in the nanoscale range (nanocrystalline metals) are expected to have ultra-high strength and hardness as predicted by the Hall–Petch equation.

When a metal is plastically deformed by cold working, the metal becomes strain-hardened, resulting in an increase in its strength and a decrease in its ductility. The strain hardening can be removed by giving the metal an annealing heat treatment. When the strain-hardened metal is slowly heated to a high temperature below its melting temperature, the processes of recovery, recrystallization, and grain growth take place, and the metal is softened. By combining strain hardening and annealing, large thickness reductions of metal sections can be accomplished without fracture.

By deforming some metals at high temperature and slow-loading rates, it is possible to achieve superplasticity, i.e., deformation of the order of 1000 to 2000%. The grain size must be ultrafine to achieve superplasticity.

Plastic deformation of metals takes place most commonly by the slip process, involving the movement of dislocations. Slip usually takes place on the closest-packed planes and in the closest-packed directions. The combination of a slip plane and a slip direction constitutes a slip system. Metals with a high number of slip systems are more ductile than those with only a few slip systems. Many metals deform by twinning when slip becomes difficult.

Grain boundaries at lower temperatures usually strengthen metals by providing barriers to dislocation movement. However, under some conditions of high-temperature deformation, grain boundaries become regions of weakness due to grain boundary sliding.

6.12 DEFINITIONS

Sec. 6.1

Hot working of metals: permanent deformation of metals and alloys above the temperature at which a strain-free microstructure is produced continuously (recrystallization temperature).

Cold working of metals: permanent deformation of metals and alloys below the temperature at which a strain-free microstructure is produced continuously (recrystallization temperature). Cold working causes a metal to be strain-hardened.

Percent cold reduction:

$$\%\ \text{cold reduction} = \frac{\text{change in cross-sectional area}}{\text{original cross-sectional area}} \times 100\%$$

Annealing: a heat treatment used on a metal to soften it.

Extrusion: a plastic-forming process in which a material under high pressure is reduced in cross section by forcing it through an opening in a die.

Forging: a primary-processing method for working metals into useful shapes in which the metal is hammered or pressed into shape.

Wire drawing: a process in which wire stock is drawn through one or more tapered dies to the desired cross section.

Deep drawing: A metal forming process for shaping flat sheets of metal into cup-shaped article.

Sec. 6.2

Elastic deformation: if a metal deformed by a force returns to its original dimensions after the force is removed, the metal is said to be elastically deformed.

Engineering stress σ: average uniaxial force divided by original cross-sectional area ($\sigma = F/A_0$).

Engineering strain ϵ: change in length of sample divided by the original length of sample ($\epsilon = \Delta l/l_0$).

Shear stress τ: shear force S divided by the area A over which the shear force acts ($\tau = S/A$).

Shear strain γ: shear displacement a divided by the distance h over which the shear acts ($\gamma = a/h$).

Sec. 6.3

Engineering stress-strain diagram: experimental plot of engineering stress versus engineering strain; σ is normally plotted as the y axis and ϵ as the x axis.

Modulus of elasticity E: stress divided by strain (σ/ϵ) in the elastic region of an engineering stress-strain diagram for a metal ($E = \sigma/\epsilon$).

Yield strength: the stress at which a specific amount of strain occurs in the engineering tensile test. In the U.S., the yield strength is determined for 0.2 percent strain.

Ultimate tensile strength (UTS): the maximum stress in the engineering stress-strain diagram.

Sec. 6.4
Hardness: a measure of the resistance of a material to permanent deformation.

Sec. 6.5
Slip: the process of atoms moving over each other during the permanent deformation of a metal.
Slipbands: line markings on the surface of a metal due to slip caused by permanent deformation.
Slip system: a combination of a slip plane and a slip direction.
Deformation twinning: a plastic deformation process that occurs in some metals and under certain conditions. In this process, a large group of atoms displaced to form a region of a metal crystal lattice that is a mirror image of a similar region along a twinning plane.

Sec. 6.6
Hall–Petch relationship: an empirical equation that relates the strength of a metal to its grain size.
Strain hardening (strengthening): the hardening of a metal or alloy by cold working. During cold working, dislocations multiply and interact, leading to an increase in the strength of the metal.

Sec. 6.7
Solid-solution hardening (strengthening): strengthening a metal by alloying additions that form solid solutions. Dislocations have more difficulty moving through a metal lattice when the atoms are different in size and electrical characteristics, as is the case with solid solutions.

Sec. 6.8
Annealing: a heat treatment process applied to a cold-worked metal to soften it.
Recovery: the first stage in the annealing process that results in removal of residual stresses and formation of low-energy dislocation configurations.
Recrystallization: the second stage of the annealing process in which new grains start to grow and dislocation density decreases significantly.
Grain growth: the third stage of the annealing process in which new grains start to grow in an equiaxed manner.

Sec. 6.9
Superplasticity: the ability of some metals to deform plastically by 1000% to 2000% at high temperatures and low loading rates.

Sec. 6.10
Nanocrystalline metals: metals with grain size smaller than 100 nm.

6.13 PROBLEMS

Answers to problems marked with an asterisk are given at the end of the book.

Knowledge and Comprehension Problems

6.1 (*a*) How are metal alloys made by the casting process? (*b*) Distinguish between wrought alloy products and cast alloy products.

6.2 Why are cast metal sheet ingots hot-rolled first instead of being cold-rolled?

6.3 What type of heat treatment is given to the rolled metal sheet after hot and "warm" rolling? What is its purpose?

6.4 Describe and illustrate the following types of extrusion processes: (*a*) direct extrusion and (*b*) indirect extrusion. What is an advantage of each process?

6.5 Describe the forging process. What is the difference between hammer and press forging?

6.6 What is the difference between open-die and closed-die forging? Illustrate. Give an example of a metal product produced by each process.

6.7 Describe the wire-drawing process. Why is it necessary to make sure the surface of the incoming wire is clean and lubricated?

6.8 Distinguish between elastic and plastic deformation (use schematics).

6.9 Define (*a*) engineering stress and strain and (*b*) true stress and strain. (*c*) What are the U.S. customary and SI units for stress and strain? (*d*) Distinguish between tensile/compressive stress (also called *normal stress*) and shear stress. (*e*) Distinguish between tensile/compressive strain (also called *normal strain*) and shear strain.

6.10 (*a*) Define the hardness of a metal. (*b*) How is the hardness of a material determined by a hardness testing machine?

6.11 What types of indenters are used in (*a*) the Brinell hardness test, (*b*) Rockwell C hardness test, and (*c*) Rockwell B hardness test?

6.12 What are slipbands and slip lines? What causes the formation of slipbands on a metal surface?

6.13 Describe the slip mechanism that enables a metal to be plastically deformed without fracture.

6.14 (*a*) Why does slip in metals usually take place on the densest-packed planes? (*b*) Why does slip in metals usually take place in the closest-packed directions?

6.15 (*a*) What are the principal slip planes and slip directions for FCC metals? (*b*) What are the principal slip planes and slip directions for BCC metals? (*c*) What are the principal slip planes and slip directions for HCP metals?

6.16 What other types of slip planes are important other than the basal planes for HCP metals with low *c*/*a* ratios?

6.17 Define the critical resolved shear stress for a pure metal single crystal. What happens to the metal from the macroscale point of view and behavior point of view once critical resolved shear stress is exceeded?

6.18 Describe the deformation twinning process that occurs in some metals when they are plastically deformed.

6.19 What is the difference between the slip and twinning mechanisms of plastic deformation of metals?

6.20 What important role does twinning play in the plastic deformation of metals with regard to deformation of metals by slip?

6.21 By what mechanism do grain boundaries strengthen metals?

6.22 What experimental evidence shows that grain boundaries arrest slip in polycrystalline metals?

6.23 (*a*) Describe the grain shape changes that occur when a sheet of alloyed copper with an original equiaxed grain structure is cold-rolled with 30 and 50 percent cold reductions. (*b*) What happens to the dislocation substructure?

6.24 How is the ductility of a metal normally affected by cold working? Why?

6.25 (*a*) What is solid-solution strengthening? Describe the two main types. (*b*) What are two important factors that affect solid-solution hardening?

6.26 What are the three main metallurgical stages that a sheet of cold-worked metal such as aluminum or copper goes through as it is heated from room temperature to an elevated temperature just below its melting point?

6.27 Describe the microstructure of a heavily cold-worked metal of an Al–0.8% Mg alloy as observed with an optical microscope at 100× (see Fig. 6.46*a*). Describe the microstructure of the same material at 20,000× (see Fig. 6.47*a*).

6.28 Describe what occurs microscopically when a cold-worked sheet of metal such as aluminum undergoes a recovery heat treatment.

6.29 When a cold-worked metal is heated into the temperature range where recovery takes place, how are the following affected: (*a*) internal residual stresses, (*b*) strength, (*c*) ductility, and (*d*) hardness?

6.30 Describe what occurs microscopically when a cold-worked sheet of metal such as aluminum undergoes a recrystallization heat treatment.

6.31 When a cold-worked metal is heated into the temperature range where recrystallization takes place, how are the following affected: (*a*) internal residual stresses, (*b*) strength, (*c*) ductility, and (*d*) hardness?

6.32 Describe two principal mechanisms whereby primary recrystallization can occur.

6.33 What are five important factors that affect the recrystallization process in metals?

6.34 What generalizations can be made about the recrystallization temperature with respect to (*a*) the degree of deformation, (*b*) the temperature, (*c*) the time of heating at temperature, (*d*) the final grain size, and (*e*) the purity of the metal?

6.35 Define superplasticity and list the conditions under which superplasticity can be achieved. Why is this an important behavior?

6.36 Discuss the major deformation mechanism that results in extensive plastic deformation in superplasticity.

6.37 Why are nanocrystalline materials stronger? Answer based on dislocation activity.

Application and Analysis Problems

***6.38** A 70% Cu–30% Zn brass sheet is 0.0955 cm thick and is cold-rolled with a 30 percent reduction in thickness. What must be the final thickness of the sheet?

6.39 A sheet of aluminum alloy is cold-rolled 30 percent to a thickness of 0.080 in. If the sheet is then cold-rolled to a final thickness of 0.064 in., what is the total percent cold work done?

6.40 Calculate the percent cold reduction when an aluminum wire is cold-drawn from a diameter of 5.25 mm to a diameter of 2.30 mm.

6.41 A brass wire is cold-drawn 25 percent to a diameter of 1.10 mm. It is then further cold-drawn to 0.900 mm. What is the total percent cold reduction?

6.42 What is the relationship between engineering strain and percent elongation?

***6.43** A tensile specimen of cartridge brass sheet has a cross section of 0.320 in. × 0.120 in. and a gage length of 2.00 in. Calculate the engineering strain that occurred during a test if the distance between gage markings is 2.35 in. after the test.

6.44 A 0.505-in.-diameter rod of an aluminum alloy is pulled to failure in a tension test. If the final diameter of the rod at the fractured surface is 0.440 in., what is the percent reduction in area of the sample due to the test?

6.45 The following engineering stress-strain data were obtained for a 0.2% C plain-carbon steel. (*a*) Plot the engineering stress-strain curve. (*b*) Determine the ultimate tensile strength of the alloy. (*c*) Determine the percent elongation at fracture.

Engineering stress (in./in.)	Engineering stress (ksi)	Engineering strain (ksi)	Engineering strain (in./in.)
0	0	76	0.08
30	0.001	75	0.10
55	0.002	73	0.12
60	0.005	69	0.14
68	0.01	65	0.16
72	0.02	56	0.18
74	0.04	51	(Fracture) 0.19
75	0.06		

6.46 Plot the data of Prob. 6.51 as engineering stress (MPa) versus engineering strain (mm/mm) and determine the ultimate strength of the steel.

6.47 The following engineering stress-strain data were obtained at the beginning of a tensile test for a 0.2% C plain carbon steel. (*a*) Plot the engineering stress-strain curve for these data. (*b*) Determine the 0.2 percent offset yield stress for this steel. (*c*) Determine the tensile elastic modulus of this steel. (Note that these data only give the beginning part of the stress-strain curve.)

Engineering stress (in./in.)	Engineering stress (ksi)	Engineering strain (ksi)	Engineering strain (in./in.)
0	0	60	0.0035
15	0.0005	66	0.004
30	0.001	70	0.006
40	0.0015	72	0.008
50	0.0020		

6.48 Plot the data of Prob. 6.53 as engineering stress (MPa) versus engineering strain (mm/mm) and determine the 0.2 percent offset yield stress of the steel.

***6.49** A 0.505-in.-diameter aluminum alloy test bar is subjected to a load of 25,000 lb. If the diameter of the bar is 0.490 in. at this load, determine (*a*) the engineering stress and strain and (*b*) the true stress and strain.

6.50 A 20-cm-long rod with a diameter of 0.250 cm is loaded with a 5000 N weight. If the diameter decreases to 0.210 cm, determine (*a*) the engineering stress and strain at this load and (*b*) the true stress and strain at this load.

***6.51** A stress of 75 MPa is applied in the [0 0 1] direction on an FCC single crystal. Calculate (*a*) the resolved shear stress acting on the (111) $[\bar{1}\,0\,1]$ slip system and (*b*) the resolved shear stress acting on the (111) $[\bar{1}\,1\,0]$ slip system.

6.52 A stress of 55 MPa is applied in the [001] direction of a BCC single crystal. Calculate (*a*) the resolved shear stress acting on the (101) $[\bar{1}11]$ system and (*b*) the resolved shear stress acting on the (110) $[\bar{1}11]$ system.

6.53 A stress of 4.75 MPa is applied in the $[0\,0\,\bar{1}]$ direction of a unit cell of an FCC copper single crystal. Calculate the resolved shear stress on the $(1\,1\,\bar{1})$ plane in the following directions: (*a*) $[\bar{1}\,0\,1]$, (*b*) $[0\,\bar{1}\,\bar{1}]$, and (*c*) $[\bar{1}\,1\,0]$.

6.54 A stress of 85 MPa is applied in the [001] direction of a unit cell of a BCC iron single crystal. Calculate the resolved shear stress for the following slip systems: (*a*) (011)[$1\bar{1}1$], (*b*) (110)[$\bar{1}11$], and (*c*) (0$\bar{1}$1)[111].

***6.55** Compare the strength of a copper specimen with an average grain diameter of 0.8 μm with another copper specimen with an average grain diameter of 80 nm using the Hall–Petch equation.

6.56 A specimen of commercially pure titanium has a strength of 140 MPa. Estimate its average grain diameter using the Hall–Petch equation.

6.57 The average grain diameter of an aluminum alloy is 14 μm with a strength of 185 MPa. The same alloy with an average grain diameter of 50 μm has a strength of 140 MPa. (*a*) Determine the constants for the Hall–Petch equation for this alloy. (*b*) How much more should you reduce the grain size if you desired a strength of 220 MPa?

6.58 An oxygen-free copper rod must have a tensile strength of 50.0 ksi and a final diameter of 0.250 in. (*a*) What amount of cold work must the rod undergo (see Fig. 6.43)? (*b*) What must the initial diameter of the rod be?

***6.59** A 70% Cu–30% Zn brass sheet is to be cold-rolled from 0.070 to 0.040 in. (*a*) Calculate the percent cold work, and (*b*) estimate the tensile strength, yield strength, and elongation from Fig. 6.44.

6.60 A 70% Cu–30% Zn brass wire is cold-drawn 20 percent to a diameter of 2.80 mm. The wire is then further cold-drawn to a diameter of 2.45 mm. (*a*) Calculate the total percent cold work that the wire undergoes. (*b*) Estimate the wire's tensile and yield strengths and elongation from Fig. 6.44.

***6.61** If it takes 115 h to 50 percent recrystallize an 1100-H18 aluminum alloy sheet at 250°C and 10 h at 285°C, calculate the activation energy in kilojoules per mole for this process. Assume an Arrhenius-type rate behavior.

6.62 If it takes 12.0 min to 50 percent recrystallize a piece of high-purity copper sheet at 140°C and 200 min at 88°C, how many minutes are required to recrystallize the sheet 50 percent at 100°C? Assume an Arrhenius-type rate behavior.

6.63 If it takes 80 h to completely recrystallize an aluminum sheet at 250°C and 6 h at 300°C, calculate the activation energy in kilojoules per mole for this process. Assume an Arrhenius-type rate behavior.

Synthesis and Evaluation Problems

6.64 How would you manufacture large propellers for large ships? What factors would influence the selection of material for this application?

6.65 If you were to make a large number of components from gold, silver, or other precious metals, what metal forming process would use and why?

6.66 If you were to make only two units of a certain component with a complicated geometry, what manufacturing process would you use?

6.67 If you were to select a material for the construction of a robotic arm which would result in the smallest amount of elastic deformation (important for positional accuracy of the arm) and weight were not a critical criterion, which one of the metals given in Fig. 6.23 would you select? Why?

6.68 Consider the casting of a thick cylindrical shell made of cast iron. If the casting process is controlled such that solidification takes place from the inner walls of the tube outward, as the outer layers solidify they shrink and compress the inner layers, what would be the advantage of developed compressive stresses?

6.69 Consider casting a cube and a sphere on the same volume from the same metal. Which one would solidify faster? Why?

6.70 Design a process that produces long bars with an "H" cross-section from steel (indicate hot or cold if applicable). Draw schematics to show your procedure.

6.71 In the rolling process, the selection of the roll material is critical. Based on your knowledge of both hot and cold rolling, what properties should the roller material have?

6.72 When manufacturing complex shapes using cold forging or shape rolling operations, the mechanical properties such as yield strength, tensile strength, and ductility measure differently dependent on the location and direction on the manufactured part. (*a*) How do you explain this from a micro point of view? (*b*) Will this happen during hot forging or rolling? Explain your answer.

6.73 (*a*) State the assumption behind the development of Eq. 6.14. (*b*) Is Eq. 6.14 (or its underlying assumption) valid throughout the engineering stress-strain curve?

6.74 Draw a generic engineering stress-strain diagram for a ductile metal and highlight the key strength points (yield, ultimate, and fracture strength) on the curve. (*a*) Schematically, show what happens if you load the specimen just below its yield point and then unload to zero. (*b*) Will the specimen behave differently if you load it again? Explain.

6.75 (*a*) Draw a generic engineering stress-strain diagram for a ductile metal and highlight the key strength points (yield, ultimate, and fracture strength) on the curve. Schematically, show what happens if you load the specimen just below its ultimate tensile strength point and then unload to zero. (*b*) Will the specimen behave differently if you load it again? Explain.

***6.76** (*a*) Derive the relationship between true strain and engineering strain. (Hint: Start with expression for engineering strain.) (*b*) Derive a relationship between true stress and engineering strain. (Hint: Start with $\sigma_t = F/A_i = (F/A_o)(A_o/A_i)$.)

***6.77** The engineering yield strength of a copper alloy is 23.9 Ksi and the modulus of elasticity is 16×10^6 psi. (*a*) Estimate the engineering strain just before yield. (*b*) What is the corresponding true strain? Are you surprised? Explain.

6.78 For the alloy in problem 6.77, the engineering ultimate tensile strength is 38.8 Ksi where the corresponding engineering strain 0.18. The reduction in area just before fracture is measured to be 34%. Determine (*a*) the true stress corresponding to the engineering ultimate tensile strength, and (*b*) the true strain just before fracture.

6.79 The material for a rod of cross-sectional area 2.70 in^2 and length 75.0 inches must be selected such that under an axial load of 120,000.0 lb, it will not yield and the elongation in the bar will remain below 0.105 inches. (*a*) Provide a list of at least three different metals that would satisfy these conditions. (*b*) Narrow the list down if cost is an issue. (*c*) Narrow the list down if corrosion is an issue. Use Appendix I for properties and cost of common alloys only.

6.80 What do E, G, ν, tell you about a material (explain the physical significance of each to a non-engineer)?

6.81 A cylindrical component is loaded in tension until the cross-sectional area is reduced by 25% (the specimen does not neck or fracture). (*a*) Determine the true strain for the specimen at this loading level. (*b*) If you were to calculate the uniaxial stress in the specimen under the given conditions, would you use the true stress or the engineering stress? Support your answer by showing the difference?

6.82 Referring to Figs. 6.20 and 6.21 (read the figure captions for details), determine (*a*) the change in length of the aluminum specimen (gage length) when the engineering stress reaches 85 ksi. (*b*) If at this point the specimen is slowly unloaded to zero load, what will the length of the specimen be in the unloaded state? (Show the unloading curve schematically).

6.83 (*a*) Show, using the definition of the Poisson's ratio, that it would be impossible to have a negative Poisson's ratio for isotropic materials. (*b*) What would it mean for a material to have a negative Poisson's ratio?

6.84 A one-inch cube of tempered stainless steel (alloy 316) is loaded along its z-direction under a tensile stress of 60.00 ksi. (*a*) Draw a schematic of the cube before and after loading showing the changes in dimension. (*b*) Repeat the problem assuming the cube is made of tempered aluminum (alloy 2024). Use Fig. 6.15*b* and Appendix I for relevant data.

6.85 A one-inch cube tempered stainless steel (alloy 316) is loaded on the same face with a shear stress of 60.00 ksi. Draw a schematic of the cube before and after loading showing any changes in the shape. ($G = 11.01 \times 10^6$ psi; use Fig. 6.17*c*)

***6.86** Three different metal alloys are tested for their hardness using the Rockwell scale. Metal 1 was rated at 60 R_B, metal 2 at 60 R_C, and metal 3 at 60 R_F. What do these ratings tell about these metals? Give an example of a component that is made of a metal that has a hardness of around 60R_c.

6.87 A fellow student asks you " What is the yield strength of titanium?" Can you answer this question? Explain.

6.88 A fellow student asks you "What is the modulus of elasticity of plain carbon steel?" Can you answer this question? Explain.

6.89 A fellow student asks you "What is the hardness of aluminum?" Can you answer this question? Explain.

6.90 Why do BCC metals in general require a higher value of τ_c than FCC metals when they both have the same number of slip systems?

***6.91** Determine the tensile stress that must be applied to the $[1\bar{1}0]$ axis of a high-purity copper single crystal to cause slip on the $(1\,\bar{1}\,\bar{1})[0\bar{1}1]$ system. The resolved shear stress for the crystal is 0.85 MPa.

6.92 In the loading of a single crystal, (*a*) determine the angles ϕ and λ for which the maximum resolved shear stress occurs. (*b*) What will resolved shear stress be at this position (in terms of σ)?

6.93 (*a*) In loading of a single crystal, how would you orient the crystal with respect to the loading axis to cause a resolved shear stress of zero? (*b*) What is the physical significance of this, i.e., under these conditions, what happens to the crystal as σ increases?

6.94 Starting with a 2-inch diameter rod of brass, we would like to process 0.2-inch diameter rods that possess minimum yield strength of 40 ksi and a minimum elongation to fracture of 40%, (see Fig. 6.44). Design a process that achieves that. Hint: Reduction of the diameter directly from 2 inches to 0.2 inches is not possible, why?

6.95 Why is it difficult to improve both strength and ductility simultaneously?

6.96 For a given application, a rod of copper of one-inch diameter is to be used. You have copper rods of various cross-sections available to you; however, all the bars are fully annealed with a yield strength of 10.0 Ksi. The material must have a yield strength of at least 30.0 Ksi and an elongation ability of at least 20.0%. Design a process that would achieve the expected goals. Use Fig. 6.43 for your solution.

6.97 Without referring to tensile strength data or tables, which of the following substitutional solid solutions would you select if higher tensile strength was the selection criterion: Cu- 30 wt% Zinc or Cu – 30 wt% Ni? Hint: Compare melt temperatures of Cu, Ni, and Zn.

6.98 The cupro-nickel substitutional solid solution alloys Cu- 40 wt% Ni and Ni- 10 wt% Cu have similar tensile strengths. For a given application that only tensile strength is important, which one would you select?

CHAPTER 7

Mechanical Properties of Metals II

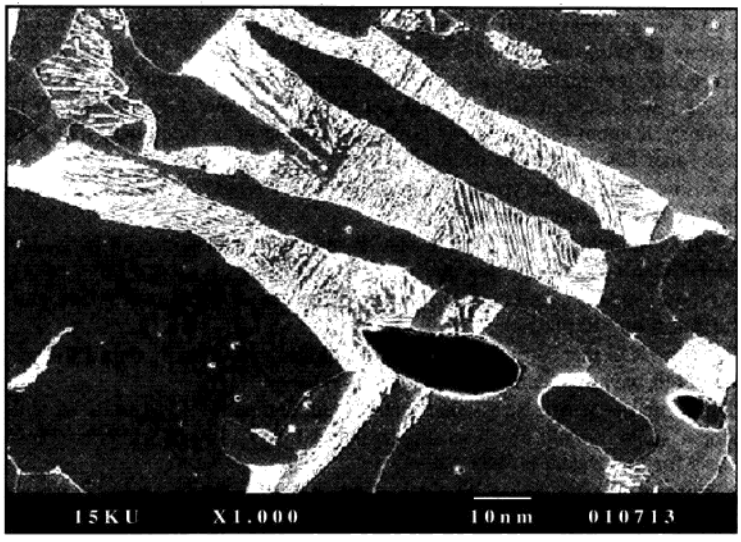

(© *The Minerals, Metals & Materials Society, 1998.*)

On April 12, 1912, at 11:40 P.M., the *Titanic,* on its maiden voyage, struck a large iceberg, damaging her hull and causing six forward compartments to rupture. The seawater temperature at the time of the accident was −2°C. The ensuing flooding of these compartments resulted in complete fracture of the hull with the tragic loss of more than 1500 lives.

The *Titanic* was found on the ocean floor September 1, 1985, by Robert Ballard. She was 3.7 km below the water surface. Based on metallurgical and mechanical tests performed on the *Titanic* steel, it was determined that the ductile-brittle transition temperature of the steel used in the *Titanic* was 32°C for the longitudinal specimens made from the hull plate, and 56°C for the transverse specimens. This reveals that the steel used in the construction of the *Titanic* behaved in a highly brittle fashion when it struck the iceberg. The microstructure of the *Titanic* steel in the chapter-opening image shows ferrite grains (gray), pearlite colonies (light lamellar), and MnS particles (dark).[1] ■

[1]www.tms.org/pubs/journals/JOM/9801/Felkins-9801.html#ToC6

LEARNING OBJECTIVES

By the end of this chapter, students will be able to . . .

1. Describe the process of fracture of metals and differentiate between ductile and brittle fracture.
2. Describe the ductile to brittle transition of metals. What type of metals are more susceptible to ductile to brittle transition?
3. Define the fracture toughness of a material and explain why this property is used in engineering design instead of toughness.
4. Define fatigue loading and failure in materials, describe the parameters that are used to characterize fluctuating stresses, and enumerate the factors that affect the fatigue strength of materials.
5. Describe creep, creep test, and the use of the Larsen-Miller parameter in the design for determination of time to stress rupture.
6. Describe why analysis of a failed component is important and what are the steps taken in the failure analysis process.
7. Describe the effect of nanograin size on the strength and ductility of a metal.

This chapter continues with a study of the mechanical properties of metals. First, the fracture of metals will be discussed. Then the fatigue and fatigue crack propagation of metals and the creep (time-dependent deformation) and stress rupture of metals are considered. A case study in fracture of a metallic component is also presented. Finally, future directions in the synthesis of nanostructured metals and their properties are discussed.

7.1 FRACTURE OF METALS

One of the important and practical aspects of materials selection in the design, development, and production of new components is the possibility of failure of the component under normal operation. Failure may be defined as the *inability* of a material or a component to (1) perform the intended function, (2) meet performance criteria although it may still be operational, or (3) perform safely and reliably even after deterioration. Yielding, wear, buckling (elastic instability), corrosion, and fracture are examples of situations in which a component has failed.

Engineers are deeply aware of the possibility of fracture in load-bearing components and its potentially detrimental effect on productivity, safety, and other economical issues. As a result all design, manufacturing, and materials engineers use safety factors in their initial analysis to reduce the possibility of fracture by essentially overdesigning the component or the machine. In many fields such as pressure vessel design and manufacturing, there exist codes and standards that are

put in place by various agencies that must be followed by all designers and manufacturers. Regardless of the extreme care taken in design, manufacturing, and materials selection for machines and components, failures are unavoidable, resulting in loss of property and unfortunately, sometimes, life. Every engineer should be (1) completely familiar with the concept of fracture or failure of materials and (2) able to extract information from a failed component as to the causes of failure. In most cases, scientists and engineers carefully analyze the failed components to determine the cause of failure. The information gained is used to advance safe performance and minimize the possibility of failure through improvements in design, manufacturing processes, and materials synthesis and selection. From a purely mechanical performance point of view, engineers are concerned with fracture failure of designed components that are made of metals, ceramics, composites, polymers, or even electronic materials. In the upcoming sections, various modes of fracture and failure of metals under operation will be presented and discussed. In future chapters, the fracture and failure of other classes of materials will also be discussed.

Fracture is the separation of a solid under stress into two or more parts. In general metal fractures can be classified as ductile or brittle, but a fracture can also be a mixture of the two. The **ductile fracture** of a metal occurs after extensive plastic deformation and is characterized by slow crack propagation. Figure 7.1 shows an example of a ductile fracture in an aluminum alloy test specimen. **Brittle fracture,** in contrast, usually proceeds along characteristic crystallographic planes called *cleavage planes* and has rapid crack propagation. Owing to their rapidity, brittle fractures generally lead to sudden, unexpected, catastrophic failures while the plastic deformation accompanying ductile fracture may be detectable before fracture occurs.

7.1.1 Ductile Fracture

Virtual Lab

Ductile fracture of a metal occurs after extensive plastic deformation. For simplicity let us consider the ductile fracture of a round (0.50-in.-diameter) tensile specimen. If a stress is applied to the specimen that exceeds its ultimate tensile strength and is sustained long enough, the specimen will fracture. Three distinct stages of ductile fracture can be recognized: (1) the specimen forms a neck, and cavities form within the necked region (Fig. 7.2*a* and *b*); (2) the cavities in the neck coalesce into a crack in the center of the specimen and propagate toward the surface of the specimen in a direction perpendicular to the applied stress (Fig. 7.2*c*); and (3) when the crack nears the surface, the direction of the crack changes to 45° to the tensile axis and a cup-and-cone fracture results (Fig. 7.2*d* and *e*). Figure 7.3 shows a scanning electron micrograph of a ductile fracture of a spring-steel specimen, and Fig. 7.4 shows internal cracks in the necked region of a deformed specimen of high-purity copper.

In practice, ductile fractures are less frequent than brittle fractures, and the main cause for their occurrence is overloading of the component. Overloading could occur as a result of (1) improper design, including the selection of materials

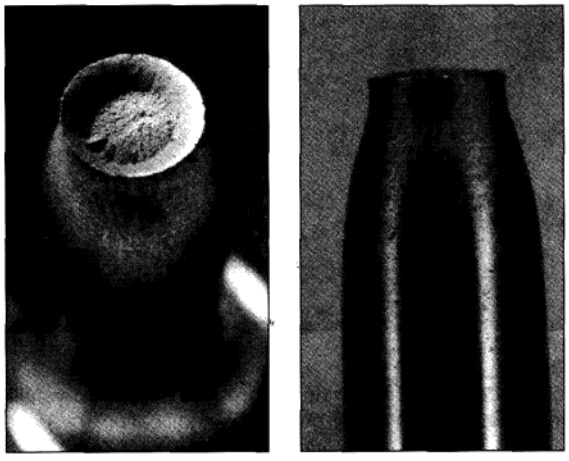

Animation

Figure 7.1
Ductile (cup-and-cone) fracture of an aluminum alloy.
(After ASM Handbook of Failure Analysis and Prevention, Vol. 11. 1992. Reprinted with permission of ASM International. All rights reserved. www.asminternational.org.)

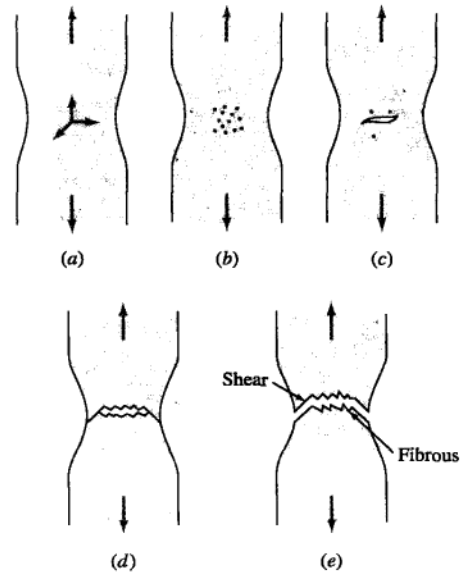

Figure 7.2
Stages in the formation of a cup-and-cone ductile fracture.
(After G. Dieter, "Mechanical Metallurgy," 2nd ed., McGraw-Hill, 1976, p. 278.)

(underdesigning), (2) improper fabrication, or (3) abuse (component is used at load levels above that allowed by the designer). An example of a ductile failure is given in Fig. 7.5. In this figure, the rear axle shaft of a vehicle is shown that has undergone significant plastic twisting (note torsion marks on the shaft) due to applied torsion. Based on engineering analysis, the cause of this failure has been attributed to a poor choice of material. AISI type S7 tool steel was used for this component with an improperly low hardness level of 22–27 HRC. The required hardness for the metal was over 50 HRC, which is usually achieved through heat treatment processes (see Chap. 9).

7.1.2 Brittle Fracture

Many metals and alloys fracture in a brittle manner with very little plastic deformation. Figure 7.6 shows a tensile specimen that failed in a brittle manner. Comparison of this figure with Fig. 7.1 reveals the drastic differences in the deformation level prior to fracture between ductile and brittle fractures. Brittle fracture usually proceeds along specific crystallographic planes called *cleavage planes* under a stress normal to the

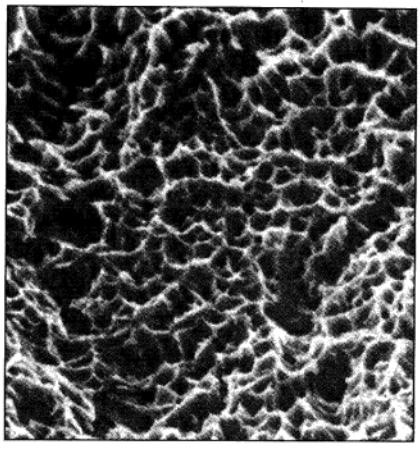

Figure 7.3
Scanning electron micrograph showing conical equiaxed dimples produced during the fracture of a spring-steel specimen. These dimples, which are formed during the microvoid coalescence of the fracture, are indicative of a ductile fracture.
(After ASM Handbook Vol. 12 – Fractography, p 14, fig. 2a, 1987. Reprinted with permission of ASM International. All rights reserved. www.asminternational.org.)

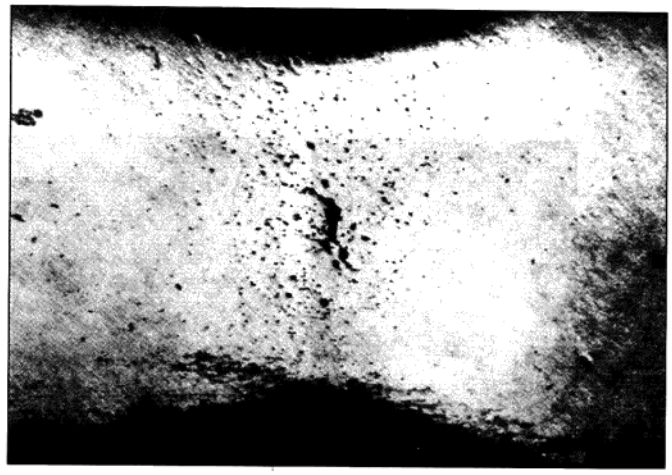

Figure 7.4
Internal cracking in the necked region of a polycrystalline specimen of high-purity copper. (Magnification 9×.)
(After K. E. Puttnick, Philos. Mag. 4:964 (1959).)

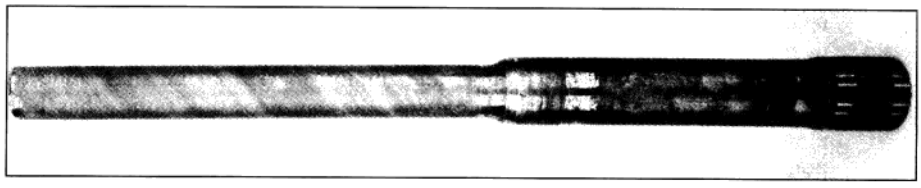

Figure 7.5
Failed axle shaft.
(ASM Handbook of Failure Analysis and Prevention, Vol. 11. 1992. Reprinted with permission of ASM International. All rights reserved. www.asminternational.org.)

cleavage plane (see Fig. 7.7). Many metals with the HCP crystal structure commonly show brittle fracture because of their limited number of slip planes. A zinc single crystal, for example, under a high stress normal to the (0001) planes will fracture in a brittle manner. Many BCC metals such as α iron, molybdenum, and tungsten also fracture in a brittle manner at low temperatures and high strain rates.

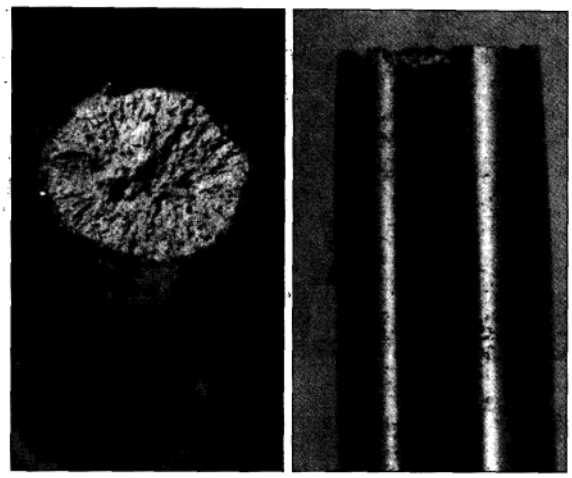

Virtual Lab

Figure 7.6
Brittle fracture of a metal alloy showing radial ridges that emanate from the center of the specimen.
(ASM Handbook of Failure Analysis and Prevention, Vol. 11. 1992. Reprinted with permission of ASM International. All rights reserved. www.asminternational.org)

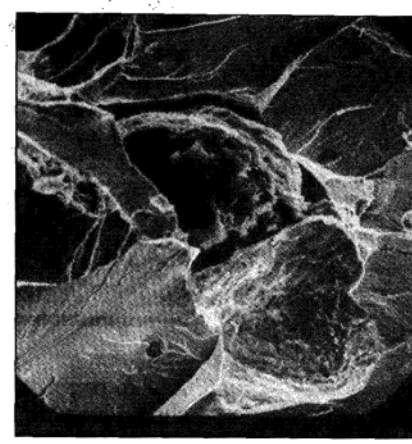

Figure 7.7
Brittle cleavage fracture in ferritic ductile iron. SEM, 1000×.
(After W.L. Bradley, Texas A&M University, From ASM Handbook, Vol. 12, p.237, fig. 97, 1987. Reprinted with permission of ASM International. All rights reserved. www.asminternational.org.)

Most brittle fractures in polycrystalline metals are **transgranular,** i.e., the cracks propagate across the matrix of the grains. However, brittle fracture can occur in an **intergranular** manner if the grain boundaries contain a brittle film or if the grain boundary region has been embrittled by the segregation of detrimental elements.

Brittle fracture in metals is believed to take place in three stages:

1. Plastic deformation concentrates dislocations along slip planes at obstacles.
2. Shear stresses build up in places where dislocations are blocked, and as a result microcracks are nucleated.
3. Further stress propagates the microcracks, and stored elastic strain energy may also contribute to the propagation of the cracks.

In many cases, brittle fractures occur because of the existence of defects in the metal. These defects are either formed during the manufacturing stage or develop during service. Undesirable defects such as folds, large inclusions, undesirable grain flow, poor microstructure, porosity, tears, and cracks may form during manufacturing operations such as forging, rolling, extrusion, and casting. Fatigue cracks, embrittlement due to the atomic hydrogen (see Sec. 13.5.11), and corrosion damage often result in final brittle fracture. When brittle fracture occurs, it consistently initiates at the defect location (*stress risers*) regardless of the cause for the formation of the defect. Certain defects, low operating temperatures, or high

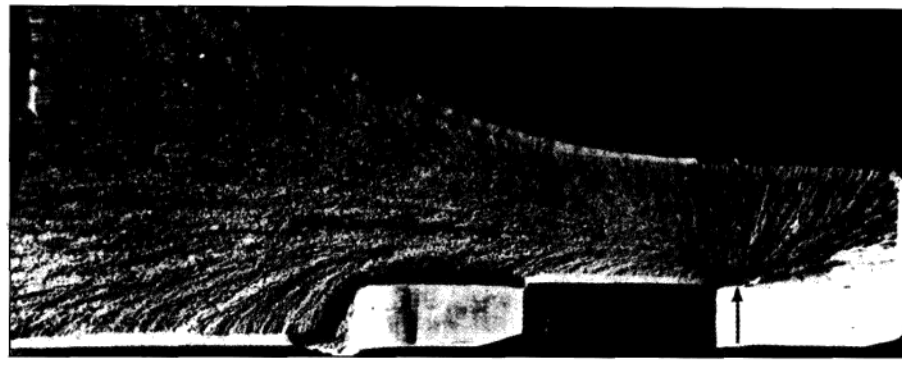

Figure 7.8
A snap ring made of 4335 steel failed in a brittle manner because of the existence of a sharp corner.
(ASM Handbook of Failure Analysis and Prevention, Vol. 11. 1992. Reprinted with permission of ASM International. All rights reserved. www.asminternational.org.)

loading rates may also cause the brittle fracture of some moderately ductile materials. The transition from ductile to brittle behavior is called a **ductile to brittle transition (DBT).** Thus, ordinarily ductile materials can, under certain circumstances, fracture in brittle manner. Figure 7.8 shows the brittle fracture of a snap ring due to the existence of a sharp corner as the defect (see arrow on the figure); note the *chevron pattern* pointing toward the origin of the fracture (typically found in a brittle fracture surface.)

7.1.3 Toughness and Impact Testing

Toughness is a measure of the amount of energy a material can absorb before fracturing. It becomes of engineering importance when the ability of a material to withstand an impact load without fracturing is considered. One of the simplest methods of measuring toughness is to use an impact-testing apparatus. A schematic diagram of a simple impact-testing machine is shown in Fig. 7.9. One method of using this apparatus is to place a Charpy V-notch specimen (shown in the upper part of Fig. 7.9) across parallel jaws in the machine. In the impact test, a heavy pendulum released from a known height strikes the sample on its downward swing, fracturing it. By knowing the mass of the pendulum and the difference between its initial and final heights, the energy absorbed by the fracture can be measured. Figure 7.10 shows the relative effect of temperature on the impact energy of some types of materials.

7.1.4 Ductile to Brittle Transition Temperature

As mentioned above, under certain conditions a marked change in the fracture resistance of some metals is observed in service, i.e., ductile to brittle transition. Low temperatures, high stress states, and fast loading rates may all cause a ductile

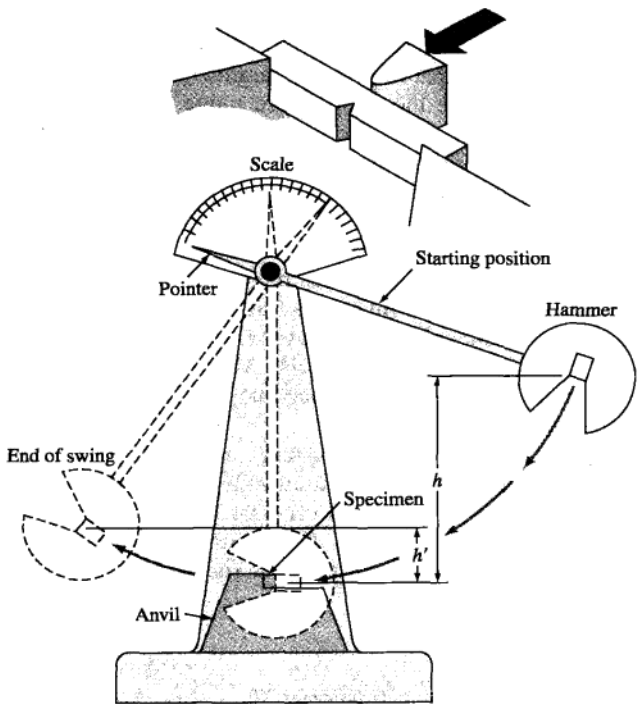

Figure 7.9
Schematic drawing of a standard impact-testing apparatus.
(After H.W. Hayden, W.G. Moffatt, and J. Wulff, "The Structure and Properties of Materials," vol. III, Wiley, 1965, p. 13.)

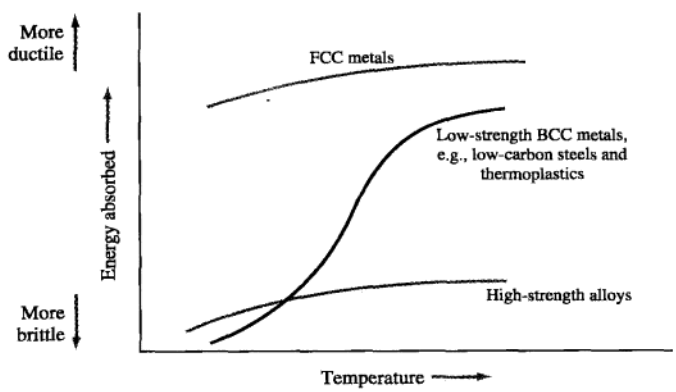

Figure 7.10
Effect of temperature on the energy absorbed upon impact by different types of materials.
(From G. Dieter, "Mechanical Metallurgy," 2nd ed., McGraw-Hill, 1976, p. 278. Reproduced with permission of The McGraw-Hill Companies.)

material to behave in a brittle manner; however, customarily the temperature is selected as the variable that represents this transition while the load rate and stress rate are held constant. The impact-testing apparatus discussed in the previous section may be used to determine the temperature range for the transition from ductile to brittle behavior of materials. The temperature of the Charpy specimen may be set using furnace and refrigeration units. Although some metals show a distinct DBT temperature, for many this transition occurs over a range of temperatures (see Fig. 7.10). Also, Fig. 7.10 shows that FCC metals do not undergo DBT and, as a consequence, are suitable for low temperature use. Factors that influence the DBT temperature are alloy composition, heat treatment, and processing. For instance, the carbon content of annealed steels affects this transition temperature range, as shown in Fig. 7.11. Low-carbon annealed steels have a lower-temperature transition range and a narrower one than high-carbon steels. Also, as the carbon content of the annealed steels is increased, the steels become more brittle, and less energy is absorbed on impact during fracture.

Ductile to brittle transition is an important consideration in materials selection for components that operate in cold environments. For instance, ships that sail in cold waters (see the chapter opener) and offshore platforms that are located in the Arctic seas are especially susceptible to DBT. For such applications, the selected materials should have a DBT temperature that is significantly lower than the operating or service temperature.

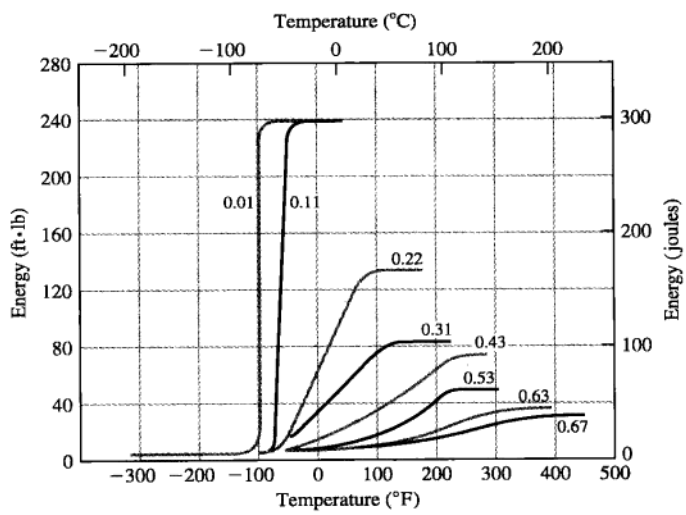

Figure 7.11
Effect of carbon content on the impact energy temperature plots for annealed steels.
[*After J.A. Rinebolt and W.H. Harris, Trans. ASM,* **43**:*1175(1951).*]

7.1.5 Fracture Toughness

Impact tests such as the one previously described give useful comparative quantitative data with relatively simple test specimens and equipment. However, these tests do not provide proper data for design purposes for material sections containing cracks or flaws. Data of this type are obtained from the discipline of fracture mechanics in which theoretical and experimental analyses are made of the fracture of structural materials containing preexisting cracks or flaws. In this book, we shall focus on the fracture toughness property of fracture mechanics and show how it can be applied to some simple component designs.

The fracture of a metal (material) starts at a place where the stress concentration is the highest, which may be at the top of a sharp crack, for example. Let us consider a plate sample under uniaxial tension that contains an edge crack (Fig. 7.12*a*) or a center-through crack (Fig. 7.12*b*). The stress at the tip of a sharp crack is highest at the tip as indicated in Fig. 7.12*c*.

The stress intensity at the crack tip is found to be dependent on both the applied stress and the width of the crack. We use the stress-intensity factor K_I to express the combination of the effects of the stress at the crack tip and the crack length. The subscript I (pronounced "one") indicates mode I testing in which a tensile stress causes the crack to open. By experiment, for the case of uniaxial tension on a metal plate containing an edge or internal crack (mode I testing), we find that

$$K_I = Y\sigma\sqrt{\pi a} \tag{7.1}$$

where K_I = stress-intensity factor
σ = applied nominal stress
a = edge-crack length or half the length of an internal through crack
Y = dimensionless geometric constant on the order of 1

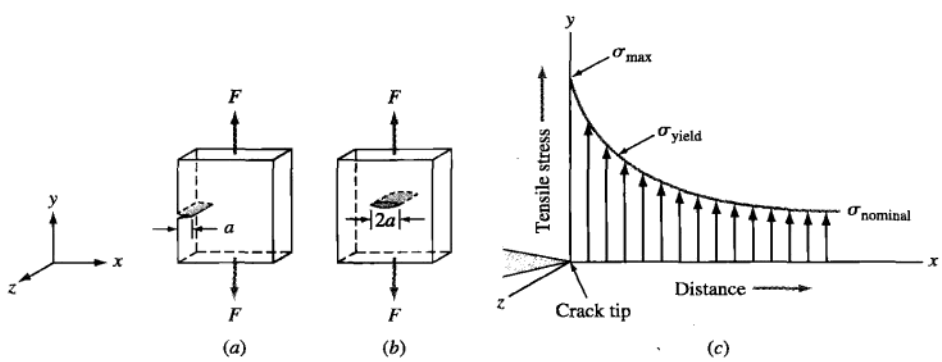

Figure 7.12
Metal alloy plate under uniaxial tension (*a*) with edge crack *a*, (*b*) with center crack 2*a*. (*c*) Stress distribution versus distance from crack tip. The stress is a maximum at the crack tip.

The critical value of the stress-intensity factor that causes failure of the plate is called the *fracture toughness* K_{IC}, (pronounced "kay-one-see") of the material. In terms of the fracture stress σ_f and the crack length a for an edge crack (or one-half of the internal crack length),

$$K_{IC} = Y\sigma_f \sqrt{\pi a} \tag{7.2}$$

Fracture-toughness (K_{IC}) values have the SI units of MPa$\sqrt{m}$ and U.S. customary units of ksi$\sqrt{in.}$ Figure 7.13*a* is a schematic diagram of the compact type of fracture-toughness test specimen. To obtain constant values for K_{IC}, the base dimension B of the specimen must be relatively large compared to the notch-depth dimension a so that so-called plain-strain conditions prevail. Plain-strain conditions require that during testing there is no strain deformation in the direction of the notch (i.e., in the z direction of Fig. 7.13*a*). Plain-strain conditions generally prevail when B (specimen thickness) = 2.5 (K_{IC}/yield strength)^2. Note that the fracture-toughness specimen has a machined notch and a fatigue crack at the end of the notch of about 3 mm depth to start the fracture during the test. Figure 7.13*b* shows a real fracture-toughness test at the time of rapid fracture.

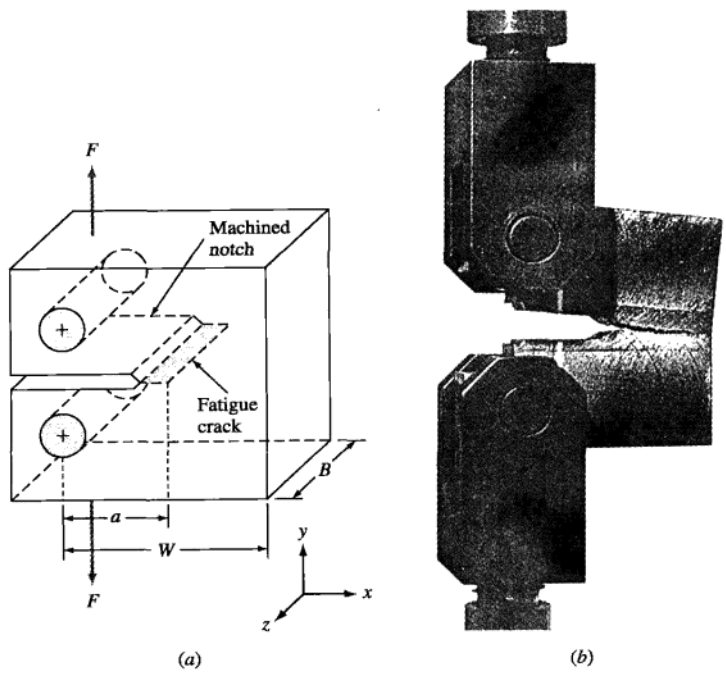

Figure 7.13
Fracture-toughness test using a compact type of specimen and plain-strain conditions. (*a*) Dimensions of specimen. (*b*) Actual test at the critical stress for fracture, using a laser beam to detect this stress. (*Courtesy of White Shell Research.*)

Table 7.1 Typical fracture-toughness values for selected engineering alloys

Material	K_{IC} MPa$\sqrt{m}$	K_{IC} ksi$\sqrt{in.}$	$\sigma_{yield\ strength}$ MPa	$\sigma_{yield\ strength}$ ksi
Aluminum alloys:				
2024-T851	26.4	24	455	66
7075-T651	24.2	22	495	72
7178-T651	23.1	21	570	83
Titanium alloy:				
Ti-6A1-4V	55	50	1035	150
Alloy steels:				
4340 (low-alloy steel)	60.4	55	1515	220
17-7 pH (precipitation hardening)	76.9	70	1435	208
350 maraging steel	55	50	1550	225

Source: R.W. Herzberg, "Deformation and Fracture Mechanics of Engineering Materials," 3rd ed., Wiley, 1989.

Fracture-toughness values of materials are most useful in mechanical design when working with materials of limited toughness or ductility such as high-strength aluminum, steel, and titanium alloys. Table 7.1 lists some K_{IC} values for some of these alloys. Materials that show little plastic deformation before fracture have relatively low fracture toughness K_{IC} values and tend to be more brittle, whereas those with higher K_{IC} values are more ductile. Fracture-toughness values can be used in mechanical design to predict the allowable flaw size in alloys with limited ductility when acted upon by specific stresses (a factor of safety is also applied for added safety). Example Problem 7.1 illustrates this design approach.

EXAMPLE PROBLEM 7.1

A structural plate component of an engineering design must support 207 MPa (30 ksi) in tension. If aluminum alloy 2024-T851 is used for this application, what is the largest internal flaw size that this material can support? (Use $Y = 1$).

■ **Solution**

$$K_{IC} = Y\sigma_f\sqrt{\pi a} \tag{7.2}$$

Using $Y = 1$ and $K_{IC} = 26.4\ \text{MPa}\sqrt{\text{m}}$ from Table 7.1,

$$a = \frac{1}{\pi}\left(\frac{K_{IC}}{\sigma_f}\right)^2 = \frac{1}{\pi}\left(\frac{26.4\ \text{MPa}\sqrt{\text{m}}}{207\ \text{MPa}}\right)^2 = 0.00518\ \text{m} = 5.18\ \text{mm}$$

Thus, the largest internal crack size that this plate can support is $2a$, or (2)(5.18 mm) = 10.36 mm.

7.2 FATIGUE OF METALS

In many types of service applications, metal parts subjected to repetitive or cyclic stresses will fail due to **fatigue** loading at a much lower stress than that which the part can withstand under the application of a single static stress. These failures that occur under repeated or cyclic stressing are called **fatigue failures.** Examples of

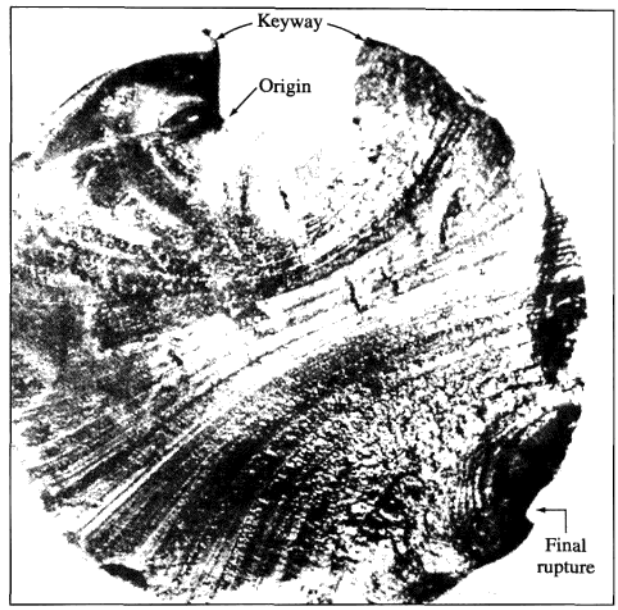

Figure 7.14
Light fractograph of the fatigue-fracture surface of a keyed shaft of 1040 steel (hardness ~ Rockwell C 30). The fatigue crack originated at the left bottom corner of the keyway and extended almost through the entire cross section before final rupture occurred. (Magnified $1\frac{7}{8}\times$.)
(After "Metals Handbook," vol. 9, 8th ed., American Society for Metals, 1974, p. 389. Reprinted with permission of ASM International. All rights reserved. www.asminternational.org.)

machine parts in which fatigue failures are common are moving parts such as shafts, connecting rods, and gears. Some estimates of failures in machines attribute about 80 percent to the direct action of fatigue failures.

A typical fatigue failure of a keyed steel shaft is shown in Fig. 7.14. A fatigue failure usually originates at a point of stress concentration such as a sharp corner or notch (Fig. 7.14) or at a metallurgical inclusion or flaw. Once nucleated, the crack propagates across the part under the cyclic or repeated stresses. During this stage of the fatigue process, clamshell or "beach" marks are created, as shown in Fig. 7.14. Finally, the remaining section becomes so small that it can no longer support the load, and complete fracture occurs. Thus, there are usually two distinct types of surface areas that can be recognized: (1) a smooth surface region due to the rubbing action between the open surface region as the crack propagates across the section and (2) a rough surface area formed by the fracture when the load becomes too high for the remaining cross section. In Fig. 7.14 the fatigue crack had propagated almost through the entire cross section before final rupture occurred.

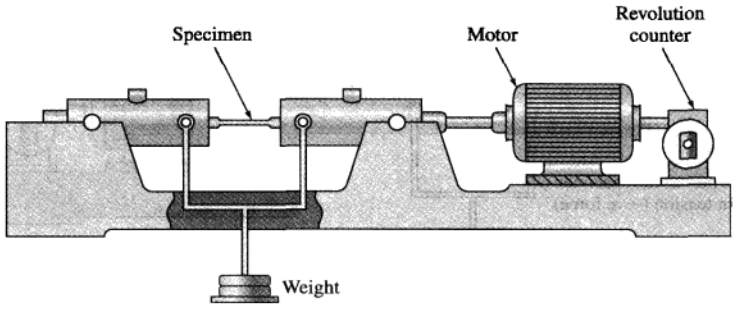

Figure 7.15
Schematic diagram of an R.R. Moore reversed-bending fatigue machine.
(After H.W. Hayden, W.G. Moffatt, and J. Wulff, "The Structure and Properties of Materials," vol. III, Wiley, 1965, p. 15.)

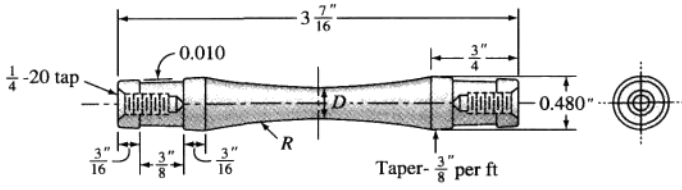

D = 0.200 to 0.400 in. selected on basis of ultimate strength of material
R = 3.5 to 10 in.

Figure 7.16
Sketch illustrating rotating-beam fatigue specimen (R.R. Moore type).
(From "Manual on Fatigue Testing," American Society for Testing and Materials, 1949.)

Many types of tests are used to determine the **fatigue life** of a material. The most commonly used small-scale fatigue test is the rotating-beam test in which a specimen is subjected to alternating compression and tension stresses of equal magnitude while being rotated (Fig. 7.15). A sketch of the specimen for the R.R. Moore reversed-bending fatigue test is shown in Fig. 7.16. The surface of this specimen is carefully polished and tapered toward the center. During the testing of a fatigue sample by this apparatus, the center of the specimen is actually undergoing tension on the lower surface and compression on the upper surface by the weight attached in the center of the apparatus (Fig. 7.15), as exaggerated in Fig. 7.17. Data from this test are plotted in the form of *SN* curves in which the stress S to cause failure is plotted against the number of cycles N at which failure occurs. Figure 7.18 shows typical *SN* curves for a high-carbon steel and a high-strength aluminum alloy. For the aluminum alloy, the stress to cause failure decreases as the number of cycles is increased. For the carbon steel, there is first a decrease in fatigue strength as the number of cycles is increased

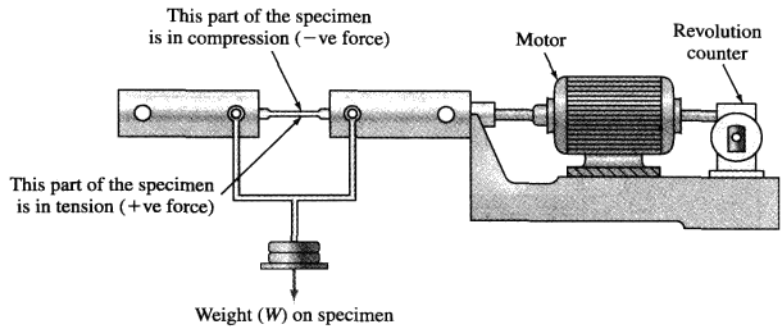

Figure 7.17
Exaggerated bending of sample to show action that produces positive tension and negative compressive forces on specimen.
(From H.W. Hayden, W.G. Moffatt and J. Wulff, "The Structure and Properties of Materials," vol. III, Wiley, 1965, p. 13.)

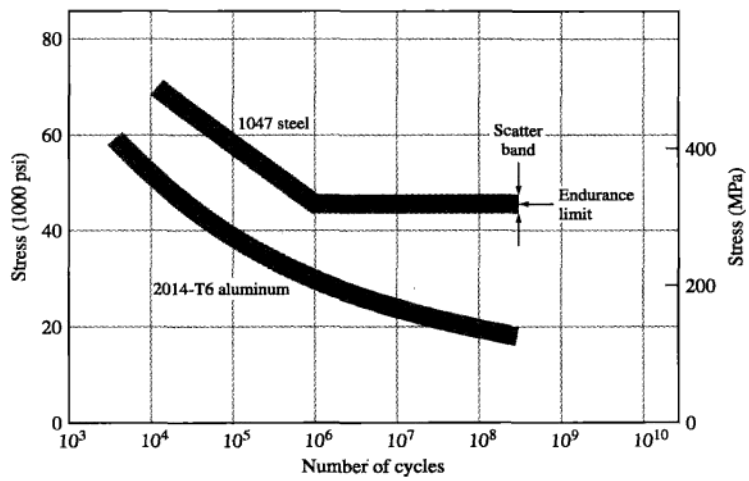

Figure 7.18
Stress versus number of cycles (*SN*) curves for fatigue failure for aluminum alloy 2014-T6 and medium-carbon steel 1047.
(After H.W. Hayden, W.G. Moffatt, and J. Wulff, "The Structure and Properties of Materials," vol. III, Wiley, 1965, p. 15.)

and then there is leveling off in the curve, with no decrease in fatigue strength as the number of cycles is increased. This horizontal part of the *SN* plot is called the *fatigue* or *endurance limit* and lies between 10^6 and 10^{10} cycles. Many ferrous alloys exhibit an endurance limit that is about one-half their tensile strength. Nonferrous alloys such as aluminum alloys do not have an endurance limit and may have fatigue strengths as low as one-third their tensile strength.

7.2.1 Cyclic Stresses

The applied fatigue stress may vary greatly in real cases and in fatigue tests. Many different kinds of fatigue test methods used in industry and research involve axial, torsional, and flexural stresses. Figure 7.19 shows graphs of fatigue stress versus number of fatigue cycles for three fatigue cycle tests. Figure 7.19*a* shows a graph of stress versus fatigue cycles for a *completely reversed stress cycle* of a sinusoidal form. This graph is typical of that produced by a rotating shaft operating at constant speed without overloads. The R.R. Moore reversed-bending fatigue machine shown in Fig. 7.15 produces similar stress versus number of fatigue cycles plots. In this fatigue cycle, the maximum and minimum stresses are equal. By definition, the tensile stresses are considered positive and the compressive stresses negative, and the maximum stress has the highest numeric value and the minimum stress the lowest.

Figure 7.19*b* shows a *repeated stress cycle* in which the maximum stress σ_{max} and the minimum stress σ_{min} are equal. In this case both maximum and minimum stresses are tensile, but a repeated stress cycle can also have maximum and minimum stresses of opposite sign, or both in compression. Finally, a cyclic stress may

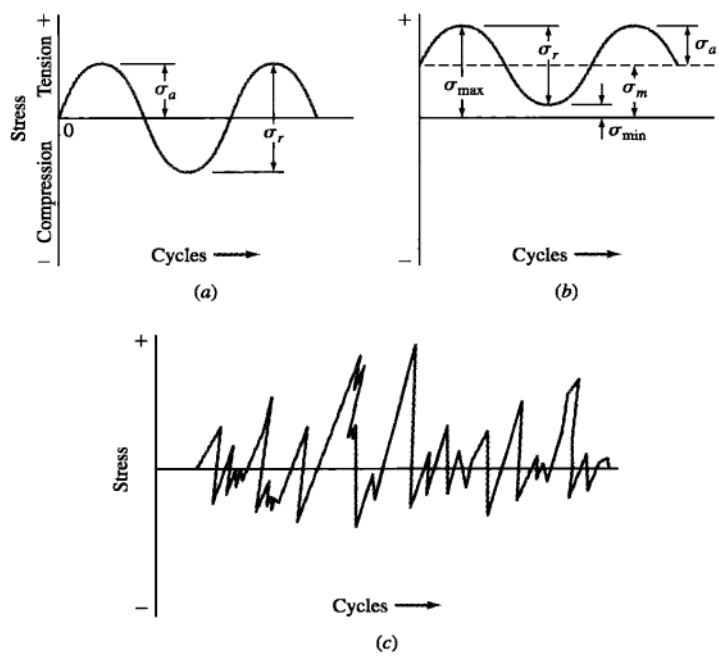

Figure 7.19
Typical fatigue stress versus cycles plots. (*a*) Completely reversed stress cycle. (*b*) Repeated stress cycle with equal σ_{max} and σ_{min}. (*c*) Random stress cycle.
(*From J.A. Rinebolt and W.H. Harris, Trans. ASM,* **43**:*1175 (1951).*)

vary randomly in amplitude and frequency, as shown in Fig. 7.19*c*. In this case there can be a spectrum of different fatigue graphs of stress versus cycles.

Fluctuating stress cycles are characterized by a number of parameters. Some of the most important ones are:

1. *Mean stress* σ_m is the algebraic mean of the maximum and minimum stresses in the fatigue cycle.

$$\sigma_m = \frac{\sigma_{\max} + \sigma_{\min}}{2} \tag{7.3}$$

2. *Range of stress* σ_r is the difference between $\sigma_{\max}$ and $\sigma_{\min}$.

$$\sigma_r = \sigma_{\max} - \sigma_{\min} \tag{7.4}$$

3. *Stress amplitude* σ_a is one-half the stress cycle.

$$\sigma_a = \frac{\sigma_r}{2} = \frac{\sigma_{\max} - \sigma_{\min}}{2} \tag{7.5}$$

4. *Stress ratio* R is the ratio of minimum and maximum stresses.

$$R = \frac{\sigma_{\min}}{\sigma_{\max}} \tag{7.6}$$

7.2.2 Basic Structural Changes that Occur in a Ductile Metal in the Fatigue Process

When a specimen of a ductile homogeneous metal is subjected to cyclic stresses, the following basic structural changes occur during the fatigue process:

1. *Crack initiation.* The early development of fatigue damage occurs.

2. *Slipband crack growth.* Crack initiation occurs because plastic deformation is not a completely reversible process. Plastic deformation in one direction and then in the reverse direction causes surface ridges and grooves called *slipband extrusions* and *slipband intrusions* to be created on the surface of the metal specimen as well as damage within the metal along *persistent slipbands* (Figs. 7.20 and 7.21). The surface irregularities and damage along the persistent slipbands cause cracks to form at or near the surface that propagate into the specimen along the planes subjected to high shear stresses. This is called *stage I of fatigue crack growth,* and the rate of the crack growth is in general very low (for example, 10^{-10} m/cycle).

3. *Crack growth on planes of high tensile stress.* During stage I, the crack may grow in a polycrystalline metal only a few grain diameters before it changes its direction to be perpendicular to the direction of the maximum tensile stress on the metal specimen. In this *stage II of crack growth,* a well-defined crack propagates at a relatively rapid rate (i.e., micrometers per cycle), and fatigue striations are created as the crack advances across the cross section of the metal specimen (Fig. 7.14). These striations are useful in fatigue failure analysis for determining the origin and direction of propagation of fatigue cracks.

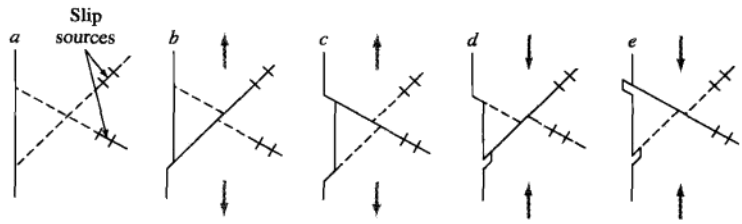

Figure 7.20
Mechanism for the formation of slipband extrusions and intrusions.
[*After A.H. Cottrell and D. Hull, Proc. R. Soc. London,* **242A**:*211–213(1957).*]

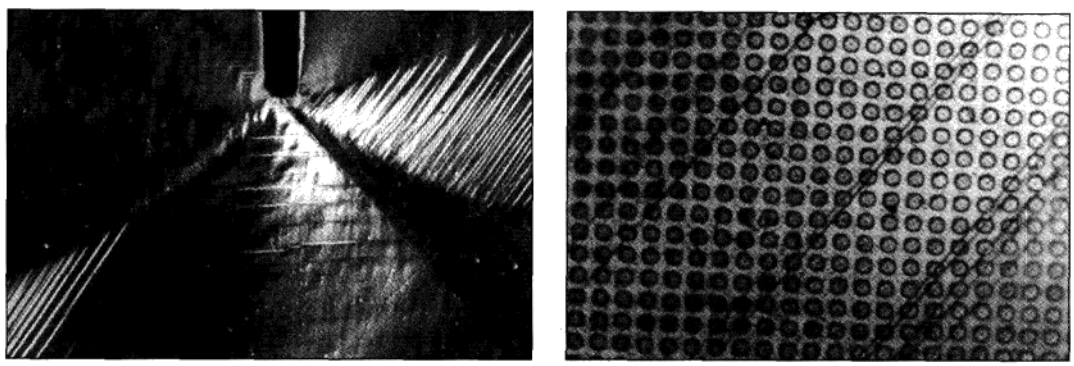

Figure 7.21
(*a*) Persistent slipbands in copper single crystal. (*b*) The polymer dots deposited on the surface are in many cases cut in half by the slipbands (dark lines on the surface) resulting in relative displacement of the two halves.
(*Courtesy of Wendy C. Crone, University of Wisconsin.*)

4. *Ultimate ductile failure.* Finally, when the crack covers a sufficient area so that the remaining metal at the cross section cannot support the applied load, the sample ruptures by ductile failure.

7.2.3 Some Major Factors that Affect the Fatigue Strength of a Metal

The fatigue strength of a metal or alloy is affected by factors other than the chemical composition of the metal itself. Some of the most important of these are:

1. *Stress concentration.* Fatigue strength is greatly reduced by the presence of stress raisers such as notches, holes, keyways, or sharp changes in cross sections. For example, the fatigue failure shown in Fig. 7.14 started at the keyway in the steel shaft. Fatigue failures can be minimized by careful design to avoid stress raisers whenever possible.

2. *Surface roughness.* In general, the smoother the surface finish on the metal sample, the higher the fatigue strength. Rough surfaces create stress raisers that facilitate fatigue crack formation.

3. *Surface condition.* Since most fatigue failures originate at the metal surface, any major change in the surface condition will affect the fatigue strength of the metal. For example, surface-hardening treatments for steels, such as carburizing and nitriding, which harden the surface, increase fatigue life. Decarburizing, on the other hand, which softens a heat-treated steel surface, lowers fatigue life. The introduction of a favorable compressive residual stress pattern on the metal surface also increases fatigue life.

4. *Environment.* If a corrosive environment is present during the cyclic stress of a metal, the chemical attack greatly accelerates the rate at which fatigue cracks propagate. The combination of corrosion attack and cyclic stresses on a metal is known as *corrosion fatigue.*

7.3 FATIGUE CRACK PROPAGATION RATE

Most fatigue data for metals and alloys for high-cycle fatigue (i.e., fatigue lives of greater than 10^4 to 10^5 cycles) have been concerned with the nominal stress required to cause failure in a given number of cycles, that is, *SN* curves such as those shown in Fig. 7.18. However, for these tests smooth or notched specimens are usually used, and thus it is difficult to distinguish between fatigue crack initiation life and fatigue crack propagation life. Thus, test methods have been developed to measure fatigue life associated with preexisting flaws in a material.

Preexisting flaws or cracks within a material component reduce or may eliminate the crack initiation part of the fatigue life of a component. Thus, the fatigue life of a component with preexisting flaws may be considerably shorter than the life of one without flaws. In this section, we will utilize fracture mechanics methodology to develop a relationship to predict fatigue life in a material with preexisting flaws and under stress-state conditions due to cyclic fatigue action.

A high-cycle fatigue experimental setup for measuring the crack growth rate in a compact-type metal test specimen containing a preexisting crack of known length is shown in Fig. 7.22. In this setup, the cyclic fatigue action is generated in the up-and-down vertical direction, and the crack length is measured by the change in electrical potential produced by the crack being further opened and extended by the fatigue action.

7.3.1 Correlation of Fatigue Crack Propagation with Stress and Crack Length

Let us now consider qualitatively how fatigue crack length varies with an increasing number of applied cyclic stresses using data obtained from an experimental setup such as that shown in Fig. 7.22. Let us use several test samples of a material each of which has a mechanical crack in its side as indicated in Fig. 7.23*a*. Now let us apply a constant-amplitude cyclic stress to the samples and measure the increase in crack length as a function of the number of applied stress cycles. Figure 7.23*b* shows qualitatively how a plot of crack length versus number of stress cycles for two levels of stress might appear for a particular material such as mild steel.

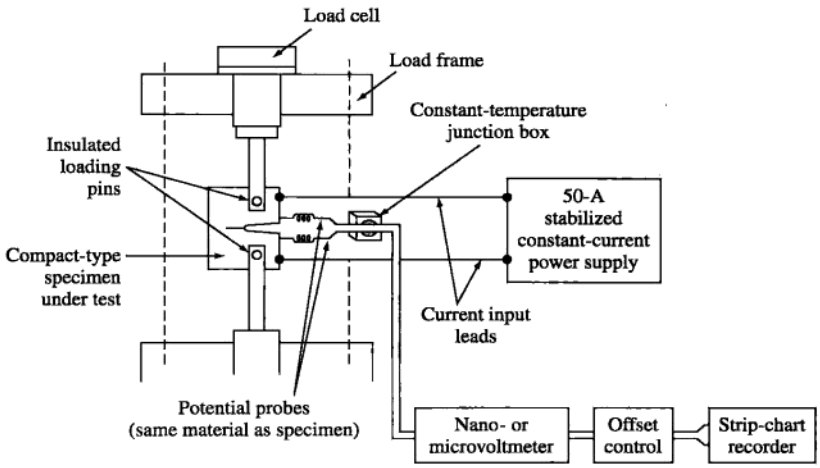

Figure 7.22
Schematic of the direct-current electrical potential crack monitoring system for the high-cycle fatigue testing of a compact test sample.
(After "Metals Handbook," vol. 8, 9th ed., American Society for Metals, 1985, p. 388.)

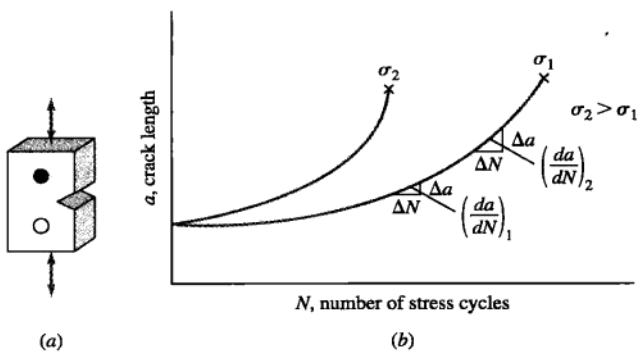

Figure 7.23
(*a*) Thin-plate test sample with edge crack under cyclic stress. (*b*) Plot of crack length versus number of stress cycles for stresses σ_1 and $\sigma_2 (\sigma_2 > \sigma_1)$.
(From H.W. Hayden, W.G. Moffatt and J. Wulff, "The Structure and Properties of Materials," vol. III, Wiley, 1965, p. 15.)

Examination of the curves of Fig. 7.23*b* indicates the following:

1. When the crack length is small, the **fatigue crack growth rate** ***da/dN*** is also relatively small.
2. The crack growth rate da/dN increases with increasing crack length.
3. An increase in cyclic stress σ increases the crack growth rate.

Thus, the crack growth rate for materials under cyclic stress that behave as indicated in Fig. 7.23*b* shows the following relationship:

$$\frac{da}{dN} \propto f(\sigma, a) \tag{7.7}$$

which reads, "the fatigue crack growth rate da/dN varies as a function of the applied cyclic stress σ and the crack length a." After much research, it has been shown that for many materials the fatigue crack growth rate is a function of the stress-intensity factor K (mode I) of fracture mechanics, which itself is a combination of stress and crack length. For many engineering alloys, the fatigue crack growth rate expressed as the differential da/dN can be related to the stress-intensity range ΔK for a constant-amplitude fatigue stress by the equation

$$\frac{da}{dN} = A\Delta K^m \tag{7.8}$$

where da/dN = fatigue crack growth rate, mm/cycle or in./cycle
ΔK = stress-intensity factor range ($\Delta K = K_{max} - K_{min}$), MPa$\sqrt{\text{m}}$ or ksi$\sqrt{\text{in.}}$
A, m = constants that are a function of the material, environment, frequency, temperature, and stress ratio

Note in Eq. 7.8 that we use the stress-intensity factor K_I (mode I) and not the fracture toughness value K_{IC}. Thus, at the maximum cyclic stress, the stress-intensity factor $K_{max} = \sigma_{max}\sqrt{\pi a}$, and at the minimum cyclic stress, $\Delta K_{min} = \sigma_{min}\sqrt{\pi a}$. For the range of stress-intensity factor, $\Delta K(\text{range}) = K_{max} - K_{min} = \Delta K = \sigma_{max}\sqrt{\pi a} - \sigma_{min}\sqrt{\pi a} = \sigma_{range}\sqrt{\pi a}$. Since the stress-intensity factor is not defined for compressive stresses, if σ_{min} is in compression, K_{min} is assigned zero value. If there is a Y geometric correction factor for the $\Delta K = \sigma_r\sqrt{\pi a}$ equation, then $\Delta K = Y\sigma_r\sqrt{\pi a}$.

7.3.2 Fatigue Crack Growth Rate versus Stress-Intensity Factor Range Plots

Usually fatigue crack length versus stress-intensity factor range data are plotted as log da/dN versus log stress-intensity factor range ΔK. These data are plotted as a log-log plot since in most cases a straight line or close to a straight-line plot is obtained. The basic reason for the straight-line plot is that the da/dN versus ΔK data closely obey the $da/dN = A\Delta K^m$ relationship, and so if the log is taken of both sides of this equation, we obtain

$$\log \frac{da}{dN} = \log(A\Delta K^m) \tag{7.9}$$

or

$$\log \frac{da}{dN} = m \log \Delta K + \log A \tag{7.10}$$

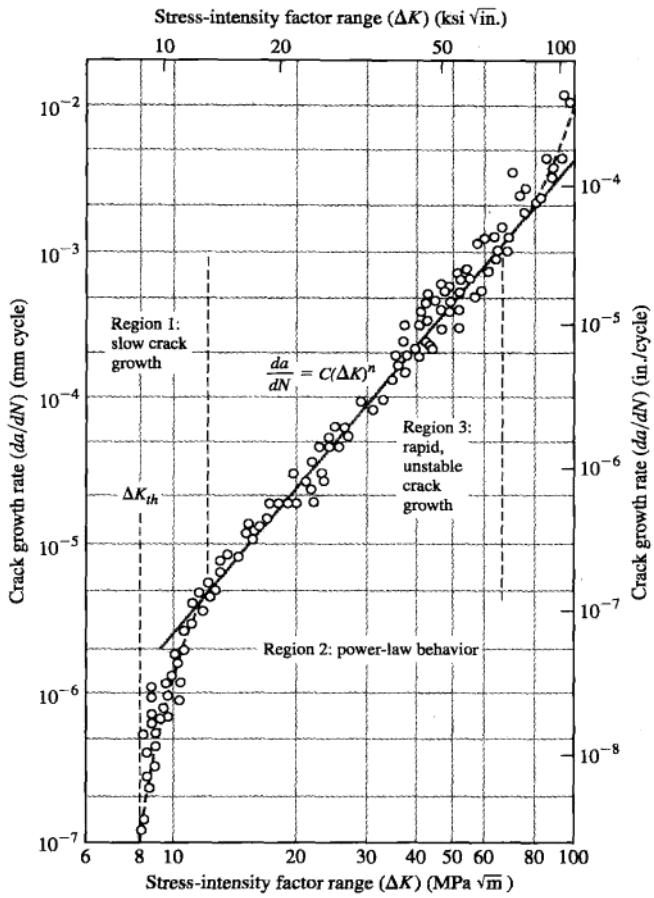

Figure 7.24
Fatigue crack growth behavior of ASTM A533 B1 steel (yield strength 470 MPa [70 ksi]). Test conditions: $R = 0.10$: ambient room air, 24°C.
(From "Manual on Fatigue Testing," American Society for Testing and Materials, 1949. Copyright ASTM International. Reprinted with permission.)

which is an equation of a straight line of the form $y = mx + b$. Thus, a plot of log (da/dN) versus log ΔK produces a straight line with a slope of m.

Figure 7.24 shows a plot of log crack growth rate versus log stress-intensity factor range for a fatigue test of an ASTM A533 B1 steel. This plot is divided into three regions: region 1 in which the fatigue crack growth rate is very slow, region 2 in which the plot is a straight line represented by the power law $da/dn = A\Delta K^m$, and region 3 in which rapid unstable crack growth takes place, approaching failure

of the sample. The limiting value of ΔK below which there is no measurable crack growth is called the *stress-intensity factor range threshold* ΔK_{th}. No crack growth should occur below this stress-intensity range level. The value of m for fatigue crack growth da/dN in region 2 usually varies from about 2.5 to 6.

7.3.3 Fatigue Life Calculations

Sometimes in designing a new engineering component using a particular material, it is desirable to obtain information about the fatigue life of the part. This can be done in many cases by combining fracture toughness data with fatigue crack growth data to produce an equation that can be used to predict fatigue life.

One type of equation for calculating fatigue life can be developed by integrating Eq. 7.8, $dA/dN = A\Delta K^m$, between an initial crack (flaw) size a_o and the critical crack (flaw) size a_f, which is produced at fatigue failure after the number of cycles to failure N_f.

We start with Eq. 7.8:

$$\frac{da}{dN} = A\Delta K^m \tag{7.11}$$

Since

$$\Delta K = Y\sigma\sqrt{\pi a} = Y\sigma\pi^{1/2}a^{1/2} \tag{7.12}$$

It follows that

$$\Delta K^m = Y^m\sigma^m\pi^{m/2}a^{m/2} \tag{7.13}$$

Substituting $Y^m\sigma^m\pi^{m/2}a^{m/2}$ of Eq. 7.13 for ΔK^m of Eq. 7.11 gives

$$\frac{da}{dN} = A(Y\sigma\sqrt{\pi a})^m = A(Y^m\sigma^m\pi^{m/2}a^{m/2}) \tag{7.14}$$

After rearranging Eq. 7.14, we integrate the crack size from the initial crack size a_o to the final crack size at failure a_f and the number of fatigue cycles from zero to the number at fatigue failure N_f. Thus,

$$\int_{a_o}^{a_f} da = AY^m\sigma^m\pi^{m/2} \cdot a^{m/2}\int_0^{N_f} dN \tag{7.15}$$

and

$$\int_0^{N_f} dN = \int_{a_o}^{a_f} \frac{da}{A\sigma^m\pi^{m/2}Y^m a^{m/2}} = \frac{1}{A\sigma^m\pi^{m/2}Y^m}\int_{a_o}^{a_f} \frac{da}{a^{m/2}} \tag{7.16}$$

Using the relationship

$$\int a^n\, da = \frac{a^{n+1}}{n+1} + c \tag{7.17}$$

we integrate Eq. 7.16,

$$\int_0^{N_f} dN = N\Big|_0^{N_f} = N_f \tag{7.18a}$$

and letting $n = -m/2$,

$$\frac{1}{A\sigma^m \pi^{m/2} Y^m} \int_{a_v}^{a_f} \frac{da}{a^{m/2}} = \frac{1}{A\sigma^m \pi^{m/2} Y^m} \left(\frac{a^{-(m/2)+1}}{-m/2+1} \right) \Bigg|_{a_o}^{a_f} \qquad (7.18b)$$

Thus,

$$N_f = \frac{a_f^{-(m/2)+1} - a_0^{-(m/2)+1}}{A\sigma^m \pi^{m/2} Y^m [-(m/2)+1]} \qquad m \neq 2 \qquad (7.19)$$

Equation 7.19 assumes that $m \neq 2$ and that Y is independent of the crack length, which is not usually the case. Thus, Eq. 7.19 may or may not be the true value for the fatigue life of the component. For the more general case, $Y = f(a)$, the calculation of N_f must take into account the change in Y, and so ΔK and ΔN must be calculated for small successive amounts of length.

EXAMPLE PROBLEM 7.2

An alloy steel plate is subjected to constant-amplitude uniaxial fatigue cyclic tensile and compressive stresses of magnitudes of 120 and 30 MPa, respectively. The static properties of the plate are a yield strength of 1400 MPa and a fracture toughness K_{IC} of 45 MPa$\sqrt{\text{m}}$. If the plate contains a uniform through thickness *edge* crack of 1.00 mm, how many fatigue cycles are estimated to cause fracture? Use the equation da/dN (m/cycle) = $2.0 \times 10^{-12} \Delta K^3$ (MPa$\sqrt{\text{m}}$)^3. Assume $Y = 1$ in the fracture toughness equation.

■ Solution

We will assume for the plate that

$$\frac{da}{dN}\,(\text{m/cycle}) = 2.0 \times 10^{-12}\,\Delta K^3\,(\text{MPa}\sqrt{\text{m}})^3$$

Thus, $A = 2.0 \times 10^{-12}$, $m = 3$, and $\sigma_r = (120 - 0)$ MPa (since compressive stresses are ignored), and $Y = 1$.

The initial crack size a_o is equal to 1.00 mm. The final crack size a_f is determined from the fracture toughness equation

$$a_f = \frac{1}{\pi}\left(\frac{K_{IC}}{\sigma_r}\right)^2 = \frac{1}{\pi}\left(\frac{45\ \text{MPa}\sqrt{\text{m}}}{120\ \text{MPa}}\right)^2 = 0.0449\ \text{m}$$

The fatigue life in cycles N_f is determined from Eq. 7.19:

$$N_f = \frac{a_f^{-(m/2)+1} - a_o^{-(m/2)+1}}{[-(m/2)+1]A\sigma^m \pi^{m/2} Y^m} \qquad m \neq 2$$

$$= \frac{(0.0449\ \text{m})^{-(3/2)+1} - (0.001\ \text{m})^{-(3/2)+1}}{(-\frac{3}{2}+1)(2.0 \times 10^{-12})(120\ \text{MPa})^3(\pi)^{3/2}(1.00)^3}$$

$$= \frac{-2}{(2 \times 10^{-12})(\pi^{3/2})(120)^3}\left(\frac{1}{\sqrt{0.0449}} - \frac{1}{\sqrt{0.001}}\right)$$

$$= \frac{-2 \times 26.88}{(2 \times 10^{-12})(5.56)(1.20)^3(10^6)} = 2.79 \times 10^6\ \text{cycles} \blacktriangleleft$$

7.4 CREEP AND STRESS RUPTURE OF METALS

7.4.1 Creep of Metals

When a metal or an alloy is under a constant load or stress, it may undergo progressive plastic deformation over a period of time. This *time-dependent strain* is called **creep.** The creep of metals and alloys is very important for some types of engineering designs, particularly those operating at elevated temperatures. For example, an engineer selecting an alloy for the turbine blades of a gas turbine engine must choose an alloy with a very low **creep rate** so that the blades can remain in service for a long period of time before having to be replaced due to their reaching the maximum allowable strain. For many engineering designs operating at elevated temperatures, the creep of materials is the limiting factor with respect to how high the operating temperature can be.

Let us consider the creep of a pure polycrystalline metal at a temperature above one-half its absolute melting point, $\frac{1}{2}T_M$ (high-temperature creep). Let us also consider a creep experiment in which an annealed tensile specimen is subjected to a constant load of sufficient magnitude to cause extensive creep deformation. When the change of length of the specimen over a period of time is plotted against time increments, a *creep curve,* such as the one shown in Fig. 7.25, is obtained.

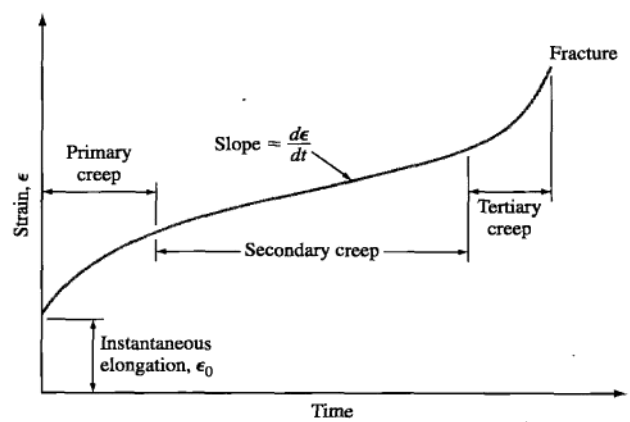

Figure 7.25
A typical creep curve for a metal. The curve represents the time versus strain behavior of a metal or alloy under a constant load at constant temperature. The second stage of creep (linear creep) is of most interest to the design engineer because extensive creep occurs under these conditions.

In the idealized creep curve of Fig. 7.25, there is first an instantaneous, rapid elongation of the specimen, ϵ_0. Following this, the specimen exhibits primary creep in which the strain rate decreases with time. The slope of the creep curve ($d\epsilon/dt$, or $\dot{\epsilon}$) is designated the *creep rate.* Thus, during primary creep the creep rate progressively decreases with time. After primary creep, a second stage of creep occurs in which the creep rate is essentially constant and is therefore also referred to as *steady-state creep.* Finally, a third or tertiary stage of creep occurs in which the creep rate rapidly increases with time up to the strain at fracture. The shape of the creep curve depends strongly on the applied load (stress) and temperature. Higher stresses and higher temperatures increase the creep rate.

During primary creep, the metal strain-hardens to support the applied load and the creep rate decreases with time as further strain hardening becomes more difficult. At higher temperatures (i.e., above about $0.5T_M$ for the metal) during secondary creep, recovery processes involving highly mobile dislocations counteract the strain hardening so that the metal continues to elongate (creep) at a steady-state rate (Fig. 7.25). The slope of the creep curve ($d\epsilon/dt = \dot{\epsilon}$) in the secondary stage of creep is referred to as the *minimum creep rate.* During secondary creep, the creep resistance of the metal or alloy is the highest. Finally, for a constant-loaded specimen, the creep rate accelerates in the tertiary stage of creep due to necking of the specimen and also to the formation of voids, particularly along grain boundaries. Figure 7.26 shows intergranular cracking in a type 304L stainless steel that has undergone creep failure.

At low temperatures (i.e., below $0.4T_M$) and low stresses, metals show primary creep but negligible secondary creep since the temperature is too low for diffusional recovery creep. However, if the stress on the metal is above the ultimate tensile strength, the metal will elongate as in an ordinary engineering tensile test. In general, as both the stress on the metal undergoing creep and its temperature are increased, the creep rate is also increased (Fig. 7.27).

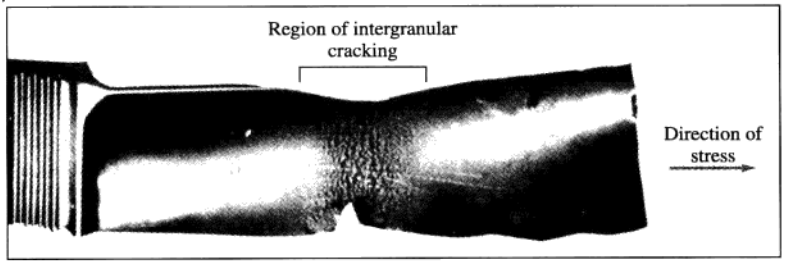

Figure 7.26
A jet engine turbine blade that has undergone creep deformation, causing local deformation and a multiplicity of intergranular cracks.
(After J. Schijive in "Metals Handbook," vol. 10, 8th ed., American Society for Metals, 1975, p.23. ASM International.)

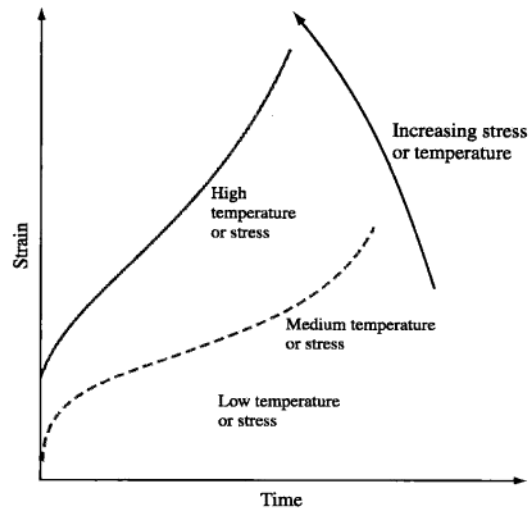

Figure 7.27
Effect of increasing stress on the shape of the creep curve of a metal (schematic). Note that as the stress increases, the strain rate increases.

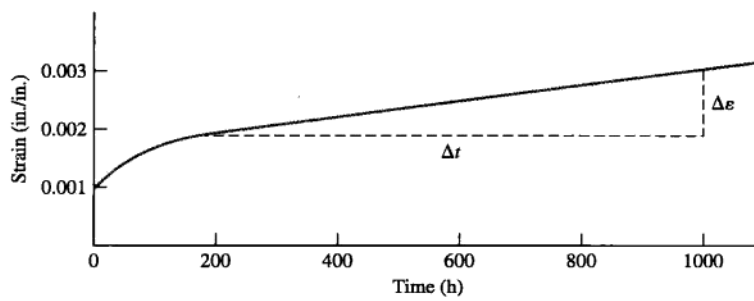

Figure 7.28
Creep curve for a copper alloy tested at 225ºC and 230 MPa (33.4 ksi). The slope of the linear part of the curve is the steady-state creep rate.
(From A.H. Cottrell and D. Hull, Proc. R. Soc. London, **242A:** *211–213 (1957).*

7.4.2 The Creep Test

The effects of temperatures and stress on the creep rate are determined by the creep test. Multiple creep tests are run using different stress levels at constant temperature or different temperatures at a constant stress, and the creep curves are plotted as shown in Fig. 7.28. The minimum creep rate or slope of the second stage

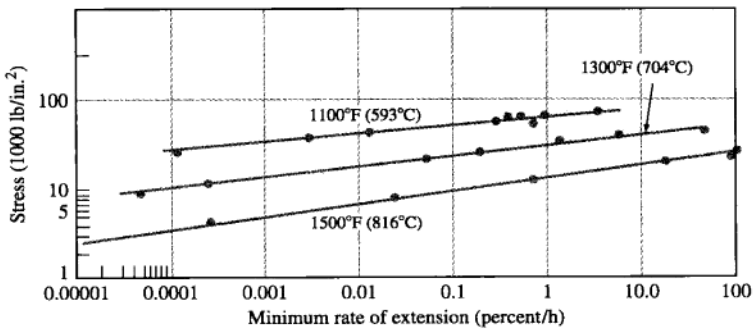

Figure 7.29
Effect of stress on the creep rate of type 316 stainless steel (18% Cr–12% Ni–2.5% Mo) at various temperatures (1100ºF, 1300ºF, 1500°F [593ºC, 704ºC, 816°C]).
(After H.E. McGannon [ed.], "The Making, Shaping, and Treating of Steel," 9th ed., United States Steel, 1971, p. 1256.)

of the creep curve is measured for each curve, as indicated in Fig. 7.28. The stress to produce a minimum creep rate of 10^{-5} percent/h at a given temperature is a common standard for creep strength. In Fig. 7.29, the stress to produce a minimum creep rate of 10^{-5} percent/h for type 316 stainless steel can be determined by extrapolation.

EXAMPLE PROBLEM 7.3

Determine the steady-state creep rate for the copper alloy whose creep curve is shown in Fig. 7.28.

■ **Solution**

The steady-state creep rate for this alloy for the creep curve shown in Fig. 7.28 is obtained by taking the slope of the linear part of the curve as indicated in the figure. Thus,

$$\text{Creep rate} = \frac{\Delta\epsilon}{\Delta t} = \frac{0.0029 - 0.0019}{1000\text{ h} - 200\text{ h}} = \frac{0.001\text{ in./in.}}{800\text{ h}} = 1.2 \times 10^{-6}\text{ in./in./h} \blacktriangleleft$$

7.4.3 Creep-Rupture Test

The **creep-rupture** or **stress-rupture test** is essentially the same as the creep test except that the loads are higher and the test is carried out to failure of the specimen. Creep-rupture data are plotted as log stress versus log rupture time, as shown in Fig. 7.30. In general, the time for stress rupture to occur is decreased as the applied stress and temperature are increased. Slope changes as observed in Fig. 7.30 are caused by factors such as recrystallization, oxidation, corrosion, or phase changes.

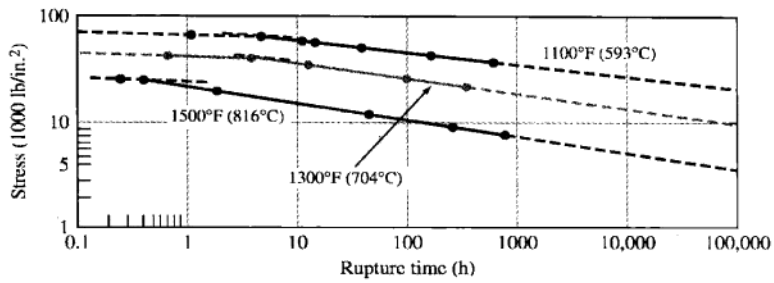

Figure 7.30
Effect of stress on the time to rupture of type 316 stainless steel (18% Cr–12% Ni–2.5% Mo) at various temperatures (1100°F, 1300°F, 1500°F [593°C, 704°C, 816°C]).
(From "Metals Handbook," vol. 8, 9th ed., American Society for Metals, 1985, p. 388. Used by permission of ASM International.)

7.5 SUMMARY

Fracture of metallic components during service is of great importance and consequence. The proper selection of a material for a component is a critical step in avoiding unwanted failures. Fracture of metals may generally be classified as either ductile or brittle. This is easily observed by performing simple static tension tests. Ductile fracture is accompanied by severe plastic deformation prior to failure. Conversely, brittle fracture shows little or no deformation prior to fracture and is therefore more problematic. In some cases, under high loading rates or lowered temperatures, originally ductile materials behave in a brittle fashion called ductile to brittle transition. Therefore, selection of materials for components that operate in cold temperatures should be done with care.

Since defects such as microcracks weaken a material, engineers use the concept of fracture toughness based on the assumption of preexisting flaws (fracture mechanics) to design components that are safer. The concept of stress intensity factor, K, at a crack tip is used to represent the combined effect of stress at the crack tip and the crack length.

The failure of metallic components under cyclic or repeated loading called fatigue failure is of tremendous importance to engineers. Its importance is due to the low level of stresses at which such failures occur, the hidden nature of the damage (inside the material), and its sudden and abrupt failure. Another form of failure that occurs at high temperatures and constant loading is called creep, which is defined as progressive plastic deformation over a period of time. Engineers are very conscious of such failures and use high factors of safety to guard against them.

Engineers and scientists always search for new materials that offer higher strength, ductility, fatigue resistance, and are in general resistant to failure. Nanocrystalline materials promise to be the materials of choice for the future offering a combination of properties that will greatly enhance a material's resistance to fracture. However, more research is needed by materials scientists to achieve this goal.

7.6 DEFINITIONS

Sec. 7.1

Ductile fracture: a mode of fracture characterized by slow crack propagation. Ductile fracture surfaces of metals are usually dull with a fibrous appearance.

Brittle fracture: a mode of fracture characterized by rapid crack propagation. Brittle fracture surfaces of metals are usually shiny and have a granular appearance.

Transgranular fracture: a type of brittle fracture in which the crack propagates across the grain.

Intergranular fracture: a type of brittle fracture in which the crack propagates along the grain boundary.

Ductile to brittle transition (DBT): observed reduced ductility and fracture resistance of a material when temperature is low.

Sec. 7.2

Fatigue: the phenomenon leading to fracture under repeated stresses having a maximum value less than the ultimate strength of the material.

Fatigue failure: failure that occurs when a specimen undergoing fatigue fractures into two parts or otherwise has been significantly reduced in stiffness.

Fatigue life: the number of cycles of stress or strain of a specific character that a sample sustains before failure.

Sec. 7.3

Fatigue crack growth rate *da/dN*: the rate of crack growth extension caused by constant-amplitude fatigue loading.

Sec. 7.4

Creep: time-dependent deformation of a material when subjected to a constant load or stress.

Creep rate: the slope of the creep-time curve at a given time.

Creep (stress)-rupture strength: the stress that will cause fracture in a creep (stress-rupture) test at a given time and in a specific environment at a particular temperature.

7.7 PROBLEMS

Answers to problems marked with an asterisk are given at the end of the book.

Knowledge and Comprehension Problems

7.1 What are the characteristics of the surface of a ductile fracture of a metal?

7.2 Describe the three stages in the ductile fracture of a metal.

7.3 What are the characteristics of the surface of a brittle fracture of a metal?

7.4 Describe the three stages in the brittle fracture of a metal.

7.5 What do chevron patterns indicate?

7.6 Why are ductile fractures less frequent in practice than brittle fractures?

7.7 Differentiate between transgranular and intergranular fractures.

7.8 Describe the simple impact test that uses a Charpy V-notch sample.

7.9 How does the carbon content of a plain-carbon steel affect the ductile-brittle transition temperature range?

7.10 Describe a metal fatigue failure.

7.11 What two distinct types of surface areas are usually recognized on a fatigue failure

surface?

7.12 Where do fatigue failures usually originate on a metal section?

7.13 What is a fatigue test *SN* curve, and how are the data for the *SN* curve obtained?

7.14 How does the *SN* curve of a carbon steel differ from that of a high-strength aluminum alloy?

7.15 Describe the four basic structural changes that take place when a homogeneous ductile metal is caused to fail by fatigue under cyclic stresses.

7.16 Describe the four major factors that affect the fatigue strength of a metal.

7.17 What is metal creep?

7.18 For which environmental conditions is the creep of metals especially important industrially?

7.19 Draw a typical creep curve for a metal under constant load and at a relatively high temperature, and indicate on it all three stages of creep.

Application and Analysis Problems

***7.20** Determine the critical crack length for a through crack contained within a thick plate of 7075-T751 aluminum alloy that is under uniaxial tension. For this alloy, $K_{IC} = 22.0\ \text{ksi}\sqrt{\text{in.}}$ and $\sigma_f = 82.0$ ksi. Assume $Y = \sqrt{\pi}$.

7.21 Determine the critical crack length for a through crack in a thick plate of 7150-T651 aluminum alloy that is in uniaxial tension. For this alloy $K_{IC} = 25.5\ \text{MPa}\sqrt{\text{m}}$ and $\sigma_f = 400$ MPa. Assume $Y = \sqrt{\pi}$.

7.22 The critical stress intensity (K_{IC}) for a material for a component of a design is $23.0\ \text{ksi}\sqrt{\text{in.}}$ What is the applied stress that will cause fracture if the component contains an internal crack 0.13 in. long? Assume $Y = 1$.

7.23 What is the largest size (mm) internal through crack that a thick plate of aluminum alloy 7075-T651 can support at an applied stress of (*a*) three-quarters of the yield strength and (*b*) one-half of the yield strength? Assume $Y = 1$.

***7.24** A Ti-6Al-4V alloy plate contains an internal through crack of 1.90 mm. What is the highest stress (MPa) that this material can withstand without catastrophic failure? Assume $Y = \sqrt{\pi}$.

7.25 Using the equation $K_{IC} = \sigma_f\sqrt{\pi a}$, plot the fracture stress (MPa) for aluminum alloy 7075-T651 versus surface crack size a (mm) for a values from 0.2 mm to 2.0 mm. What is the minimum size surface crack that will cause catastrophic failure?

7.26 Determine the critical crack length (mm) for a through crack in a thick 2024-T6 alloy plate that has a fracture toughness $K_{IC} = 23.5\ \text{MPa}\sqrt{\text{m}}$ and is under a stress of 300 MPa. Assume $Y = 1$.

***7.27** A fatigue test is made with a maximum stress of 25 ksi (172 MPa) and a minimum stress of −4.00 ksi (−27.6 MPa). Calculate (*a*) the stress range, (*b*) the stress amplitude, (*c*) the mean stress, and (*d*) the stress ratio.

7.28 A fatigue test is made with a mean stress of 17,500 psi (120 MPa) and a stress amplitude of 24,000 psi (165 MPa). Calculate (*a*) the maximum and minimum stresses, (*b*) the stress ratio, and (*c*) the stress range.

7.29 A large flat plate is subjected to constant-amplitude uniaxial cyclic tensile and compressive stresses of 120 and 35 MPa, respectively. If before testing the largest surface crack is 1.00 mm and the plain-strain fracture toughness of the plate is $35\ \text{MPa}\sqrt{\text{m}}$, estimate the fatigue life of the plate in cycles to failure. For the plate,

$m = 3.5$ and $A = 5.0 \times 10^{-12}$ in MPa and m units. Assume $Y = 1.3$.

*7.30 Refer to Prob. 7.29: If the initial and critical crack lengths are 1.25 and 12 mm, respectively, in the plate and the fatigue life is 2.0×10^6 cycles, calculate the maximum tensile stress in MPa that will produce this life. Assume $m = 3.0$ and $A = 6.0 \times 10^{-13}$ in MPa and m units. Assume $Y = 1.20$.

7.31 Refer to Prob. 7.29: Compute the final critical surface crack length if the fatigue life must be a minimum of 7.0×10^5 cycles. Assume the initial maximum edge surface crack length of 1.80 mm and a maximum tensile stress of 160 MPa. Assume $m = 1.8$ and $A = 7.5 \times 10^{-13}$ in MPa and meter units. Assume $Y = 1.25$.

7.32 Refer to Prob. 7.29: Compute the critical surface edge crack if the fatigue life must be 8.0×10^6 cycles and maximum tensile stress is 21,000 psi. $m = 3.5$ and $A = 4.0 \times 10^{-11}$ in ksi and in. units. Initial crack (edge) is 0.120 in. $Y = 1.15$.

7.33 The following creep data were obtained for a titanium alloy at 50 ksi and 400°C. Plot the creep strain versus time (hours), and determine the steady-state creep rate for these test conditions.

Strain (in./in.)	Time (h)	Strain (in./in.)	Time (h)
0.010×10^{-2}	2	0.075×10^{-2}	80
0.030×10^{-2}	18	0.090×10^{-2}	120
0.050×10^{-2}	40	0.11×10^{-2}	160

Synthesis and Evaluation Problems

*7.34 A Charpy V-notch specimen is tested by the impact-testing machine in Fig. 7.9. In the test, the 15 kg hammer of arm-length 120 cm (measured from the fulcrum to the point of impact) is raised to 90° and then released. (*a*) What is the potential energy stored in the mass at this point? (*b*) After fracture of the specimen, the hammer swings to 45°. What is the potential energy at this point? (*c*) How much energy was expended in the fracture of the specimen? Hint: potential energy = mass × g × height.

7.35 Assuming that the maximum angle the pendulum in problem 43 can rise to is 120° and if the V-notch specimen requires 220 J of energy for fracture, will the above system have sufficient capacity to achieve the fracture of the specimen? How much will the pendulum rise if it achieves fracture of the specimen?

*7.36 The circumferential stress, σ, (also called hoop stress) in a pressurized cylindrical vessel is calculated by the equation $\sigma = Pr/t$, where P is the internal pressure, r is radius of the vessel, and t its thickness. For a vessel of 36 in diameter, 0.25 in thickness and an internal pressure of 5000 psi, what would be the critical crack length if the vessel were made of (*a*) Al 7178-T651, (*b*) alloy steel (17-7 pH)? What is your conclusion? Use Table 6.1 for properties. (Use Y = 1.0 and assume center crack geometry.)

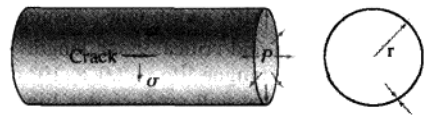

7.37 For the vessel in problem 7.36, consider that it is made of Titanium alloy (Ti-6Al-4V). (*a*) If cracks of length a=0.005 inch are detected in the vessel, what should the safe operating pressure be? What if cracks of length a=0.2 inches are detected, what should the safe operating pressure be? Use Y=1.0 and assume center crack geometry.

***7.38** An ultrasonic crack detection equipment used by Company A can find cracks of length a = 0.25 inches and longer. A lightweight component is to be designed and manufactured and then inspected for cracks using the above machine. The maximum uniaxial stress applied to the component will be 60 ksi. Your choices of metals for the component are Al 7178 T651, Ti-6Al-4V, or 4340 steel as listed in Table 7.1. (*a*) Which metal would you select to make the component from? (*b*) Which metal would you choose when considering both safety and weight? (Use Y=1.0 and assume center crack geometry.)

7.39 In problem 7.38, if you did not consider the existence of cracks at all and only considered yielding under uniaxial stress as a failure criterion, (*a*) which metal would you select to avoid yielding? (*b*) Which metal would you select to avoid yielding and have the lightest component? (Use data in Table 7.1)? Is it a safe design practice to assume that no initial cracks exist? Explain.

7.40 It is a common practice in inspection of bridges (and other structures) that if a crack is found in the steel, the engineers will drill a small hole just ahead of the crack tip. How will this help?

7.41 An alloy steel plate is subjected to a tensile stress of 120 Mpa. The fracture toughness of the materials is given to be 45 Mpa.m1/2. (*a*) Determine the critical crack length to assure the plate will not fail under the static loading conditions (assume Y=1). (*b*) Consider the same plate under the action of cyclic tensile/compressive stresses of 120 Mpa and 30 Mpa respectively. Under the cyclic conditions, a crack length reaching 50% of the critical crack length under static conditions (part a) would be considered unacceptable. If the component is to remain safe for 3 million cycles, what is largest allowable initial crack length?

7.42 A cylindrical rod made of directionally solidified alloy CM 247 is to carry a 10,000 N load at a temperature of 900° C and for a period of 300 hours. Using the Larson-Miller plot in Fig. 7.32, design the appropriate dimensions for the cross section.

7.43 In the manufacturing of connecting rods, 4340 alloy steel heat treatable to 260 Ksi may be used. There are two options for the manufacturing of the component, (*i*) heat treat the component and use, and (*ii*) heat treat and ground the surface. Which option would you use and why?

7.44 In aircraft applications, aluminum panels are riveted together through holes drilled in the sheets. It is the industry practice to plastically expand the holes to the desired diameter at room temperature (this introduces compressive stresses on the circumference of the hole). (*a*) Explain why this process is done and how it benefits the structure. (*b*) Design a system that would accomplish the cold expansion process effectively and cheaply. (*c*) What are some precautions that must be taken during the cold expansion process?

7.45 What factors would you consider in selecting materials for coins? Suggest materials for this application.

7.46 If you had a choice between an aluminum alloy, stainless steel, a plain low carbon steel alloy, and a plain high carbon steel alloy (all of which offer appropriate strength for the application) for a structural application in the Arctic regions which would you choose? Why? (Cost is not an issue.)

7.47 Examine the fracture surface of a fractured steel tube. How would you classify this fracture? Can you tell where the fracture started from? How?

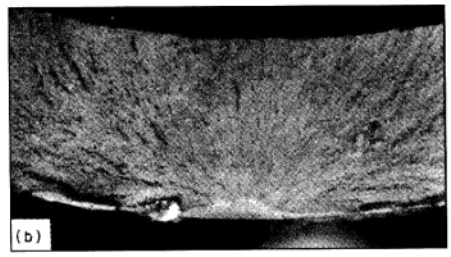

Figure P7.47
(*"ASM Handbook of Failure Analysis and Prevention," vol. 11, p. 21, Fig. 3b.*)

7.48 Examine the fracture surfaces below and discuss the differences in surface features. Can you identify the type and nature of the fracture?

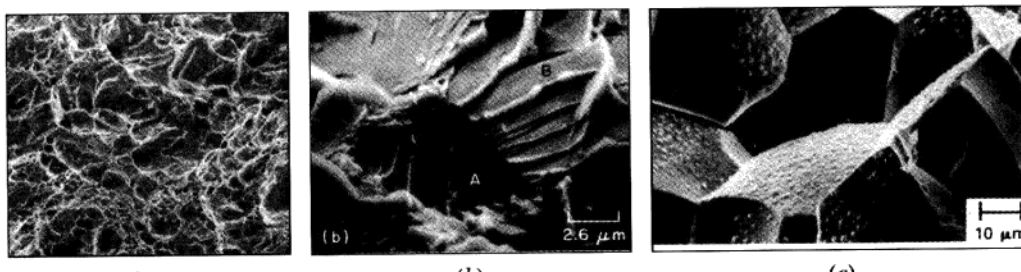

(*a*) (*b*) (*c*)

Figure P7.48
(*"ASM Handbook of Failure Analysis and Prevention," vol. 11.*)

7.49 The components in Fig. P7.54 is high strength steel racecar transmission shaft, which is cyclically loaded in torsion and some bending. The one at the bottom of

Fig. P7.54*a* is fractured. Figure P7.54*b* shows a higher magnification image of the fracture path around the shaft. Figure P7.54*c* shows that cross-section of the fractured shaft. Based on this visual evidence speculate as much as possible about what happened to this shaft and where did the fracture start from. Especially, list your observations of Fig. P7.54*c*.

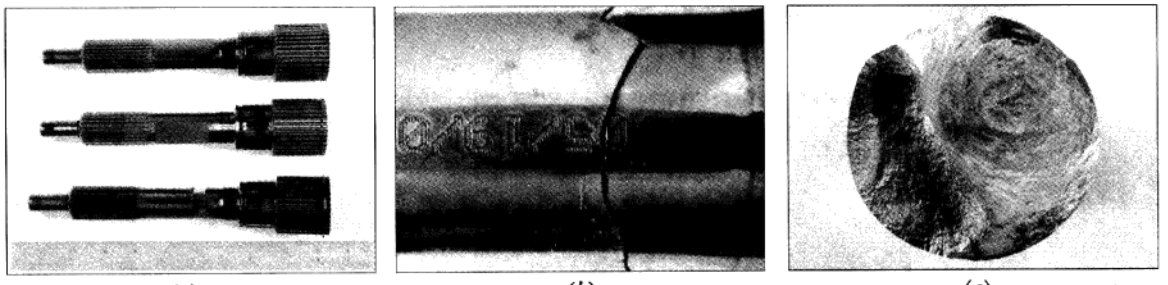

(*a*) (*b*) (*c*)

Figure P7.49
(*Courtesy of Met-Tech*)

CHAPTER 8

Phase Diagrams

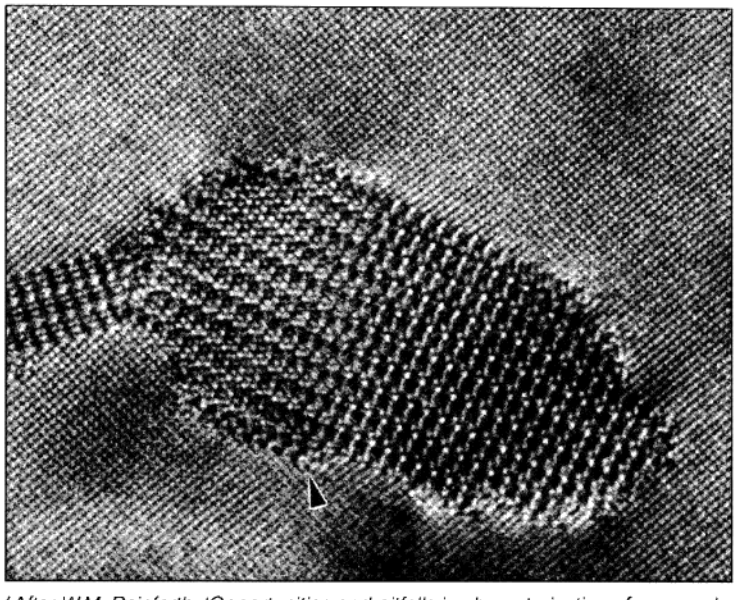

(After W.M. Rainforth, 'Opportunities and pitfalls in characterization of nanoscale features,' Materials Science and Technology, vol. 16 (2000) 1349–1355.)

Precipitation hardening or age hardening is a heat-treatment process used to produce a mixture of uniformly distributed hard phases in a soft matrix. The precipitated phase interferes with the movement of dislocations and, as a result, strengthens the alloy. The chapter-opening figure is a high-resolution electron microscope image of the Al_2CuMg phase in an aluminum matrix.[1]

A **phase** in a material is a region that differs in its microstructure and/or composition from another region. *Phase diagrams* are graphical representations of what phases are present in a materials system at various temperatures, pressures, and compositions. Most phase diagrams are constructed by using equilibrium conditions[2] and are used by engineers and scientists to understand and predict many aspects of the behavior of materials. ■

[1]http://www.shef.ac.uk/uni/academic/D-H/em/research/centres/sorbcent.html

[2]**Equilibrium phase diagrams** are determined by using slow cooling conditions. In most cases, equilibrium is approached but never fully attained.

LEARNING OBJECTIVES

By the end of this chapter, students will be able to . . .

1. Describe equilibrium, phase, and degrees of freedom for a materials system.
2. Describe the application of Gibbs rule in a material system.
3. Describe cooling curves and phase diagrams and the type of information that may be extracted from them.
4. Describe a binary isomorphous phase diagram and be able to draw a generic diagram showing all phase regions and relevant information.
5. Be able to apply tie line and lever rule to phase diagrams in order to determine the phase composition and phase fraction in a mixture.
6. Describe nonequilibrium solidification of metals and explain the general differences in microstructure when compared to equilibrium solidification.
7. Describe a binary eutectic phase diagram and be able to draw a generic diagram showing all phase regions and relevant information.
8. Describe the microstructure evolution during equilibrium cooling as metal solidifies at various regions of the phase diagram.
9. Define various invariant reactions.
10. Define intermediate phase compounds and intermetallics.
11. Describe ternary phase diagrams.

8.1 PHASE DIAGRAMS OF PURE SUBSTANCES


Animation

A pure substance such as water can exist in solid, liquid, or vapor phases, depending on the conditions of temperature and pressure. An example familiar to everyone of two phases of a pure substance in **equilibrium** is a glass of water containing ice cubes. In this case, solid and liquid water are two separate and distinct phases that are separated by a phase boundary, the surface of the ice cubes. During the boiling of water, liquid water and water vapor are two phases in equilibrium. A graphical representation of the phases of water that exist under different conditions of temperature and pressure is shown in Fig. 8.1.

In the *pressure-temperature* (*PT*) phase diagram of water, there exists a *triple point* at low pressure (4.579 torr) and low temperature (0.0098°C) where solid, liquid, and vapor phases of water coexist. Liquid and vapor phases exist along the vaporization line and liquid and solid phases along the freezing line, as shown in Fig. 8.1. These lines are two-phase equilibrium lines.

Pressure-temperature equilibrium phase diagrams also can be constructed for other pure substances. For example, the equilibrium *PT* phase diagram for pure iron is shown in Fig. 8.2. One major difference with this phase diagram is that there are three separate and distinct *solid phases:* alpha (α) Fe, gamma (γ) Fe, and delta (δ) Fe. Alpha and delta iron have BCC crystal structures, whereas gamma iron has an FCC structure. The

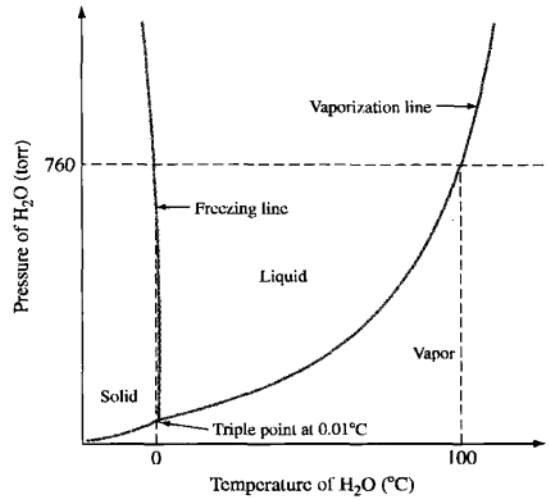

Figure 8.1
Approximate *PT* equilibrium phase diagram for pure water. (The axes of the diagram are distorted to some extent.)

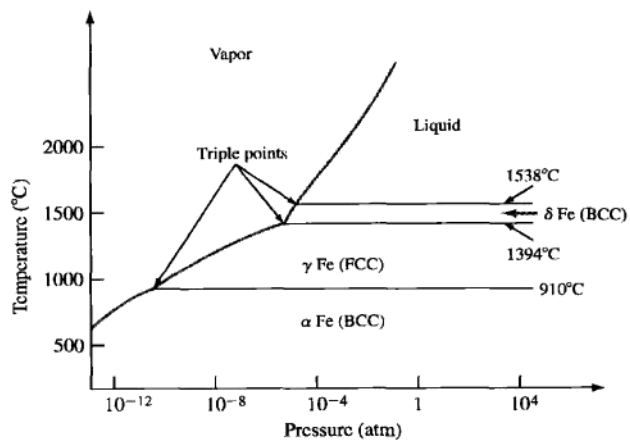

Figure 8.2
Approximate *PT* equilibrium phase diagram for pure iron.
(*From W.G. Moffatt, G.W. Pearsall, and J. Wulff, "The Structure and Properties of Materials," vol. 1: "Structure," Wiley, 1964, p. 151.*)

Animation

phase boundaries in the solid state have the same properties as the liquid and solid phase boundaries. For example, under equilibrium conditions, alpha and gamma iron can exist at a temperature of 910°C and 1 atm pressure. Above 910°C only single-phase gamma exists, and below 910°C only single-phase alpha exists (Fig. 8.2). There are also three

triple points in the iron *PT* diagram where three different phases coexist: (1) liquid, vapor, and δFe, (2) vapor, δFe, and γFe, and (3) vapor, γFe, and αFe.

8.2 GIBBS PHASE RULE

From thermodynamic considerations, J.W. Gibbs[3] derived an equation that computes the number of phases that can coexist in equilibrium in a chosen system. This equation, called **Gibbs phase rule,** is

$$P + F = C + 2 \tag{8.1}$$

where P = number of phases that coexist in a chosen system

C = **number of components** in the system

F = degrees of freedom

Usually a component C is an element, compound, or solution in the system. F, the **degrees of freedom,** is the number of variables (pressure, temperature, and composition) that can be changed independently without changing the number of phases in equilibrium in the chosen system.

Let us consider the application of Gibbs phase rule to the *PT* phase diagram of pure water (Fig. 8.1). At the triple point, three phases coexist in equilibrium, and since there is one component in the **system** (water), the number of degrees of freedom can be calculated:

$$P + F = C + 2$$

$$3 + F = 1 + 2$$

or

$$F = 0 \qquad \text{(zero degrees of freedom)}$$

Since none of the variables (temperature or pressure) can be changed and still keep the three phases in balance, the triple point is called an *invariant point.*

Consider next a point along the liquid-solid freezing curve of Fig. 8.1. At any point along this line two phases will coexist. Thus, from the phase rule,

$$2 + F = 1 + 2$$

or

$$F = 1 \qquad \text{(one degree of freedom)}$$

This result tells us that there is one degree of freedom, and thus one variable (T or P) can be changed independently and still maintain a system with two coexisting phases. Thus, if a particular pressure is specified, there is only one temperature at which both liquid and solid phases can coexist. For a third case, consider a point on the water *PT* phase diagram inside a single phase. Then there will be only one phase present ($P = 1$), and substituting into the phase-rule equation gives

$$1 + F = 1 + 2$$

[3]Josiah Willard Gibbs (1839–1903). American physicist. He was a professor of mathematical physics at Yale University and made great contributions to the science of thermodynamics, which included the statement of the phase rule for multiphase systems.

or

$$F = 2 \qquad \text{(two degrees of freedom)}$$

This result tells us that two variables (temperature and pressure) can be varied independently and the system will still remain a single phase.

Most binary phase diagrams used in materials science are temperature composition diagrams in which pressure is kept constant, usually at 1 atm. In this case, we have the condensed phase rule, which is given by

$$P + F = C + 1 \qquad \textbf{(8.1}a\textbf{)}$$

Equation 8.1a will apply to all subsequent binary phase diagrams discussed in this chapter.

8.3 COOLING CURVES

Cooling curves can be used to determine phase transition temperatures for both pure metals and alloys. A **cooling curve** is obtained by recording the temperature of a material versus time as it cools from a temperature at which it is molten through solidification and finally to room temperature. The cooling curve for a pure metal is shown in Fig. 8.3. If the metal is allowed to cool under equilibrium conditions (slow cooling), its temperature drops continuously along line AB of the curve. At the melting point (freezing temperature) solidification begins and the cooling curve becomes flat (horizontal segment BC, also called a **plateau** or **region of thermal arrest**) and remains flat until solidification is complete. In region BC, the metal is in the form of a mixture of solid and liquid phases. As point C is approached, the weight fraction of solid in the mixture grows until solidification is complete. The temperature remains constant because there is a balance between the heat lost by the metal through the mold and the latent heat supplied by the solidifying metal. Simply stated, the latent heat keeps the mixture at the freezing temperature until complete solidification is achieved. After solidification is complete at C, the cooling curve will again show a drop in temperature with time (segment CD of the curve).

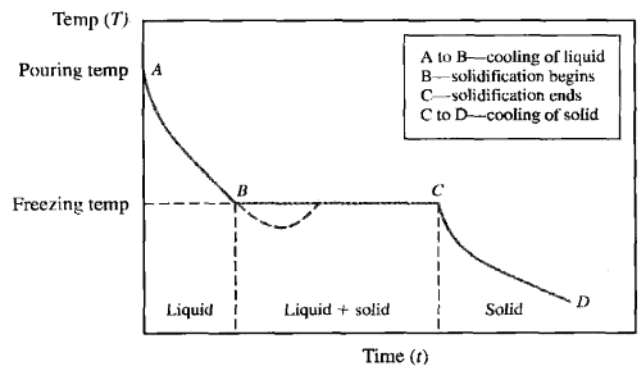

Figure 8.3
The cooling curve for a pure metal.

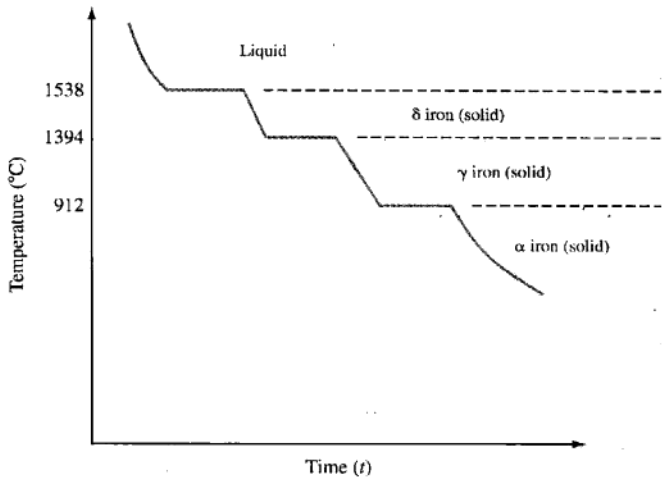

Figure 8.4
Cooling curve for pure iron at a pressure of 1 atm.

As discussed in the sections on the solidification of pure metals in Chap. 4, a degree of undercooling (cooling below the freezing temperature) is required for the formation of solid nuclei. The undercooling will appear on the cooling curve as a drop below the freezing temperature as shown in Fig. 8.3.

The cooling curve may also provide information regarding the solid state phase transformation in metals. An example of such a cooling curve would be that of pure iron. The pure iron cooling curve under atmospheric pressure conditions ($P = 1$ atm) shows a freezing temperature of 1538°C at which point a high-temperature solid of BCC structure is formed called δ *iron* (Fig. 8.4). Upon additional cooling, at a temperature of approximately 1394°C, the cooling curve shows a second plateau. At this temperature, a solid-solid phase transformation of BCC δ ferrite to an FCC solid called γ *iron* (polymorphic transformation, see Sec. 3.10) takes place. With further cooling, a second solid-solid phase transformation takes place at a temperature of 912°C. In this transformation, the FCC γ iron reverts back to a BCC iron structure called α *iron.* This solid-solid transformation has important technological implications in steel-processing industries and will be discussed in Chap. 9.

8.4 BINARY ISOMORPHOUS ALLOY SYSTEMS

Let us now consider a mixture or alloy of two metals instead of pure substances. A mixture of two metals is called a *binary alloy* and constitutes a *two-component* system since each metallic element in an alloy is considered a separate component. Thus, pure copper is a one-component system, whereas an alloy of copper and nickel is a two-component system. Sometimes a compound in an alloy is also considered a separate component. For example, plain-carbon steels containing mainly iron and iron carbide are considered two-component systems.

In some binary metallic systems, the two elements are completely soluble in each other in both the liquid and solid states. In these systems, only a single type of crystal structure exists for all compositions of the components, and therefore they are called **isomorphous systems.** In order for the two elements to have complete solid solubility in each other, they usually satisfy one or more of the following conditions formulated by Hume-Rothery[4] and known as the Hume-Rothery solid solubility rules:

1. The size of the atoms of each of the two elements must not differ by more than 15 percent.
2. The elements should not form compounds with each other, i.e., there should be no appreciable difference in the electronegativities of the two elements.
3. The crystal structure of each element of the solid solution must be the same.
4. The elements should have the same valence.

The Hume-Rothery rules are not all applicable for every pair of elements that shows complete solid solubility.

An important example of an isomorphous binary alloy system is the copper-nickel system. A phase diagram of this system with temperature as the ordinate and chemical composition in weight percent as the abscissa is shown in Fig. 8.5. This diagram has been determined for slow cooling or equilibrium conditions at atmospheric pressure and does not apply to alloys that have been rapidly cooled through the solidification temperature range. The area above the upper line in the diagram, called the **liquidus,** corresponds to the region of stability of the liquid phase, and the area below the lower line, or **solidus,** represents the region of stability for the solid phase. The region between the liquidus and solidus represents a two-phase region where both the liquid and solid phases coexist.

For the binary isomorphous phase diagram of Cu and Ni, according to the Gibbs phase rule ($F = C - P + 1$), at the melting point of the pure components, the number of components C is 1 (either Cu or Ni) and the number of phases available P is 2 (liquid or solid), resulting in a degree of freedom of 0 ($F = 1 - 2 + 1 = 0$). These points are referred to as *invariant points* ($F = 0$). This means that any change in temperature will change the microstructure either into solid or liquid. Accordingly, in the single-phase regions (liquid or solid), the number of components, C, is 2 and the number of phases available, P, is 1, resulting in a degree of freedom of 2 ($F = 2 - 1 + 1 = 2$). This means that we can maintain the microstructure of the system in this region by varying either the temperature or composition independently. In the two-phase region, the number of components, C, is 2 and the number of phases available, P, is 2, resulting in a degree of freedom of 1 ($F = 2 - 2 + 1 = 1$). This means that only one variable (either temperature or composition) can be changed independently while maintaining the two-phase structure of the system. If the temperature is changed, the phase composition will also change.

[4]William Hume-Rothery (1899–1968). English metallurgist who made major contributions to theoretical and experimental metallurgy and who spent years studying alloy behavior. His empirical rules for solid solubility in alloys were based on his alloy design work.

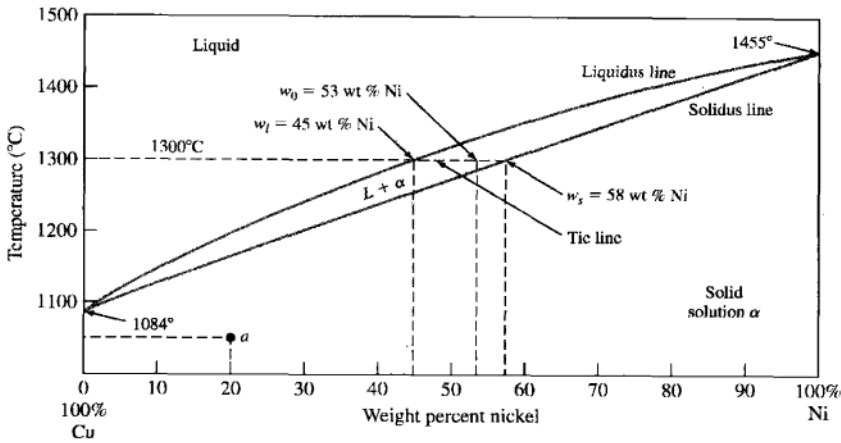

Figure 8.5
The copper-nickel phase diagram. Copper and nickel have complete liquid solubility and complete solid solubility. Copper-nickel solid solutions melt over a range of temperatures rather than at a fixed temperature, as is the case for pure metals. (*Adapted from "Metals Handbook," vol. 8, 8th ed., American Society for Metals, 1973, p. 294.*)

In the single-phase region of solid solution α, both the temperature and the composition of the alloy must be specified in order to locate a point on the phase diagram. For example, the temperature 1050°C and 20 percent Ni specify the point *a* on the Cu-Ni phase diagram of Fig. 8.5. The microstructure of solid solution α at this temperature and composition appears the same as that of a pure metal, i.e., the only observable feature in the optical microscope will be grain boundaries. However, because the alloy is a solid solution of 20 percent Ni in copper, the alloy will have higher strength and electrical resistivity than pure copper.

In the region between the liquidus and solidus lines, both liquid and solid phases exist. The amount of each phase present depends on the temperature and chemical composition of the alloy. Let us consider an alloy of 53 wt % Ni–47 wt % Cu at 1300°C in Fig. 8.5. Since this alloy contains both liquid and solid phases at 1300°C, neither of these phases can have the average composition of 53% Ni–47% Cu. The compositions of the liquid and solid phases at 1300°C can be determined by drawing a horizontal *tie line* at 1300°C from the liquidus line to the solidus line and then dropping vertical lines to the horizontal composition axis. The composition of the liquid phase (w_l) at 1300°C is 45 wt % Ni and that of the solid phase (w_S) is 58 wt % Ni, as indicated by the intersection of the dashed vertical lines with the composition axis.

Binary equilibrium phase diagrams for components that are completely soluble in each other in the solid state can be constructed from a series of liquid-solid cooling curves, as shown for the Cu-Ni system in Fig. 8.6. As discussed in the previous section, the cooling curves for pure metals show horizontal thermal arrests at their freezing points, as shown for pure copper and nickel in Fig. 8.6*a* at *AB* and *CD*. Binary solid solutions exhibit slope changes in their cooling curves at the liquidus and

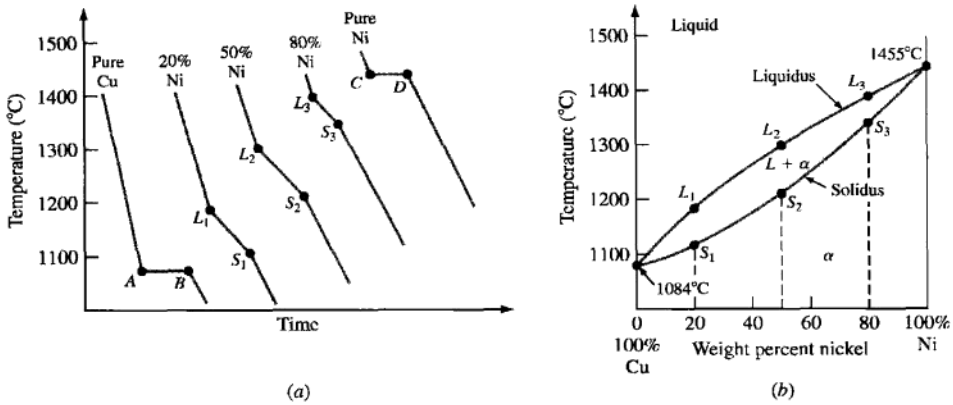

Figure 8.6
Construction of the Cu–Ni equilibrium phase diagram from liquid-solid cooling curves. (*a*) Cooling curves and (*b*) equilibrium phase diagram.
(From "Metals Handbook," vol. 8, 8th ed., American Society for Metals, 1973, p. 294. Used by permission of ASM International.)

solidus lines, as shown in Fig. 8.6*a* at compositions of 80% Cu–20% Ni, 50% Cu–50% Ni, and 20% Cu–80% Ni. The slope changes at L_1, L_2, and L_3 in Fig. 8.6*a* correspond to the liquidus points L_1, L_2, and L_3 of Fig. 8.6*b*. Similarly, the slope changes of S_1, S_2, and S_3 of Fig. 8.6*a* correspond to the points S_1, S_2, and S_3 on the solidus line of Fig. 8.6*b*. Further accuracy in the construction of the Cu-Ni phase diagram can be attained by determining more cooling curves at intermediate alloy compositions.

The cooling curve for metal alloys in an isomorphous system does not contain the thermal arrest region that one observes in the solidification of a pure metal. Instead, solidification begins at a specific temperature and ends at a lower temperature as presented by L and S symbols in Fig. 8.6. As a result, unlike pure metals, alloys solidify over a range of temperatures. Thus, when we refer to the freezing temperature of a metal alloy, we are speaking of the temperature at which the solidification process is complete.

8.5 THE LEVER RULE

The weight percentages of the phases in any two-phase region of a binary equilibrium phase diagram can be calculated by using the **lever rule.** For example, by using the lever rule, the weight percent liquid and weight percent solid for any particular temperature can be calculated for any average alloy composition in the two-phase liquid-plus-solid region of the binary copper-nickel phase diagram of Fig. 8.5.

To derive the lever-rule equations, let us consider the binary equilibrium phase diagram of two elements A and B that are completely soluble in each other, as shown in Fig. 8.7. Let x be the alloy composition of interest and its weight fraction of B in A be w_0. Let T be the temperature of interest, and let us construct a **tie line** (LS) at temperature T from the liquidus at point L to the solidus line at point S, forming the tie line LOS. At temperature T, the alloy x consists of a mixture of liquid of w_l weight fraction of B and solid of w_s weight fraction of B.

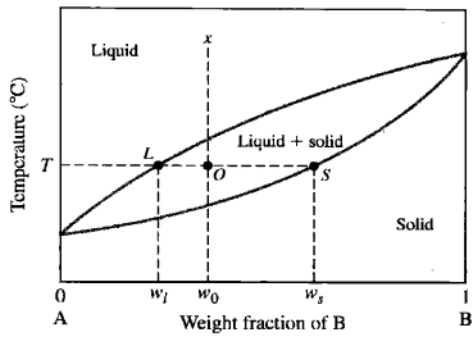

Figure 8.7
Binary phase diagram of two metals A and B completely soluble in each other being used to derive the lever-rule equations. At temperature T, the composition of the liquid phase is w_l and that of the solid is w_s.

The lever-rule equations can be derived by using weight balances. One equation for the derivation of the lever-rule equations is obtained from the fact that the sum of the weight fraction of the liquid phase, X_l, and the weight fraction of the solid phase, X_s, must equal 1. Thus,

$$X_l + X_s = 1 \tag{8.2}$$

or

$$X_l = 1 - X_s \tag{8.2a}$$

and

$$X_s = 1 - X_l \tag{8.2b}$$

A second equation for the derivation of the lever rule can be obtained by a weight balance of B in the alloy as a whole and the sum of B in the two separate phases. Let us consider 1 g of the alloy, and make this weight balance:

$$\begin{array}{ccccc} \text{Grams of B in two-phase mixture} & = & \text{Grams of B in liquid phase} & + & \text{Grams of B in solid phase} \\ \text{Grams of two-phase mixture} & & \text{Grams of liquid phase} & & \text{Grams of solid} \end{array}$$

$$\overbrace{(1\text{ g})(1)}\left(\frac{\%w_0}{100}\right) = \overbrace{(1\text{ g})(X_l)}\left(\frac{\%w_l}{100}\right) + \overbrace{(1\text{ g})(X_s)}\left(\frac{\%w_s}{100}\right)$$

Wt fraction of phase mixture — Average wt fraction of B in phase mixture

Wt fraction of liquid phase — Wt fraction of B in liquid phase

Wt fraction of solid phase — Wt fraction of B in solid phase

(8.3)

Thus, $$w_0 = X_l w_l + X_s w_s \quad (8.4)$$

combined with $$X_l = 1 - X_s \quad (8.2a)$$

gives $$w_0 = (1 - X_s)\, w_l + X_s w_s$$

or $$w_0 = w_l - X_s w_l + X_s w_s$$

Rearranging, $$X_s w_s - X_s w_l = w_0 - w_l$$

$$\boxed{\text{Wt fraction of solid phase} = X_s = \frac{w_0 - w_l}{w_s - w_l}} \quad (8.5)$$

Similarly, $$w_0 = X_l w_l + X_s w_s \quad (8.4)$$

combined with $$X_s = 1 - X_l \quad (8.2b)$$

gives $$\boxed{\text{Wt fraction of liquid phase} = X_l = \frac{w_s - w_0}{w_s - w_l}} \quad (8.6)$$

Equations 8.5 and 8.6 are the lever-rule equations. Effectively, the lever-rule equations state that to calculate the weight fraction of one phase of a two-phase mixture, one must use the segment of the tie line that is on the opposite side of the alloy of interest and is farthest away from the phase for which the weight fraction is being calculated. The ratio of this line segment of the tie line to the total tie line provides the weight fraction of the phase being determined. Thus, in Fig. 8.7, the weight fraction of the liquid phase is the ratio *OS/LS*, and the weight fraction of the solid phase is the ratio *LO/LS*.

Weight fractions can be converted to weight percentages by multiplying by 100 percent. Example Problem 8.1 shows how the lever rule can be used to determine the weight percentage of a phase in a binary alloy at a particular temperature.

EXAMPLE PROBLEM 8.1

Derive the lever rule for the case shown in Fig. EP8.1.

■ Solution

To derive the lever rule, let us consider the binary equilibrium diagram of two elements A and B that are completely soluble in each other, as shown in Fig. EP8.1. Let x be the alloy composition of interest and its weight fraction of B in A be w_0. Let T be the temperature of interest, and let us construct a tie line from the solidus line at point S forming the tie line *SOL*. From the solution of these equations:

The weight fraction of the liquid phase would equal

$$\frac{w_0 - w_s}{w_l - w_s} = \frac{SO}{LS}$$

The weight fraction of the solid phase would equal

$$\frac{w_l - w_0}{w_l - w_s} = \frac{OL}{LS}$$

This problem is illustrated in Example Problem 8.3 at 1200°C.

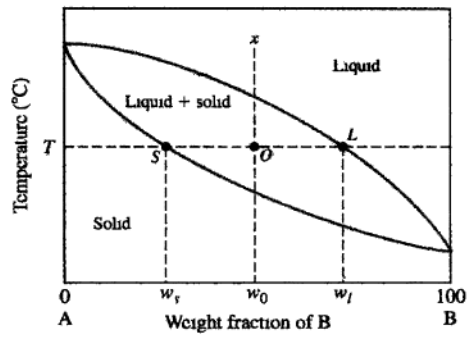

Figure EP8.1

EXAMPLE PROBLEM 8.2

A copper-nickel alloy contains 47 wt % Cu and 53 wt % Ni and is at 1300°C. Use Fig. 8.5 and answer the following:

a. What is the weight percent of copper in the liquid and solid phases at this temperature?
b. What weight percent of this alloy is liquid, and what weight percent is solid?

■ Solution

a. From Fig. 8.5 at 1300°C, the intersection of the 1300°C tie line with the liquidus gives 55 wt % Cu in the liquid phase and the intersection of the solidus of the 1300°C tie line gives 42 wt % Cu in the solid phase.

b. From Fig. 8.5 and using the lever rule on the 1300°C tie line,

$$w_0 = 53\%\ \text{Ni} \qquad w_l = 45\%\ \text{Ni} \qquad w_s = 58\%\ \text{Ni}$$

$$\text{Wt fraction of liquid phase} = X_l = \frac{w_s - w_0}{w_s - w_l}$$

$$= \frac{58 - 53}{58 - 45} = \frac{5}{13} = 0.38$$

$$\text{Wt \% of liquid phase} = (0.38)(100\%) = 38\% \blacktriangleleft$$

$$\text{Wt fraction of solid phase} = X_s = \frac{w_0 - w_l}{w_s - w_l}$$

$$= \frac{53 - 45}{58 - 45} = \frac{8}{13} = 0.62$$

$$\text{Wt \% of solid phase} = (0.62)(100\%) = 62\% \blacktriangleleft$$

EXAMPLE PROBLEM 8.3

Calculate the percent liquid and solid for the Ag-Pd phase diagram shown in Fig. EP8.3 at 1200°C and 70 wt % Ag. Assume $W_l = 74$ without Ag and $W_s = 64$ without Ag.

■ Solution

$$W(\%)\ \text{liquid} = \frac{70 - 64}{74 - 64} = \frac{6}{10} = 60\%$$

$$W(\%)\ \text{solid} = \frac{74 - 70}{74 - 64} = \frac{4}{10} = 40\%$$

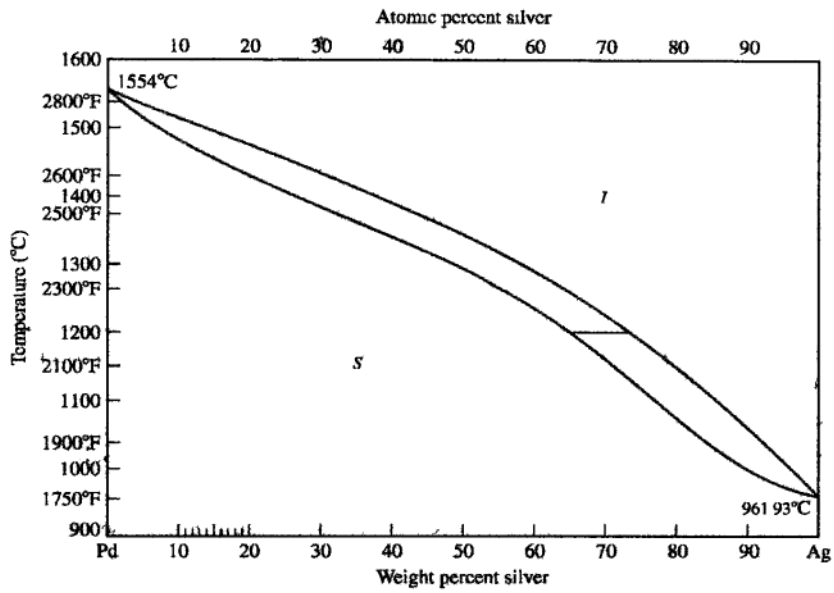

Figure EP8.3
The Ag-Pd equilibrium phase diagram.

8.6 NONEQUILIBRIUM SOLIDIFICATION OF ALLOYS

The phase diagram for the Cu-Ni system previously referred to was constructed by using very slow cooling conditions approaching equilibrium. That is, when the Cu-Ni alloys were cooled through the two-phase liquid + solid regions, the compositions of the liquid and solid phases had to readjust continuously by solid-state diffusion as the temperature was lowered. Since atomic diffusion is very slow in the solid state, an extensive period of time is required to eliminate concentration

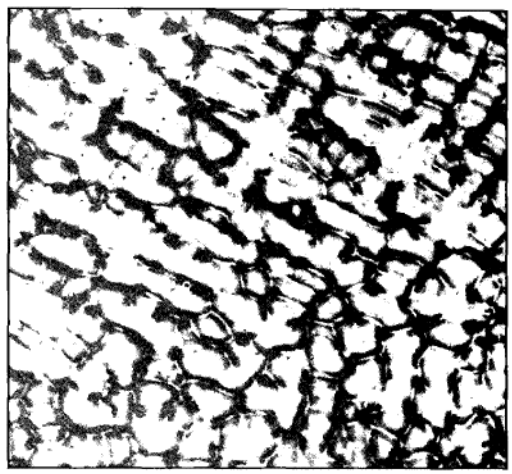

Figure 8.8
The microstructure of an as-cast 70% Cu–30% Ni alloy showing a cored structure.
(After W.G. Moffat et al., "Structure and Properties of Materials," vol. I, Wiley, 1964, p. 177.)

gradients. Thus, the as-cast microstructures of slowly solidified alloys usually have a **cored structure** (Fig. 8.8) caused by regions of different chemical composition.

The copper-nickel alloy system provides a good example to describe how such a cored structure originates. Consider an alloy of 70% Ni–30% Cu that is cooled from a temperature T_0 at a rapid rate (Fig. 8.9). The first solid forms at temperature T_1 and has the composition α_1 (Fig. 8.9). Upon further rapid cooling to T_2, additional layers of composition α_2 will form without much change in the composition of the solid primarily solidified. The overall composition at T_2 lies somewhere between α_1 and α_2 and will be designated α'_2. Since the tie line $\alpha'_2 L_2$ is longer than $\alpha_2 L_2$, there will be more liquid and less solid in the rapidly cooled alloy than if it were cooled under equilibrium conditions to the same temperature. Thus, solidification has been delayed at that temperature by the rapid cooling.

As the temperature is lowered to T_3 and T_4, the same processes occur and the average composition of the alloy follows the *nonequilibrium solidus* $\alpha_1 \alpha'_2 \alpha'_3 \cdots$. At T_6 the solid freezing has less copper than the original composition of the alloy, which is 30 percent Cu. At temperature T_7 the average composition of the alloy is 30 percent Cu, and freezing is complete. Regions in the microstructure of the alloy will thus consist of compositions varying from α_1 to α'_7 as the cored structure forms during solidification (Fig. 8.10). Figure 8.8 shows a cored microstructure of rapidly solidified 70% Cu–30% Ni alloy.

Most as-cast microstructures are cored to some extent and thus have composition gradients. In many cases, this structure is undesirable, particularly if the alloy

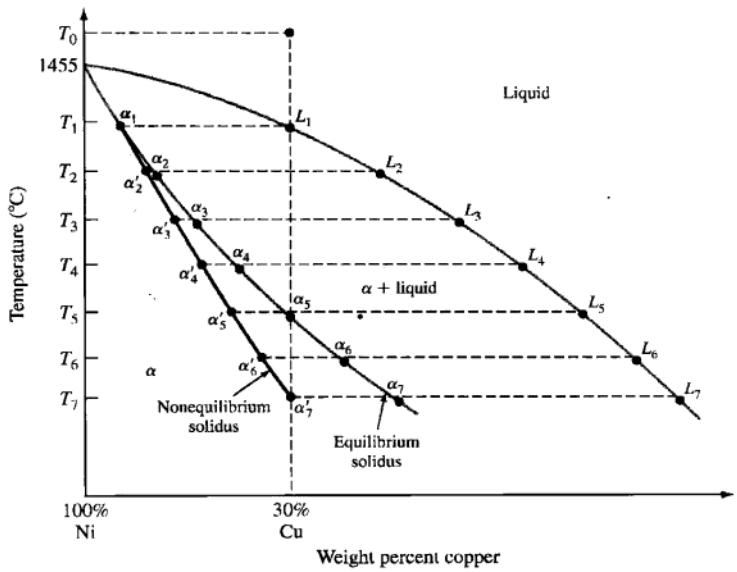

Figure 8.9
Nonequilibrium solidification of a 70% Ni–30% Cu alloy. This phase diagram has been distorted for illustrative purposes. Note the nonequilibrium solidus α_1 to α'_7. The alloy is not completely solidified until the nonequilibrium solidus reaches α'_7 at T_7.

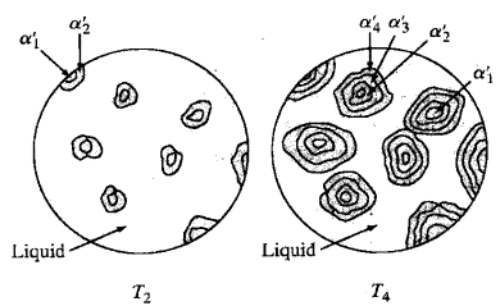

Figure 8.10
Schematic microstructures at temperature T_2 and T_4 of Fig. 8.9 for the nonequilibrium solidification of a 70% Ni–30% Cu alloy illustrating the development of a cored structure.

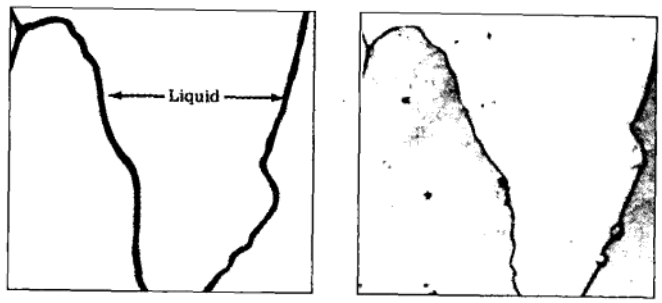

Figure 8.11
Liquation in a 70% Ni–30% Cu alloy. Heating only slightly above the solidus temperature so that melting just begins, produces a liquated structure such as shown in (*a*). In (*b*) the grain-boundary region was slightly melted, and then upon subsequent freezing, the melted zone became copper-rich and caused the grain boundaries to appear as broad dark lines. (*Courtesy of F. Rhines.*)

is to be subsequently worked. To eliminate the cored structure, as-cast ingots or castings are heated to elevated temperatures to accelerate solid-state diffusion. This process is called **homogenization** since it produces a homogeneous structure in the alloy. The homogenizing heat treatment must be carried out at a temperature that is lower than the lowest-melting solid in the as-cast alloy or else melting will occur. For homogenizing the 70% Ni–30% Cu alloy just discussed, a temperature just below T_7 indicated in Fig. 8.9 should be used. If the alloy is overheated, localized melting or *liquation* may take place. If the liquid phase forms a continuous film along the grain boundaries, the alloy will lose strength and may break up during subsequent working. Figure 8.11 shows liquation in the microstructure of a 70% Ni–30% Cu alloy.

8.7 BINARY EUTECTIC ALLOY SYSTEMS

Many binary alloy systems have components that have limited solid solubility in each other as, for example, in the lead-tin system (Fig. 8.12). The regions of restricted solid solubility at each end of the Pb-Sn diagram are designated as alpha and beta phases and are called *terminal solid solutions* since they appear at the ends of the diagram. The alpha phase is a lead-rich solid solution and can dissolve in solid solution a maximum of 19.2 wt % Sn at 183°C. The beta phase is a tin-rich solid solution and can dissolve a maximum of 2.5 wt % Pb at 183°C. As the temperature is decreased below 183°C, the maximum solid solubility of the solute elements decreases according to the **solvus** lines of the Pb-Sn phase diagram.

In simple binary eutectic systems like the Pb-Sn one, there is a specific alloy composition known as the **eutectic composition** that freezes at a lower temperature than all other compositions. This low temperature, which corresponds to the lowest temperature at which the liquid phase can exist when cooled slowly, is called the **eutectic temperature.** In the Pb-Sn system, the eutectic composition (61.9 percent Sn and 38.1 percent Pb) and the eutectic temperature (183°C) determine a point on the phase diagram called the **eutectic point.** When liquid of eutectic composition is slowly cooled to the eutectic temperature, the single liquid phase transforms simultaneously into two solid forms (solid solutions α and β). This transformation is known as the **eutectic reaction** and is written as

$$\text{Liquid} \xrightarrow[\text{cooling}]{\text{eutectic temperature}} \alpha \text{ solid solution} + \beta \text{ solid solution} \qquad \textbf{(8.7)}$$

The eutectic reaction is called an **invariant reaction** since it occurs under equilibrium conditions at a specific temperature and alloy composition that cannot be

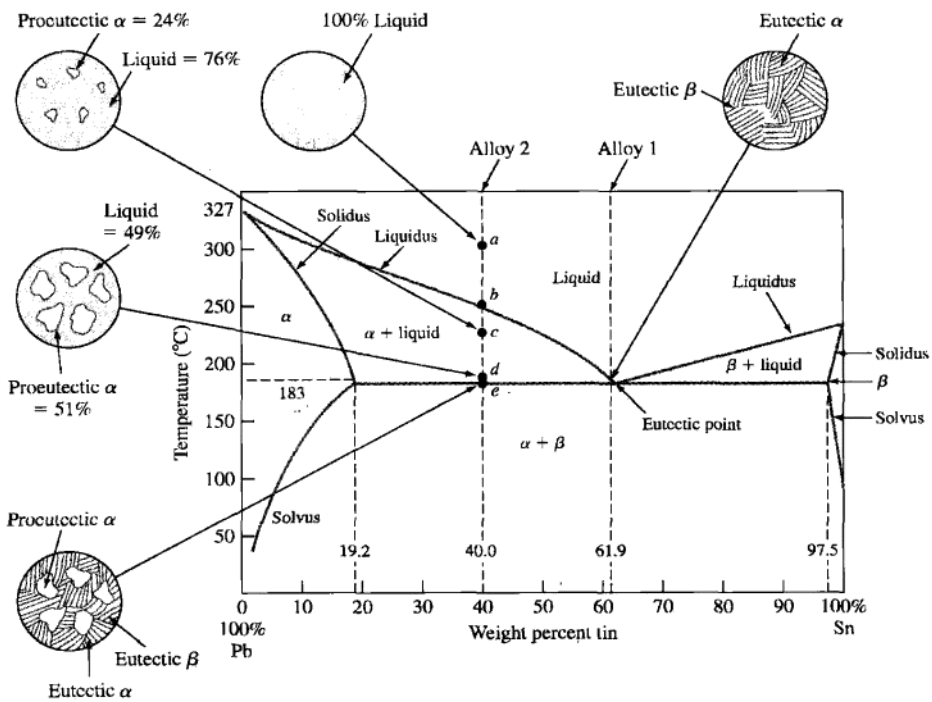

Figure 8.12
The lead-tin equilibrium phase diagram. This diagram is characterized by the limited solid solubility of each terminal phase (α and β). The eutectic invariant reaction at 61.9% Sn and 183°C is the most important feature of this system. At the eutectic point, α (19.2% Sn), β (97.5% Sn), and liquid (61.9% Sn) can coexist.

varied (according to Gibbs rule, $F = 0$). During the progress of the eutectic reaction, the liquid phase is in equilibrium with the two solid solutions α and β, and thus during a eutectic reaction, three phases coexist and are in equilibrium. Since three phases in a binary phase diagram can only be in equilibrium at one temperature, a horizontal thermal arrest appears at the eutectic temperature in the cooling curve of an alloy of eutectic composition.

Slow cooling of a Pb-Sn alloy of eutectic composition. Consider the slow cooling of a Pb-Sn alloy (alloy 1 of Fig. 8.12) of eutectic composition (61.9 percent Sn) from 200°C to room temperature. During the cooling period from 200°C to 183°C, the alloy remains liquid. At 183°C, which is the eutectic temperature, all the liquid solidifies by the eutectic reaction and forms a eutectic mixture of solid solutions α (19.2 percent Sn) and β (97.5 percent Sn) according to the reaction

$$\text{Liquid}\,(61.9\%\ \text{Sn}) \xrightarrow[\text{cooling}]{183^\circ\text{C}} \alpha\,(19.2\%\ \text{Sn}) + \beta\,(97.5\%\ \text{Sn}) \qquad \textbf{(8.8)}$$

After the eutectic reaction has been completed, upon cooling the alloy from 183°C to room temperature, there is a decrease in solid solubility of solute in the α and β solid solutions, as indicated by the solvus lines. However, since diffusion is slow at the lower temperatures, this process does not normally reach equilibrium, and thus solid solutions α and β can still be distinguished at room temperature, as shown in the microstructure of Fig. 8.13*a*.

Compositions to the left of the eutectic point are called **hypoeutectic,** Fig. 8.13*b*. Conversely, compositions to the right of the eutectic point are called **hypereutectic,** Fig. 8.13*d*.

Slow cooling of a 60% Pb–40% Sn alloy. Next consider the slow cooling of a 40% Sn–60% Pb alloy (alloy 2 of Fig. 8.12) from the liquid state at 300°C to room temperature. As the temperature is lowered from 300°C (point *a*), the alloy will remain liquid until the liquidus line is intersected at point *b* at about 245°C. At this temperature, solid solution α containing 12 percent Sn will begin to precipitate from the liquid. The first solid to form in this type of alloy is called **primary** or **proeutectic** *alpha.* The term proeutectic alpha is used to distinguish this constituent from the alpha that forms later by the eutectic reaction.

As the liquid cools from 245°C to slightly above 183°C through the two-phase liquid + alpha region of the phase diagram (points *b* to *d*), the composition of the solid phase (alpha) follows the solidus and varies from 12 percent Sn at 245°C to 19.2 percent Sn at 183°C. Likewise, the composition of the liquid phase varies from 40 percent Sn at 245°C to 61.9 percent Sn at 183°C. These composition changes are possible since the alloy is cooling very slowly and atomic diffusion occurs to equalize compositional gradients. At the eutectic temperature (183°C) all the remaining liquid solidifies by the eutectic reaction (Eq. 8.8). After the eutectic reaction is completed, the alloy consists of proeutectic alpha and a eutectic mixture of alpha (19.2 percent Sn) and beta (97.5 percent Sn). Further cooling below 183°C to room temperature

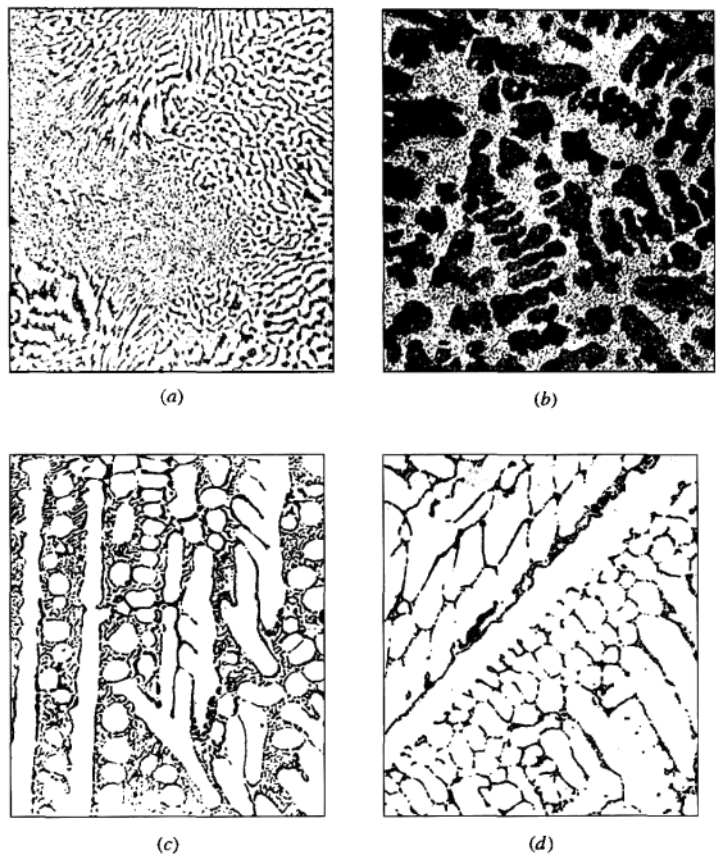

Figure 8.13
Microstructures of slowly cooled Pb–Sn alloys: (*a*) eutectic composition (63% Sn–37% Pb), (*b*) 40% Sn–60% Pb, (*c*) 70% Sn–30% Pb, (*d*) 90% Sn–10% Pb. (Magnification 75×.)
(From J. Nutting and R.G. Baker, "Microstructure of Metals," Institute of Metals, London, 1965, p. 19.)

lowers the tin content of the alpha phase and the lead content of the beta phase. However, at the lower temperatures the diffusion rate is much lower, and equilibrium is not attained. Figure 8.13*b* shows the microstructure of a 40% Sn–60% Pb alloy that has been slowly cooled. Note the dark-etching dendrites of the lead-rich alpha phase surrounded by eutectic. Figure 8.14 shows a cooling curve for a 60% Pb–40% Sn alloy. Note that a slope change occurs at the liquidus at 245°C and a horizontal thermal arrest appears during the freezing of the eutectic.

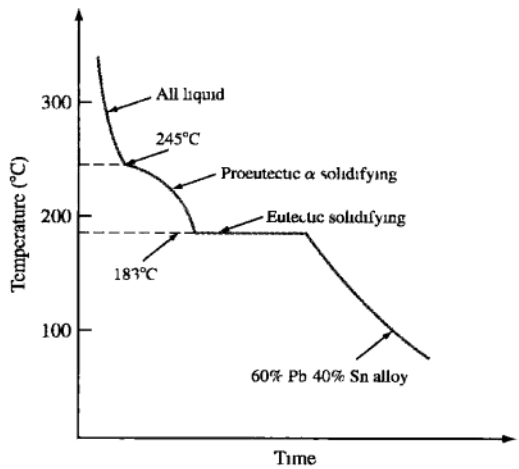

Figure 8.14
Schematic temperature-time cooling curve for a 60% Pb–40% Sn alloy

---

EXAMPLE PROBLEM 8.4

Make phase analyses of the equilibrium (ideal) solidification of lead-tin alloys at the following points in the lead-tin phase diagram of Fig. 8.12:

a. At the eutectic composition just below 183°C (eutectic temperature).
b. The point c at 40% Sn and 230°C.
c. The point d at 40% Sn and 183°C + ΔT.
d. The point e at 40% Sn and 183°C − ΔT.

■ Solution

a. At the eutectic composition (61.9 percent Sn) just below 183°C:

Phases present:	alpha	beta
Compositions of phases:	19.2% Sn in alpha phase	97.5% Sn in beta phase
Amounts of phases.	Wt % alpha phase* $= \dfrac{97.5 - 61.9}{97.5 - 19.2}(100\%)$ $= 45.5\%$	Wt % beta phase* $= \dfrac{61.9 - 19.2}{97.5 - 19.2}(100\%)$ $= 54.5\%$

*Note that in the lever-rule calculations one uses the ratio of the tie-line segment that is *farthest away* from the phase for which the weight percent is being determined to the whole tie line

b. The point c at 40 percent Sn and 230°C:

Phases present:	liquid	alpha
Compositions of phases.	48% Sn in liquid phase	15% Sn in alpha phase
Amounts of phases:	Wt % liquid phase $= \frac{40 - 15}{48 - 15}(100\%)$ $= 76\%$	Wt % alpha phase $= \frac{48 - 40}{48 - 15}(100\%)$ $= 24\%$

c The point d at 40 percent Sn and 183°C + ΔT·

Phases present:	liquid	alpha
Compositions of phases.	61.9% Sn in liquid phase	19.2% Sn in alpha phase
Amounts of phases:	Wt % liquid phase $= \frac{40 - 19.2}{61.9 - 19.2}(100\%)$ $= 49\%$	Wt % alpha phase $= \frac{61.9 - 40}{61.9 - 19.2}(100\%)$ $= 51\%$

d. The point e at 40 percent Sn and 183°C − ΔT:

Phases present:	alpha	beta
Compositions of phases:	19.2% Sn in alpha phase	97.5% Sn in beta phase
Amounts of phases:	Wt % alpha phase $= \frac{97.5 - 40}{97.5 - 19.2}(100\%)$ $= 73\%$	Wt % beta phase $= \frac{40 - 19.2}{97.5 - 19.2}(100\%)$ $= 27\%$

EXAMPLE PROBLEM 8.5

One kilogram of an alloy of 70 percent Pb and 30 percent Sn is slowly cooled from 300°C. Refer to the lead-tin phase diagram of Fig. 8.12 and calculate the following:

a. The weight percent of the liquid and proeutectic alpha at 250°C.
b. The weight percent of the liquid and proeutectic alpha just above the eutectic temperature (183°C) and the weight in kilograms of these phases.
c. The weight in kilograms of alpha and beta formed by the eutectic reaction.

■ Solution

a. From Fig. 8.12 at 250°C,

$$\text{Wt \% liquid}^* = \frac{30 - 12}{40 - 12}(100\%) = 64\% \blacktriangleleft$$

$$\text{Wt \% proeutectic } \alpha^* = \frac{40 - 30}{40 - 12}(100\%) = 36\% \blacktriangleleft$$

b. The weight percent liquid and proeutectic alpha just above the eutectic temperature, 183°C + ΔT, is

$$\text{Wt \% liquid} = \frac{30 - 19.2}{61.9 - 19.2}(100\%) = 25.3\% \blacktriangleleft$$

$$\text{Wt \% proeutectic } \alpha = \frac{61.9 - 30.0}{61.9 - 19.2}(100\%) = 74.7\% \blacktriangleleft$$

$$\text{Weight of liquid phase} = 1 \text{ kg} \times 0.253 = 0.253 \text{ kg} \blacktriangleleft$$

$$\text{Weight of proeutectic } \alpha = 1 \text{ kg} \times 0.747 = 0.747 \text{ kg} \blacktriangleleft$$

c. At 183°C − ΔT,

$$\text{Wt \% total } \alpha \text{ (proeutectic } \alpha + \text{ eutectic } \alpha) = \frac{97.5 - 30}{97.5 - 19.2}(100\%)$$

$$= 86.2\%$$

$$\text{Wt \% total } \beta \text{ (eutectic } \beta) = \frac{30 - 19.2}{97.5 - 19.2}(100\%)$$

$$= 13.8\%$$

$$\text{Wt total } \alpha = 1 \text{ kg} \times 0.862 = 0.862 \text{ kg}$$

$$\text{Wt total } \beta = 1 \text{ kg} \times 0.138 = 0.138 \text{ kg}$$

The amount of proeutectic alpha will remain the same before and after the eutectic reaction. Thus,

$$\text{Wt of } \alpha \text{ created by eutectic reaction} = \text{total } \alpha - \text{proeutectic } \alpha$$

$$= 0.862 \text{ kg} - 0.747 \text{ kg}$$

$$= 0.115 \text{ kg} \blacktriangleleft$$

$$\text{Wt of } \beta \text{ created by eutectic reaction} = \text{total } \beta$$

$$= 0.138 \text{ kg} \blacktriangleleft$$

*See note in Example Problem 8.4

EXAMPLE PROBLEM 8.6

A lead-tin (Pb-Sn) alloy contains 64 wt % proeutectic α and 36 wt % eutectic $\alpha + \beta$ at 183°C − ΔT. Calculate the average composition of this alloy (see Fig. 8.12).

■ Solution

Let x be the wt % Sn in the unknown alloy. Since this alloy contains 64 wt % proeutectic α, the alloy must be hypoeutectic, and x will therefore lie between 19.2 and 61.9 wt % Sn as indicated in Fig. EP8.6. At 183°C + ΔT, using Fig. EP8.6 and the lever rule gives

$$\% \text{ proeutectic } \alpha = \frac{61.9 - x}{61.9 - 19.2}(100\%) = 64\%$$

or

$$61.9 - x = 0.64(42.7) = 27.3$$
$$x = 34.6\%$$

Thus, the alloy consists of 34.6 percent Sn and 65.4 percent Pb. ◀ Note that we use the lever-rule calculation above the eutectic temperature since the percentage of the proeutectic α remains the same just above and just below the eutectic temperature.

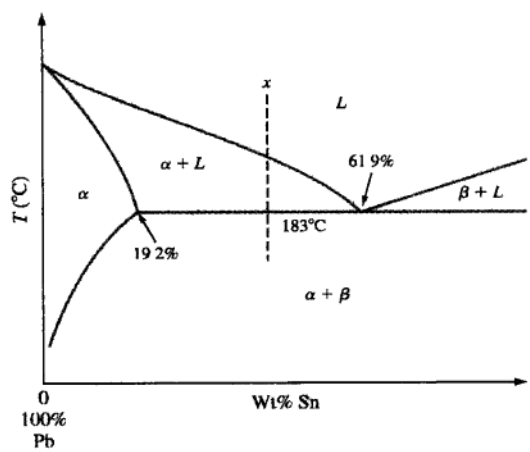

Figure EP8.6
Lead-rich end of the Pb–Sn phase diagram.

In a binary eutectic reaction, the two solid phases ($\alpha + \beta$) can have various morphologies. Figure 8.15 shows schematically some varied eutectic structures. The shape that will be created depends on many factors. Of prime importance is a minimization of free energy at the $\alpha - \beta$ interfaces. An important factor that determines the eutectic shape is the manner in which the two phases (α and β) nucleate and

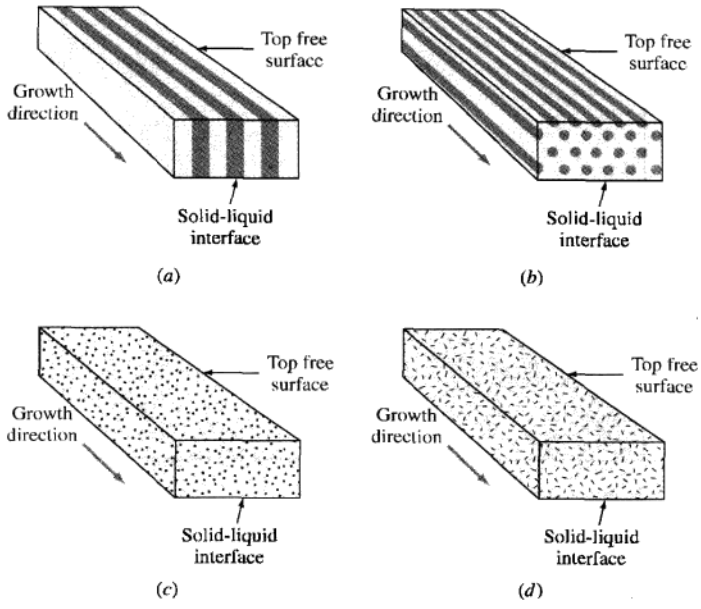

Figure 8.15
Schematic illustration of various eutectic structures: (*a*) lamellar, (*b*) rodlike, (*c*) globular, (*d*) acicular.
(After W.C. Winegard, "An Introduction to the Solidification of Metals," Institute of Metals, London, 1964.)

grow. For example, rod- and plate-type eutectics form when repeated nucleation of the two phases is not required in certain directions. An example of a *lamellar eutectic structure* formed by a Pb-Sn eutectic reaction is shown in Fig. 8.16. Lamellar eutectic structures are very common. A mixed irregular eutectic structure found in the Pb-Sn system is shown in Fig. 8.13*a*.

8.8 BINARY PERITECTIC ALLOY SYSTEMS

Another type of reaction that often occurs in binary equilibrium phase diagrams is the **peritectic reaction.** This reaction is commonly present as part of more-complicated binary equilibrium diagrams, particularly if the melting points of the two components are quite different. In the peritectic reaction a liquid phase reacts with a solid phase to form a new and different solid phase. In the general form, the peritectic reaction can be written as

$$\text{Liquid} + \alpha \xrightarrow[\text{cooling}]{} \beta \qquad \textbf{(8.9)}$$

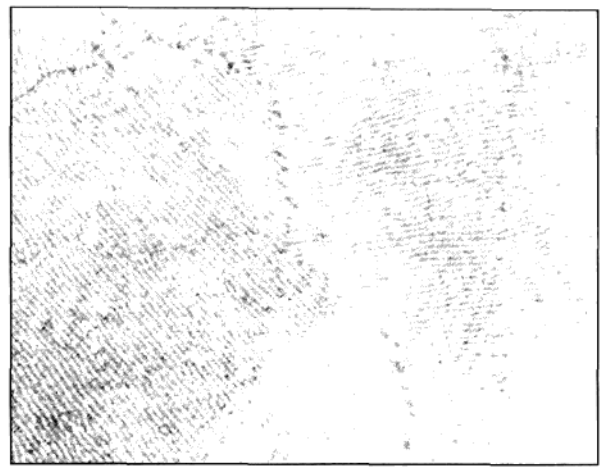

Figure 8.16
Lamellar eutectic structure formed by the Pb–Sn eutectic reaction. (Magnification 500×.)
(After W.G. Moffatt et al., "Structure and Properties of Materials," vol. I, Wiley, 1964.)

Figure 8.17 shows the peritectic region of the iron-nickel phase diagram. In this diagram, there are solid phases (δ and γ) and one liquid phase. The δ phase is a solid solution of nickel in BCC iron, whereas the γ phase is a solid solution of nickel in FCC iron. The peritectic temperature of 1517°C and the peritectic composition of 4.3 wt % Ni in iron define the peritectic point c in Fig. 8.17. This point is invariant since the three phases δ, γ, and liquid coexist in equilibrium. The peritectic reaction occurs when a slowly cooled alloy of Fe–4.3 wt % Ni passes through the peritectic temperature of 1517°C. This reaction can be written as

$$\text{Liquid (5.4 wt \% Ni)} + \delta\,\text{(4.0 wt \% Ni)} \xrightarrow[\text{cooling}]{1517^\circ\text{C}} \gamma\,\text{(4.3 wt \% Ni)} \qquad \textbf{(8.10)}$$

To further understand the peritectic reaction, consider an alloy of Fe–4.3 wt % Ni (peritectic composition) that is slowly cooled from 1550°C to slightly under 1517°C (points a to c in Fig. 8.17). From 1550°C to about 1525°C (points a to b in Fig. 8.17) the alloy cools as a homogeneous liquid of Fe–4.3% Ni. When the liquidus is intersected at about 1525°C (point b), solid δ begins to form. Further cooling to point c results in more and more solid δ being formed. At the peritectic temperature of 1517°C (point c), solid δ of 4.0 percent Ni and liquid of 5.4 percent Ni are in equilibrium, and at this temperature all the liquid reacts with all the δ solid phase to

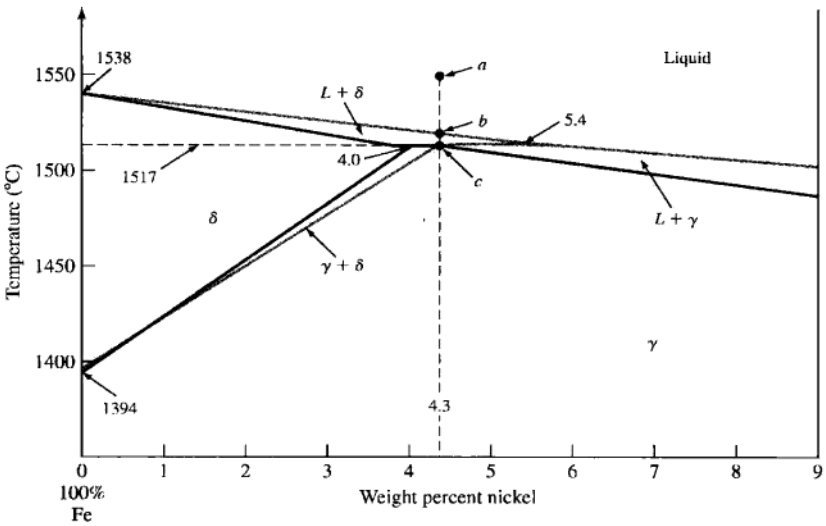

Figure 8.17
The peritectic region of the iron-nickel phase diagram. The peritectic point is located at 4.3% Ni and 1517°C, which is point *c*.

produce a new and different solid phase γ of 4.3 percent Ni. The alloy remains as single-phase γ solid solution until another phase change occurs at a lower temperature with which we are not concerned. The lever rule can be applied in the two-phase regions of the peritectic diagram in the same way as for the eutectic diagram.

If an alloy in the Fe-Ni system has less than 4.3 percent Ni and is slowly cooled from the liquid state through the liquid $+\delta$ region, there will be an excess of δ phase after the peritectic reaction is completed. Similarly, if an Fe-Ni alloy of more than 4.3 percent Ni but less than 5.4 percent Ni is slowly cooled from the liquid state through the $\delta+$ liquid region, there will be an excess of the liquid phase after the peritectic reaction is completed.

The silver-platinum binary equilibrium phase diagram is an excellent example of a system that has a single invariant peritectic reaction (Fig. 8.18). In this system, the peritectic reaction $L + \alpha \rightarrow \beta$ occurs at 42.4 percent Ag and 1186°C. Figure 8.19 schematically illustrates how the peritectic reaction progresses isothermally in the Pt-Ag system. In Example Problem 8.7, phase analyses are made at various points on this phase diagram. However, during the natural freezing of peritectic alloys, the departure from equilibrium is usually very large because of the relatively slow atomic diffusion rate through the solid phase created by this reaction.

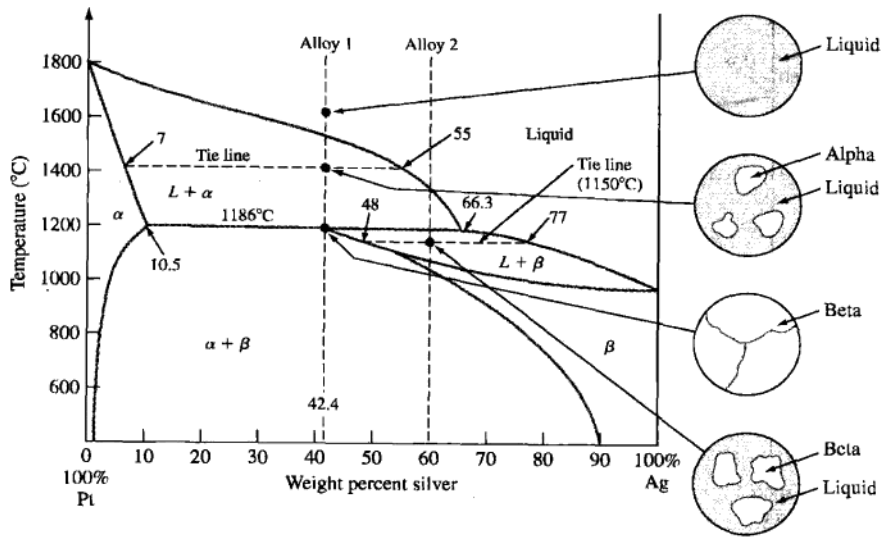

Figure 8.18
The platinum-silver phase diagram. The most important feature of this diagram is the peritectic invariant reaction at 42.4% Ag and 1186°C. At the peritectic point, liquid (66.3% Ag), alpha (10.5% Ag), and beta (42.4% Ag) can coexist.

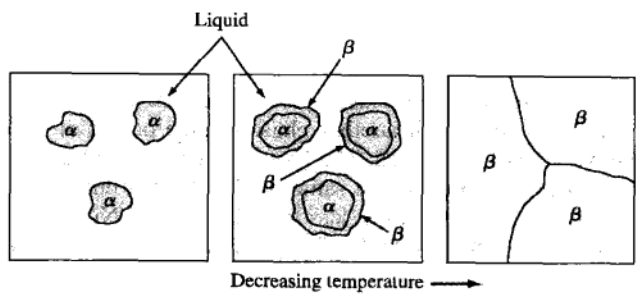

Figure 8.19
Schematic representation of the progressive development of the peritectic reaction liquid + $\alpha \rightarrow \beta$.

EXAMPLE PROBLEM 8.7

Make phase analyses at the following points in the platinum-silver equilibrium phase diagram of Fig. 8.18.

a. The point at 42.4 percent Ag and 1400°C.
b. The point at 42.4 percent Ag and 1186°C + ΔT.
c. The point at 42.4 percent Ag and 1186°C − ΔT.
d. The point at 60 percent Ag and 1150°C.

■ **Solution**

a. At 42.4 percent Ag and 1400°C:

Phases present:	liquid	alpha
Compositions of phases:	55% Ag in liquid phase	7% Ag in alpha phase
Amounts of phases:	Wt % liquid phase $= \frac{42.4 - 7}{55 - 7}(100\%)$ $= 74\%$	Wt % alpha phase $= \frac{55 - 42.4}{55 - 7}(100\%)$ $= 26\%$

b. At 42.4 percent Ag and 1186°C + ΔT:

Phases present:	liquid	alpha
Compositions of phases:	66.3% Ag in liquid phase	10.5% Ag in alpha phase
Amounts of phases:	Wt % liquid phase $= \frac{42.4 - 10.5}{66.3 - 10.5}(100\%)$ $= 57\%$	Wt % alpha phase $= \frac{66.3 - 42.4}{66.3 - 10.5}(100\%)$ $= 43\%$

c. At 42.4 percent Ag and 1186°C − ΔT:

Phase present:	beta only
Composition of phase:	42.4% Ag in beta phase
Amounts of phase:	100% beta phase

d. At 60 percent Ag and 1150°C:

Phases present:	liquid	beta
Compositions of phases:	77% Ag in liquid phase	48% Ag in beta phase
Amounts of phases:	Wt % liquid phase $= \frac{60 - 48}{77 - 48}(100\%)$ $= 41\%$	Wt % beta phase $= \frac{77 - 60}{77 - 48}(100\%)$ $= 59\%$

During the equilibrium or very slow cooling of an alloy of peritectic composition through the peritectic temperature, all the solid-phase alpha reacts with all the liquid to produce a new solid-phase beta, as indicated in Fig. 8.19. However, during the rapid solidification of a cast alloy through the peritectic temperature, a nonequilibrium phenomenon called *surrounding* or *encasement* occurs. During the peritectic reaction of $L + \alpha \rightarrow \beta$, the beta phase created by the peritectic reaction surrounds

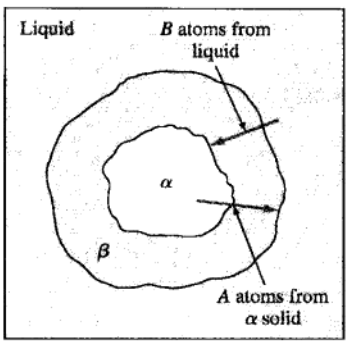

Figure 8.20
Surrounding during the peritectic reaction. The slow rate of atoms diffusing from the liquid to the alpha phase causes the beta phase to surround the alpha phase.

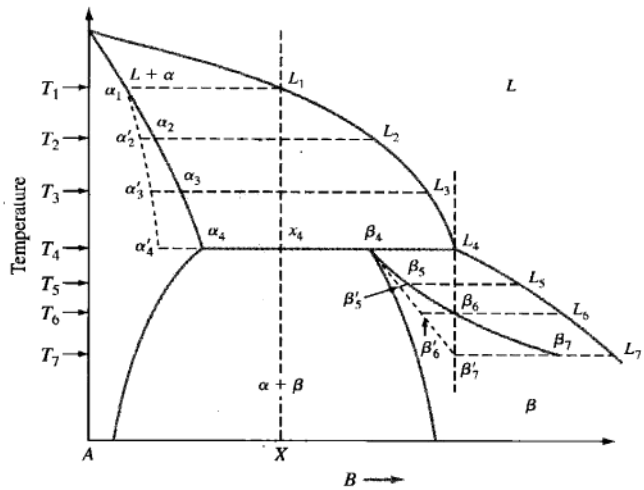

Figure 8.21
A hypothetical binary peritectic phase diagram to illustrate how coring occurs during natural freezing. Rapid cooling causes a nonequilibrium change of solidus α_1 to α'_4 and β_4 to β'_7, which lead to cored alpha phase and cored beta phase. The surrounding phenomenon also occurs during the rapid solidification of peritectic-type alloys.
(After F. Rhines, "Phase Diagrams in Metallurgy," McGraw-Hill, 1956, p. 86.)

or encases the primary alpha, as shown in Fig. 8.20. Since the beta phase formed is a solid phase and since solid-state diffusion is relatively slow, the beta formed around the alpha creates a diffusion barrier and the peritectic reaction proceeds at an ever-decreasing rate. Thus, when a peritectic-type alloy is rapidly cast, coring occurs during the formation of the primary alpha (Fig. 8.21 along α_1 to α'_4), and encasement of the cored α by β occurs during the peritectic reaction. Figure 8.22 schematically illustrates these combined nonequilibrium structures. The microstructure of a 60% Ag–40% Pt alloy that was rapidly cast is shown in Fig. 8.23. This structure shows cored alpha and its encasement by the beta phase.

8.9 BINARY MONOTECTIC SYSTEMS

Another three-phase invariant reaction that occurs in some binary phase diagrams is the **monotectic reaction** in which a liquid phase transforms into a solid phase and another liquid phase as

$$L_1 \xrightarrow{\text{cooling}} \alpha + L_2 \qquad \textbf{(8.11)}$$

Over a certain range of compositions, the two liquids are immiscible like oil in water and so constitute individual phases. A reaction of this type occurs in the copper-lead

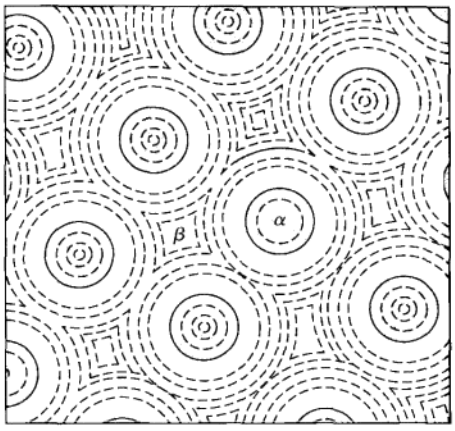

Figure 8.22
Schematic representation of surrounding or encasement in a cast peritectic-type alloy. A residue of cored primary α is represented by the solid circles concentric about smaller dashed circles; surrounding the cored α is a layer of β of peritectic composition. The remaining space is filled with cored β, represented by dashed curved lines.
(From F. Rhines, "Phase Diagrams in Metallurgy," McGraw-Hill, 1956, p. 86. Reproduced with permission of The McGraw-Hill Companies.)

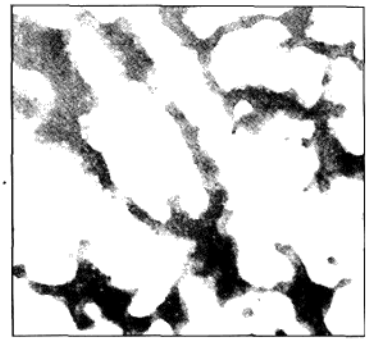

Figure 8.23
Cast 60% Ag–40% Pt hyperperitectic alloy. White and light gray areas are residual cored α; dark two-toned areas are β, the outer portions being of peritectic composition and the darkest central areas being the cored β that formed at temperatures below that of the peritectic reaction. (Magnification 1000×.)
(From F. Rhines, "Phase Diagrams in Metallurgy," McGraw-Hill, 1956. p. 87. Reproduced with permission of The McGraw-Hill Companies.)

system at 955°C and 36 percent Pb, as shown in Fig. 8.24. The copper-lead phase diagram has a eutectic point at 326°C and 99.94 percent Pb, and as a result terminal solid solutions of almost pure lead (0.007 percent Cu) and pure copper (0.005 percent Pb) are formed at room temperature. Figure 8.25 shows the microstructure of a cast monotectic alloy of Cu–36% Pb. Note the distinct separation of the lead-rich phase (dark) and the copper matrix (light).

Lead is added in small amounts up to about 0.5 percent to many alloys (e.g., the Cu-Zn brasses) to make the machining of alloys easier by reducing ductility sufficiently to cause machined metal chips to break away from the workpiece. This small addition of lead reduces the strength of the alloy only slightly. Leaded alloys are also used for bearings where small amounts of lead smear out at wear surfaces between the bearing and shaft and thus reduce friction.

8.10 INVARIANT REACTIONS

Three invariant reactions that commonly occur in binary phase diagrams have been discussed so far: the eutectic, peritectic, and monotectic types. Table 8.1 summarizes these reactions and shows their phase-diagram characteristics at their reaction

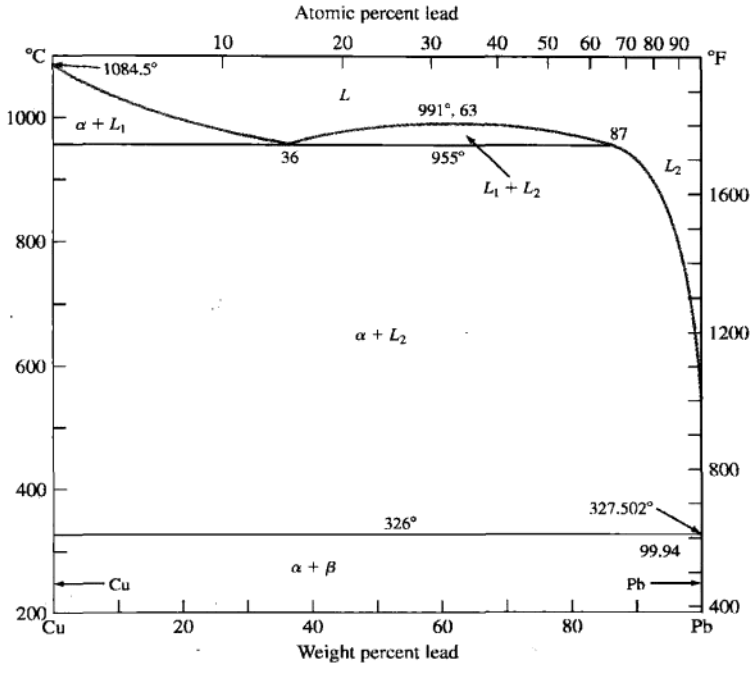

Figure 8.24
The copper-lead phase diagram. The most important feature of this diagram is the monotectic invariant reaction at 36% Pb and 955°C. At the monotectic point α (100% Cu), L_1 (36% Pb), and L_2 (87% Pb) can coexist. Note that copper and lead are essentially insoluble in each other.
(*"Metals Handbook," vol. 8: "Metallography, Structures, and Phase Diagrams," 8th ed., American Society for Metals, 1973, p. 296.*)

Figure 8.25
The microstructure of cast monotectic alloy Cu–36% Pb. Light areas are the Cu-rich matrix of the monotectic constituent; dark areas are the Pb-rich portion, which existed as L_2 at the monotectic temperature. (Magnification 100×.)
(*From F. Rhines, "Phase Diagrams in Metallurgy," McGraw-Hill, 1956, p. 87. Reproduced with the permission of The McGraw-Hill Companies.*)

Table 8.1 Types of three-phase invariant reactions occurring in binary phase diagrams

Name of reaction	Equation	Phase-diagram characteristic
Eutectic	$L \xrightarrow{\text{cooling}} \alpha + \beta$	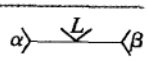
Eutectoid	$\alpha \xrightarrow{\text{cooling}} \beta + \gamma$	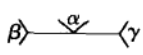
Peritectic	$\alpha + L \xrightarrow{\text{cooling}} \beta$	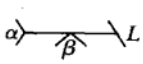
Peritectoid	$\alpha + \beta \xrightarrow{\text{cooling}} \gamma$	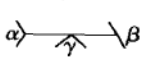
Monotectic	$L_1 \xrightarrow{\text{cooling}} \alpha + L_2$	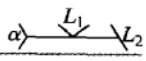

points. Two other important invariant reactions occurring in binary systems are the *eutectoid* and *peritectoid types*. Eutectic and eutectoid reactions are similar in that two solid phases are formed from one phase on cooling. However, in the eutectoid reaction, the decomposing phase is solid, whereas in the eutectic reaction, it is liquid. In the peritectoid reaction, two solid phases react to form a new solid phase, whereas in the peritectic reaction, a solid phase reacts with a liquid phase to produce a new solid phase. It is interesting to note that the peritectic and peritectoid reactions are the inverse of the corresponding eutectic and eutectoid reactions. The temperatures and compositions of the reacting phases are fixed for all these invariant reactions, i.e., according to the phase rule, there are zero degrees of freedom at the reaction points.

8.11 PHASE DIAGRAMS WITH INTERMEDIATE PHASES AND COMPOUNDS

The phase diagrams considered so far have been relatively simple and contained only a small number of phases and have had only one invariant reaction. Many equilibrium diagrams are complex and often show intermediate phases or compounds. In phase-diagram terminology, it is convenient to distinguish between two types of solid solutions: **terminal phases** and **intermediate phases.** Terminal solid-solution phases occur at the ends of phase diagrams, bordering on pure components. The α and β solid solutions of the Pb-Sn diagram (Fig. 8.12) are examples. Intermediate solid-solution phases occur in a composition range inside the phase diagram and are separated from other phases in a binary diagram by two-phase regions. The Cu-Zn phase diagram has both terminal and intermediate phases (Fig. 8.26). In this system, α and η are terminal phases, and β, γ, δ, and ϵ are intermediate phases. The Cu-Zn diagram contains five invariant peritectic points and one eutectoid invariant point at the lowest point of the δ intermediate-phase region.

Intermediate phases are not restricted to binary metal phase diagrams. In the ceramic phase diagram of the $Al_2O_3-SiO_2$ system, an intermediate phase called

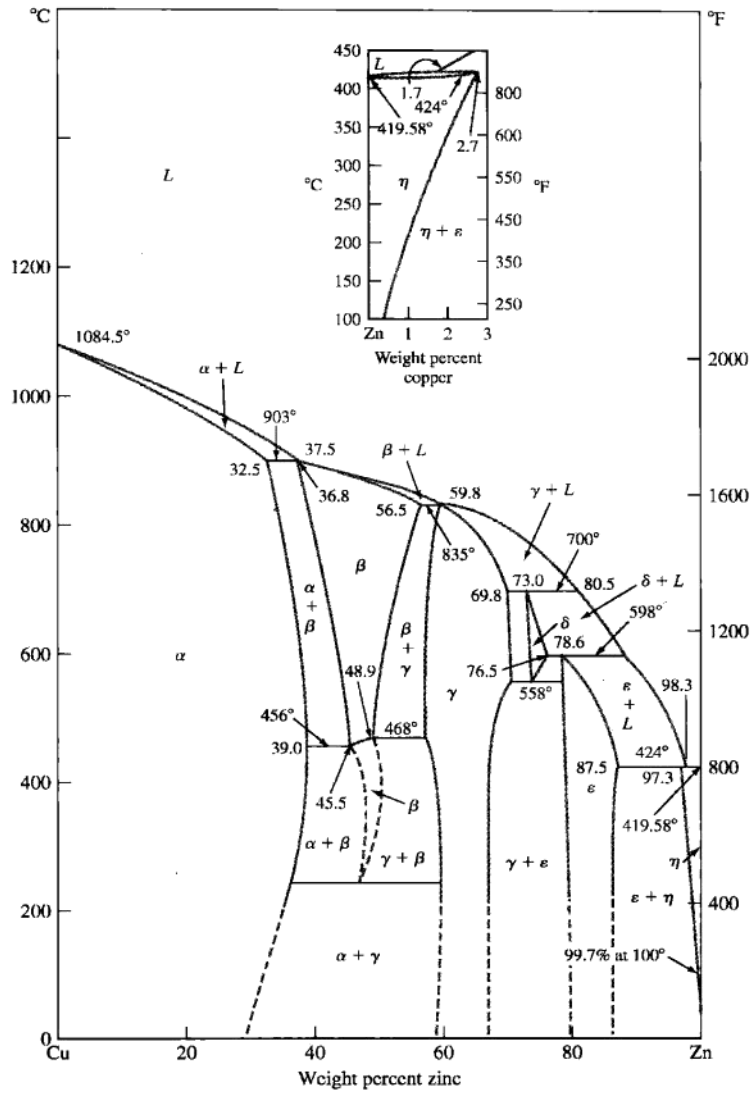

Figure 8.26
The copper-zinc phase diagram. This diagram has terminal phases α and η and intermediate phases β, γ, δ, and ϵ There are five invariant peritectic points and one eutectoid point.
(After "Metals Handbook," vol. 8: "Metallography, Structures, and Phase Diagrams," 8th ed., American Society for Metals, 1973, p. 301.)

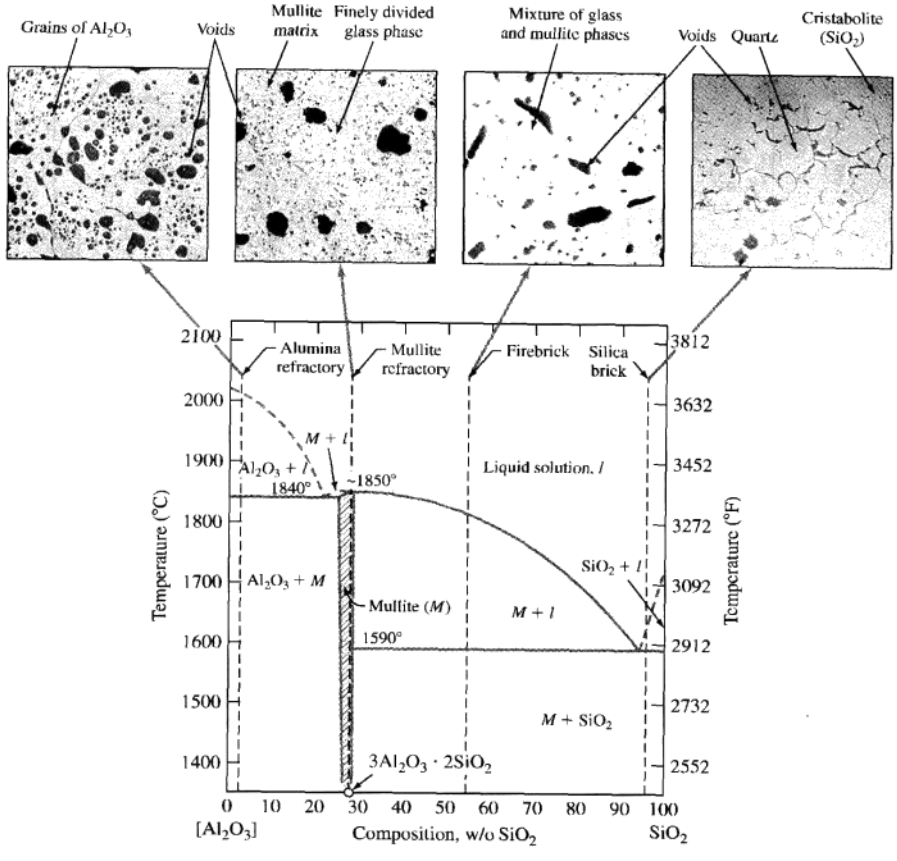

Figure 8.27
The phase diagram of the Al_2O_3–SiO_2 system, which contains mullite as an intermediate phase. Typical compositions of refractories having Al_2O_3 and SiO_2 as their main components are shown.
(After A.G. Guy, "Essentials of Materials Science," McGraw-Hill, 1976.)

mullite is formed, which includes the compound $3Al_2O_3 \cdot 2SiO_2$ (Fig. 8.27). Many refractories[5] have Al_2O_3 and SiO_2 as their main components. These materials will be discussed in Chap. 11 on ceramic materials.

If the intermediate compound is formed between two metals, the resulting material is a crystalline material called an *intermetallic compound* or simply an *intermetallic*. Generally speaking, the intermetallic compounds should have a distinct chemical formula or be stoichiometric (fixed ratio of involved atoms). However, in

[5]A refractory is a heat-resisting ceramic material.

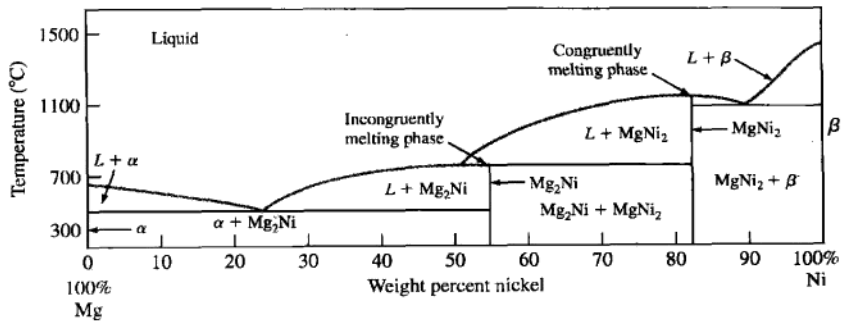

Figure 8.28
The magnesium-nickel phase diagram. In this diagram there are two intermetallic compounds, Mg_2Ni and $MgNi_2$.
(From A.G. Guy, "Essentials of Materials Science," McGraw-Hill, 1976.)

many cases, a certain degree of atomic substitution takes place that accommodates large deviations from stoichiometry. In a phase diagram, intermetallics appear either as a single vertical line, signifying the stoichiometric nature of the compound (see $TiNi_3$ line in Fig. EP8.8), or sometimes as a range of composition, signifying a non-stoichiometric compound (for example, the substitution of Cu for Zn or Zn for Cu atoms in the β and γ phases of the Cu-Zn phase diagram shown in Fig. 8.26). The majority of the intermetallic compounds possess a mixture of metallic-ionic or metallic-covalent bonds. The percentage of ionic or covalent bonds formed in intermetallic compounds depends on the differences in the electronegativities of the elements involved (see Sec. 2.4).

The Mg-Ni phase diagram contains the intermediate compounds Mg_2Ni and $MgNi_2$, which are primarily metallically bonded and have fixed compositions and definite stoichiometries (Fig. 8.28). The intermetallic compound $MgNi_2$ is said to be a *congruently melting compound* since it maintains its composition right up to the melting point. On the other hand, Mg_2Ni is said to be an *incongruently melting compound* since, upon heating, it undergoes peritectic decomposition at 761°C into liquid and $MgNi_2$ phases. Other examples of intermediate compounds that occur in phase diagrams are Fe_3C and Mg_2Si. In Fe_3C, the bonding is mainly metallic in character, but in Mg_2Si, the bonding is mainly covalent.

EXAMPLE PROBLEM 8.8

Consider the titanium-nickel (Ti-Ni) phase diagram in Fig. EP8.8. This phase diagram has six points where three phases coexist. For each of these three-phase points:

a. List the coordinates of composition (weight percent) and temperature for each point.
b. Write the invariant reaction that occurs during slow cooling of the Ti-Ni alloy through each point.
c. Name the type of invariant reaction that takes place at each point.

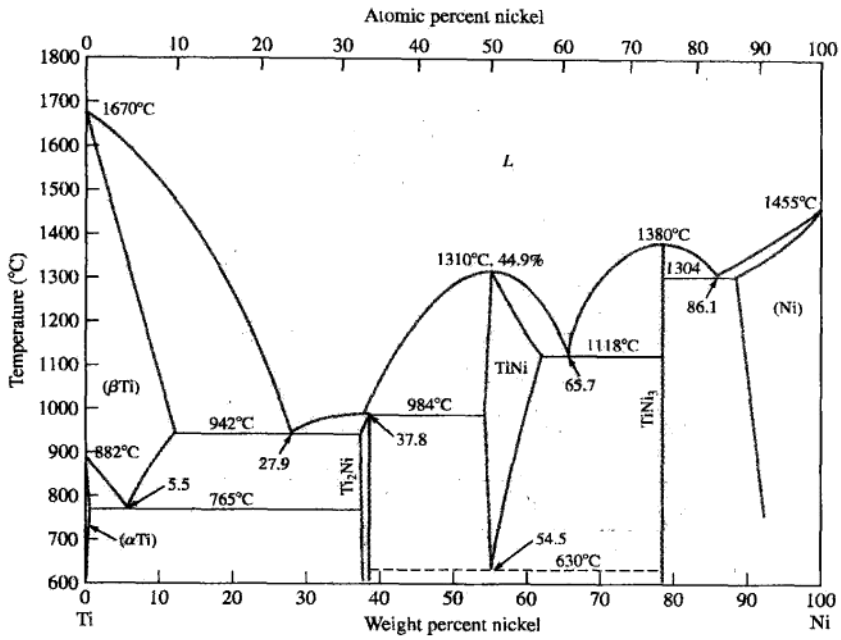

Figure EP8.8
Titanium-nickel phase diagram.
(After "Binary Alloy Phase Diagrams," ASM Int., 1986, p. 1768.)

■ Solution

a. (i) 5.5 wt % Ni, 765°C
(ii) $(\beta\ \text{Ti}) \longrightarrow (\alpha\ \text{Ti}) + \text{Ti}_2\text{Ni}$
(iii) Eutectoid reaction

b. (i) 27.9 wt % Ni, 942°C
(ii) $L \longrightarrow (\beta\ \text{Ti}) + \text{Ti}_2\text{Ni}$
(iii) Eutectic reaction

c. (i) 37.8 wt % Ni, 984°C
(ii) $L + \text{TiNi} \longrightarrow \text{Ti}_2\text{Ni}$
(iii) Peritectic reaction

d. (i) 54.5 wt % Ni, 630°C
(ii) $\text{TiNi} \longrightarrow \text{Ti}_2\text{Ni} + \text{TiNi}_3$
(iii) Eutectoid reaction

e. (i) 65.7 wt % Ni, 1118°C
(ii) $L \longrightarrow \text{TiNi} + \text{TiNi}_3$
(iii) Eutectic reaction

f. (i) 86.1 wt % Ni, 1304°C
(ii) $L \longrightarrow \text{TiNi}_3 + (\text{Ni})$
(iii) Eutectic reaction

8.12 TERNARY PHASE DIAGRAMS

Until now we have discussed only binary phase diagrams in which there are two components. We shall now turn our attention to ternary phase diagrams that have three components. Compositions on ternary phase diagrams are usually constructed by using an equilateral triangle as a base. Compositions of ternary systems are

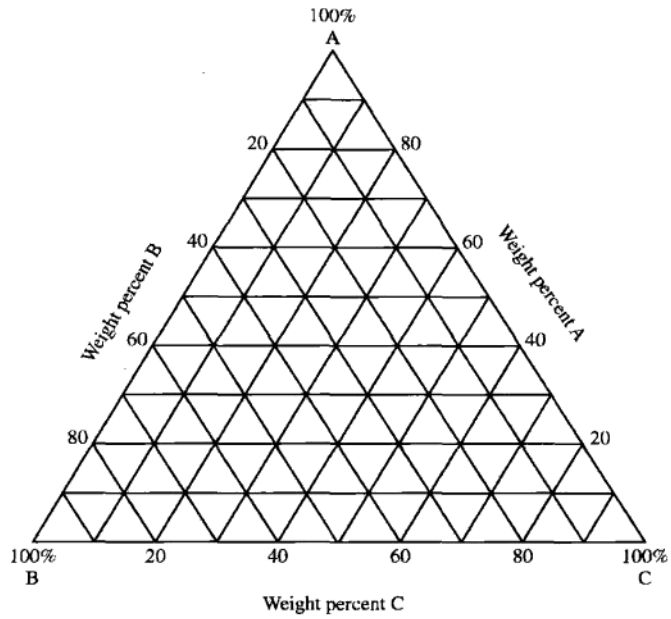

Figure 8.29
Composition base for a ternary phase diagram for a system with pure components A, B, and C.
(From "Metals Handbook," vol. 8, 8th ed., American Society for Metals, 1973, p. 314. Used by permission of ASM International.)

represented on this base with the pure component at each end of the triangle. Figure 8.29 shows the composition base of a ternary phase diagram for a ternary metal alloy consisting of pure metals A, B, and C. The binary alloy compositions AB, BC, and AC are represented on the three edges of the triangle.

Ternary phase diagrams with a triangular composition base are normally constructed at a constant pressure of 1 atm. Temperature can be represented as uniform throughout the whole diagram. This type of ternary diagram is called an *isothermal section.* To show a range of temperatures at varying compositions, a figure with temperature on a vertical axis with a triangular composition base can be constructed. However, more commonly, temperature contour lines are drawn on a triangular composition base to indicate temperature ranges just as different elevations are shown on a flat-page map of a terrain.

Let us now consider the determination of the composition of a ternary alloy indicated by a point on a ternary diagram of the type shown in Fig. 8.29. In Fig. 8.29 the *A* corner of the triangle indicates 100 percent metal A, the *B* corner indicates 100 percent metal B, and the *C* corner indicates 100 percent metal C. The weight percent of each pure metal in the alloy is determined in the following way: A perpendicular line is drawn from a pure metal corner to the side of the triangle opposite that corner, and the distance *from* the side to the corner along the perpendicular line is measured as

a fraction of 100 percent for the whole line. This percentage is the weight percent of the pure metal of that corner in the alloy. Example Problem 8.9 explains this procedure in more detail.

EXAMPLE PROBLEM 8.9

Determine the weight percents of metals A, B, and C for a ternary alloy ABC at point x on the ternary phase diagram grid shown in Fig. EP8.9.

■ Solution

The composition at a point in a ternary phase diagram grid of the type shown in Fig. EP8.9 is determined by separately determining the compositions of each of the pure metals from the diagram. To determine the percent A at point x in Fig. EP8.9, we first draw the perpendicular line AD from the corner A to point D on the side of the triangle opposite corner A. The total length of the line from D to A represents 100 percent A. At point D, the percent A in the alloy is zero. The point x is on an isocomposition line at 40 percent A, and thus the percentage of A in the alloy is 40 percent. In a similar manner, we draw line BE and determine that the percentage of B in the alloy is also 40 percent. A third line CF is drawn, and the percentage of C in the alloy is determined to be 20 percent. Thus, the composition of the ternary alloy at point x is 40 percent A, 40 percent B, and 20 percent C. Actually only two percentages need to be determined since the third can be obtained by subtracting the sum of the two from 100 percent.

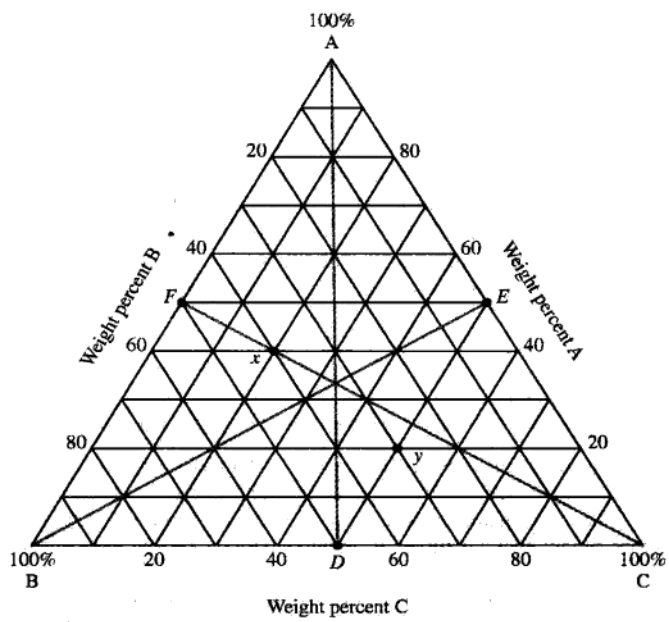

Figure EP8.9
Ternary phase diagram composition base for an ABC alloy.

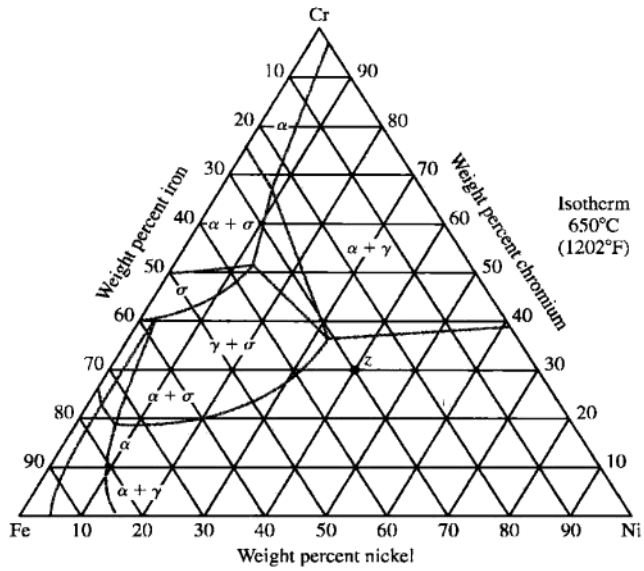

Figure 8.30
Ternary phase diagram of an isothermal section at 650°C (1202°F) for the iron-chromium-nickel system.
(After "Metals Handbook," vol. 8, 8th ed., American Society for Metals, 1973, p. 425.)

The ternary phase diagram of iron, chromium, and nickel is important since the commercially most important stainless steel has a composition essentially of 74 percent iron, 18 percent chromium, and 8 percent nickel. Figure 8.30 shows an isothermal section at 650°C (1202°F) for the iron-chromium-nickel ternary system.

Ternary phase diagrams also are important for the study of some ceramic materials. Figure 11.34 shows a ternary phase diagram of the important silica-leucite-mullite system.

8.13 SUMMARY

Phase diagrams are graphical representations of what phases are present in an alloy (or ceramic) system at various temperatures, pressures, and compositions. Phase diagrams are constructed using the information gathered from cooling curves. Cooling curves are time temperature plots generated for various alloy compositions and provide information about phase transition temperatures. In this chapter, the emphasis has been placed on temperature-composition binary equilibrium phase diagrams. These diagrams tell us which phases are present at different compositions and temperatures for slow cooling or heating conditions that approach equilibrium. In two-phase regions of these diagrams, the chemical compositions of each of the two phases is indicated by the intersection of the isotherm with the phase boundaries. The weight fraction of each phase in a two-phase region can be determined by using the lever rule along an isotherm (tie line at a particular temperature).

In binary equilibrium *isomorphous phase diagrams*, the two components are completely soluble in each other in the solid state, and so there is only one solid phase. In binary equilibrium alloy (ceramic) phase diagrams, *invariant reactions* involving three phases in equilibrium often occur The most common of these reactions are

1. Eutectic reaction: $L \rightarrow \alpha + \beta$
2. Eutectoid reaction: $\alpha \rightarrow \beta + \gamma$
3. Peritectic reaction: $\alpha + L \rightarrow \beta$
4. Peritectoid reaction: $\alpha + \beta \rightarrow \gamma$
5. Monotectic reaction. $L_1 \rightarrow \alpha + L_2$

In many binary equilibrium phase diagrams, intermediate phase(s) and/or compounds are present The intermediate phases have a range of compositions, whereas the intermediate compounds have only one composition. If the components are both metal, the intermediate compound is called an *intermetallic*.

During the rapid solidification of many alloys, compositional gradients are created and *cored* structures are produced A cored structure can be eliminated by homogenizing the cast alloy for long times at high temperatures just below the melting temperature of the lowest melting phase in the alloy. If the cast alloy is overheated slightly so that melting occurs at the grain boundaries, a *liquated* structure is produced. This type of structure is undesirable since the alloy loses strength and may break up during subsequent working.

8.14 DEFINITIONS

Sec. 8.1

Phase: a physically homogeneous and distinct portion of a material system.

Equilibrium: a system is said to be in equilibrium if no macroscopic changes take place with time

Equilibrium phase diagram: a graphical representation of the pressures, temperatures, and compositions for which various phases are stable at equilibrium. In materials science, the most common phase diagrams involve temperature versus composition.

Sec. 8.2

System: a portion of the universe that has been isolated so that its properties can be studied

Gibbs phase rule: the statement that at equilibrium the number of phases plus the degrees of freedom equals the number of components plus 2. $P + F = C + 2$. In the condensed form with pressure $\approx$ 1 atm, $P + F = C + 1$.

Degrees of freedom F: the number of variables (temperature, pressure, and composition) that can be changed *independently* without changing the phase or phases of the system.

Number of components of a phase diagram: the number of elements or compounds that make up the phase-diagram system. For example, the Fe-Fe_3C system is a two-component system; the Fe-Ni system is also a two-component system.

Sec 8.3

Cooling curve: plots of temperature vs time acquired during solidification of a metal. It provides phase change information as the temperature is lowered.

Thermal arrest: a region of the cooling curve for a pure metal where temperature does not change with time (plateau), representing the freezing temperature.

Sec. 8.4

Isomorphous system: a phase diagram in which there is only one solid phase, i e , there is only one solid-state structure.

Liquidus: the temperature at which liquid starts to solidify under equilibrium conditions.
Solidus: the temperature during the solidification of an alloy at which the last of the liquid phase solidifies.

Sec. 8.5
Lever rule: the weight percentages of the phases in any two-phase region of a binary phase diagram can be calculated using this rule if equilibrium conditions prevail.
Tie line: a horizontal working line drawn at a particular temperature between two phase boundaries (in a binary phase diagram) to be used to apply the lever rule. Vertical lines are drawn from the intersection of the tie line with the phase boundaries to the horizontal composition line. A vertical line is also drawn from the tie line to the horizontal line at the intersection point of the tie line with the alloy of interest to use with the lever rule.

Sec. 8.6
Cored structure: a type of microstructure that occurs during rapid solidification or non-equilibrium cooling of a metal.
Homogenization: a heat treatment process given to a metal to remove undesirable cored structures.

Sec. 8.7
Solvus: a phase boundary below the isothermal liquid + proeutectic solid phase boundary and between the terminal solid solution and two-phase regions in a binary eutectic phase diagram.
Eutectic composition: the composition of the liquid phase that reacts to form two new solid phases at the eutectic temperature.
Eutectic temperature: the temperature at which a eutectic reaction takes place.
Eutectic point: the point determined by the eutectic composition and temperature.
Eutectic reaction (in a binary phase diagram): a phase transformation in which all the liquid phase transforms on cooling into two solid phases isothermally.
Hypoeutectic composition: one that is to the left of the eutectic point.
Hypereutectic composition: one that is to the right of the eutectic point.
Primary phase: a solid phase that forms at a temperature above that of an invariant reaction and is still present after the invariant reaction is completed.
Proeutectic phase: a phase that forms at a temperature above the eutectic temperature.

Sec. 8.8
Peritectic reaction (in a binary phase diagram): a phase transformation in which, upon cooling, a liquid phase combines with a solid phase to produce a new solid phase.

Sec. 8.9
Monotectic reaction (in a binary phase diagram): a phase transformation in which, upon cooling, a liquid phase transforms into a solid phase and a new liquid phase (of different composition than the first liquid phase).

Sec. 8.10
Invariant reactions: those reactions in which the reacting phases have fixed temperature and composition. The degree of freedom, F, is zero at these reaction points.

Sec. 8.11
Terminal phase: a solid solution of one component in another for which one boundary of the phase field is a pure component.
Intermediate phase: a phase whose composition range is between those of the terminal phases.

8.15 PROBLEMS

Answers to problems marked with an asterisk are given at the end of the book.

Knowledge and Comprehension Problems

8.1 Define (*a*) a phase in a material and (*b*) a phase diagram.

8.2 In the pure water pressure-temperature equilibrium phase diagram (Fig. 8.1), what phases are in equilibrium for the following conditions: (*a*) along the freezing line, (*b*) along the vaporization line, and (*c*) at the triple point.

8.3 How many triple points are there in the pure iron pressure-temperature equilibrium phase diagram of Fig. 8.2? What phases are in equilibrium at each of the triple points?

8.4 Write the equation for Gibbs phase rule and define each of the terms.

8.5 Refer to the pressure-temperature equilibrium phase diagram for pure water (Fig. 8.1) and answer the following:

(*a*) How many degrees of freedom are there at the triple point?

(*b*) How many degrees of freedom are there along the freezing line?

8.6 (*a*) What is a cooling curve? (*b*) What type of information may be extracted from a cooling curve? (*c*) Draw a schematic of a cooling curve for a pure metal and one for an alloy. Discuss the differences.

8.7 What is a binary isomorphous alloy system?

8.8 What are the four Hume-Rothery rules for the solid solubility of one element in another?

8.9 Describe how the liquidus and solidus of a binary isomorphous phase diagram can be determined experimentally.

8.10 Explain how a cored structure is produced in a 70% Cu–30% Ni alloy.

8.11 How can the cored structure in a 70% Cu–30% Ni alloy be eliminated by heat treatment?

8.12 Explain what is meant by the term *liquation*. How can a liquated structure be produced in an alloy? How can it be avoided?

8.13 Describe the mechanism that produces the phenomenon of *surrounding* in a peritectic alloy that is rapidly solidified through the peritectic reaction.

8.14 Can coring and surrounding occur in a peritectic-type alloy that is rapidly solidified? Explain.

8.15 What is a monotectic invariant reaction? How is the monotectic reaction in the copper-lead system important industrially?

8.16 Write equations for the following invariant reactions: eutectic, eutectoid, peritectic, and peritectoid. How many degrees of freedom exist at invariant reaction points in binary phase diagrams?

8.17 How are eutectic and eutectoid reactions similar? What is the significance of the *−oid* suffix?

8.18 Distinguish between (*a*) a terminal phase and (*b*) an intermediate phase.

8.19 Distinguish between (*a*) an intermediate phase and (*b*) an intermediate compound.

8.20 What is the difference between a congruently melting compound and an incongruently melting one?

Application and Analysis Problems

***8.21** Consider an alloy containing 70 wt % Ni and 30 wt % Cu (see Fig. 8.5).

(*a*) At 1350°C, make a phase analysis assuming equilibrium conditions. In the phase analysis, include the following:

(*i*) What phases are present?

(*ii*) What is the chemical composition of each phase?

(*iii*) What amount of each phase is present?

(*b*) Make a similar phase analysis at 1500°C.

(*c*) Sketch the microstructure of the alloy at each of these temperatures by using circular microscopic fields.

8.22 Consider the binary eutectic copper-silver phase diagram in Fig. P8.22. Make phase analyses of an 88 wt % Ag–12 wt % Cu alloy at the temperatures (*a*) 1000°C, (*b*) 800°C, (*c*) 780°C + ΔT, and (*d*) 780°C − ΔT. In the phase analyses, include:

(*i*) The phases present

(*ii*) The chemical compositions of the phases

(*iii*) The amounts of each phase

(*iv*) Sketch the microstructure by using 2-cm diameter circular fields.

8.23 If 500 g of a 40 wt % Ag–60 wt % Cu alloy is slowly cooled from 1000°C to just below 780°C (see Fig. P8.22):

(*a*) How many grams of liquid and proeutectic alpha are present at 850°C?

(*b*) How many grams of liquid and proeutectic alpha are present at 780°C + ΔT?

(*c*) How many grams of alpha are present in the eutectic structure at 780°C − ΔT?

(*d*) How many grams of beta are present in the eutectic structure at 780°C − ΔT?

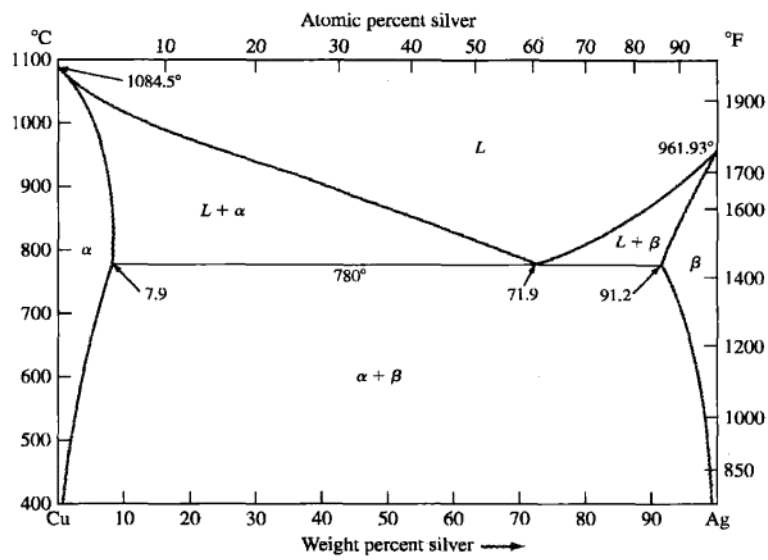

Figure P8.22
The copper-silver phase diagram.
(After "Metals Handbook," vol. 8, 8th ed., American Society for Metals, 1973, p. 253.)

8.24 A lead-tin (Pb–Sn) alloy consists of 60 wt % proeutectic β and 60 wt % eutectic $\alpha + \beta$ at 183°C $- \Delta T$. Calculate the average composition of this alloy (see Fig. 8.12).

8.25 A Pb–Sn alloy (Fig. 8.12) contains 40 wt % β and 60 wt % α at 50°C. What is the average composition of Pb and Sn in this alloy?

***8.26** An alloy of 30 wt % Pb– 70 wt % Sn is slowly cooled from 250°C to 27°C (see Fig. 8.12).

(*a*) Is this alloy hypoeutectic or hypereutectic?

(*b*) What is the composition of the first solid to form?

(*c*) What are the amounts and compositions of each phase that is present at 183°C + ΔT?

(*d*) What is the amount and composition of each phase that is present at 183°C $- \Delta T$?

(*e*) What are the amounts of each phase present at room temperature?

8.27 Consider the binary peritectic iridium-osmium phase diagram of Fig. P8.27. Make phase analyses of a 70 wt % Ir–30 wt % Os at the temperatures (*a*) 2600°C, (*b*) 2665°C + ΔT, and (*c*) 2665°C $- \Delta T$. In the phase analyses include:

(*i*) The phases present

(*ii*) The chemical compositions of the phases

(*iii*) The amounts of each phase

(*iv*) Sketch the microstructure by using 2 cm diameter circular fields.

8.28 Consider the binary peritectic iridium-osmium phase diagram of Fig. P8.27. Make phase analyses of a 40 wt % Ir–60 wt % Os at the temperatures (*a*) 2600°C, (*b*) 2665°C + ΔT, (*c*) 2665°C $- \Delta T$, and (*d*) 2800°C. Include in the phase analyses the four items listed in Prob. 8.20.

8.29 Consider the binary peritectic iridium-osmium phase diagram of Fig. P8.27. Make phase analyses of a 70 wt % Ir–30 wt % Os at the temperatures (*a*) 2600°C, (b) 2665°C + ΔT, and (*c*) 2665°C $- \Delta T$. In the phase analyses include:

(*i*) The phases present

(*ii*) The chemical compositions of the phases

(*iii*) The amounts of each phase

(*iv*) Sketch the microstructure by using 2-cm diameter circular fields.

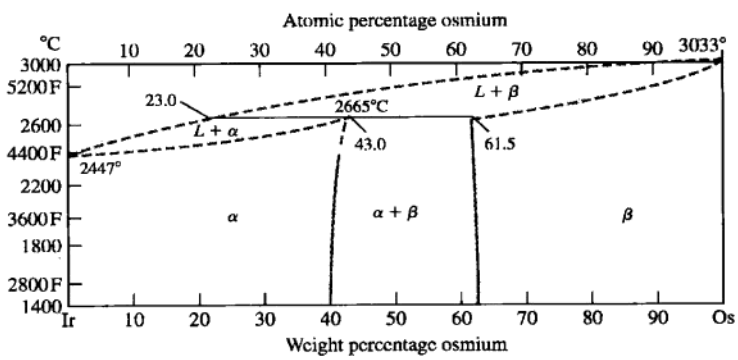

Figure P8.27
The iridium-osmium phase diagram.
(From "Metals Handbook," vol. 8, 8th ed., American Society for Metals, 1973, p. 425. Used by permission of ASM International.)

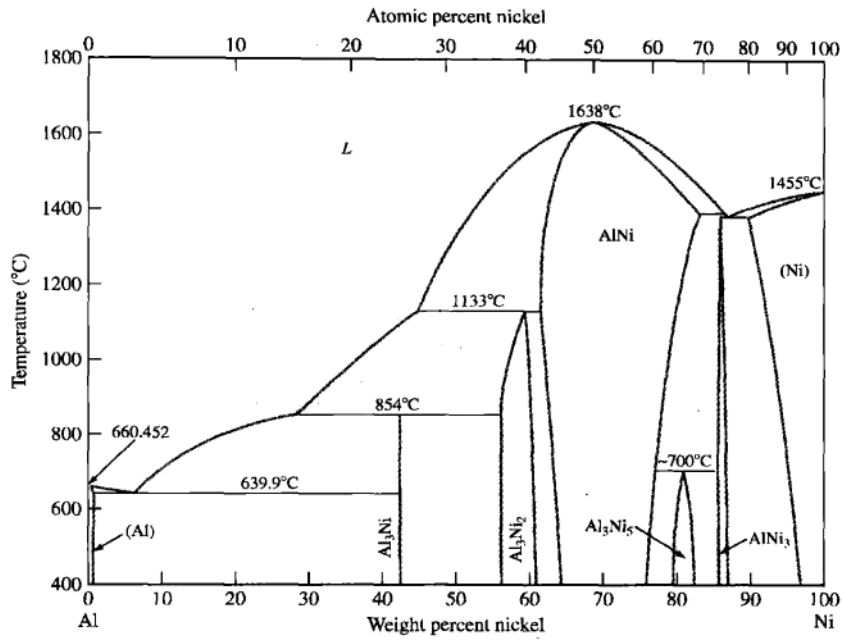

Figure P8.39
Aluminum-nickel phase diagram.
(From "Metals Handbook", vol. 8, 8th ed., American Society for Metals, 1973, p. 253. Used by permission of ASM International.)

***8.30** In the copper-lead (Cu-Pb) system (Fig. 8.24) for an alloy of Cu–10 wt % Pb, determine the amounts and compositions of the phases present at (*a*) 1000°C, (*b*) 955°C + ΔT, (*c*) 955°C − ΔT, and (*d*) 200°C.

8.31 For an alloy of Cu–70 wt % Pb (Fig. 8.24), determine the amounts and compositions in weight percent of the phases present at (*a*) 955°C + ΔT, (*b*) 955°C − ΔT, and (*c*) 200°C.

8.32 What is the average composition (weight percent) of a Cu-Pb alloy that contains 30 wt % L_1 and 70 wt % α at 955°C + ΔT?

8.33 Consider an Fe–4.2 wt % Ni alloy (Fig. 8.17) that is slowly cooled from 1550°C to 1450°C. What weight percent of the alloy solidifies by the peritectic reaction?

***8.34** Consider an Fe–5.0 wt % Ni alloy (Fig. 8.17) that is slowly cooled from 1550°C to 1450°C. What weight percent of the alloy solidifies by the peritectic reaction?

8.35 Determine the weight percent and composition in weight percent of each phase present in an Fe–4.2 wt % Ni alloy (Fig. 8.17) at 1517°C + ΔT.

8.36 Determine the composition in weight percent of the alloy in the Fe–Ni system (Fig. 8.17) that will produce a structure of 40 wt % δ and 60 wt % γ just below the peritectic temperature.

8.37 Draw, schematically, the liquidus and the solidus lines for Cu-Zn diagram (Fig. 8.26). Show all the critical zinc contents and temperatures. Which one of these temperatures should be important to metal-forming processes? Why?

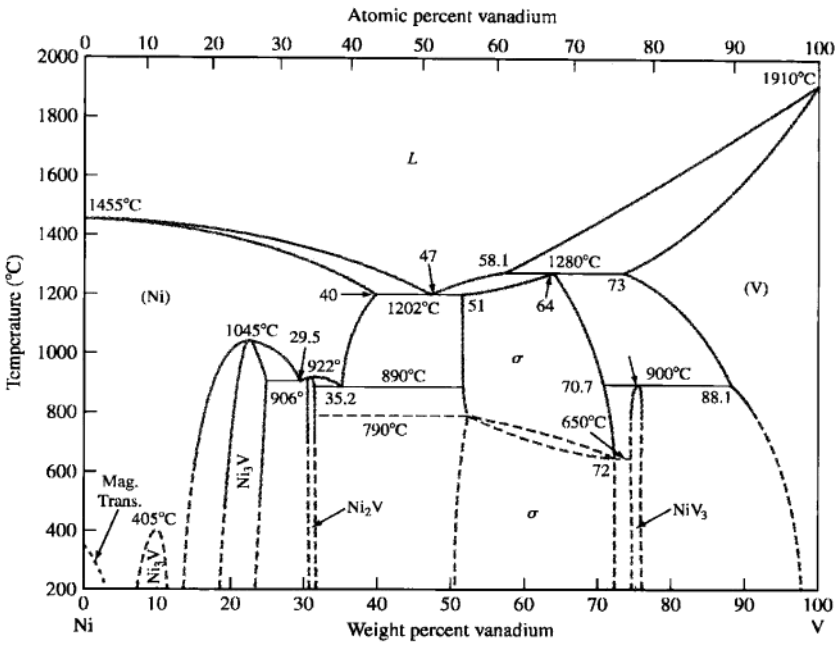

Figure P8.40
Nickel-vanadium phase diagram.
(From "Metals Handbook," vol. 8, 8th ed., American Society for Metals, 1973, p. 332. Used by permission of ASM International.)

***8.38** Consider the Cu-Zn phase diagram of Fig. 8.26.
- (*a*) What is the maximum solid solubility in weight percent of Zn in Cu in the terminal solid solution α?
- (*b*) Identify the intermediate phases in the Cu-Zn phase diagram.
- (*c*) Identify the three-phase invariant reactions in the Cu-Zn diagram.
  - (*i*) Determine the composition and temperature coordinates of the invariant reactions.
  - (*ii*) Write the equations for the invariant reactions.
  - (*iii*) Name the invariant reactions.

8.39 Consider the aluminum-nickel phase diagram of Fig. P8.39. For this phase diagram:
- (*a*) Determine the coordinates of the composition and temperature of the invariant reactions.
- (*b*) Write the equations for the three-phase invariant reactions and name them.
- (*c*) Label the two-phase regions in the phase diagram.

8.40 Consider the nickel-vanadium phase diagram of Fig. P8.40. For this phase diagram, repeat questions of Prob. 8.38.

8.41 Consider the titanium-aluminum phase diagram of Fig. P8.41. For this phase diagram, repeat the questions of Prob. 8.38.

8.42 What is the composition of point *y* in Fig. EP8.9?

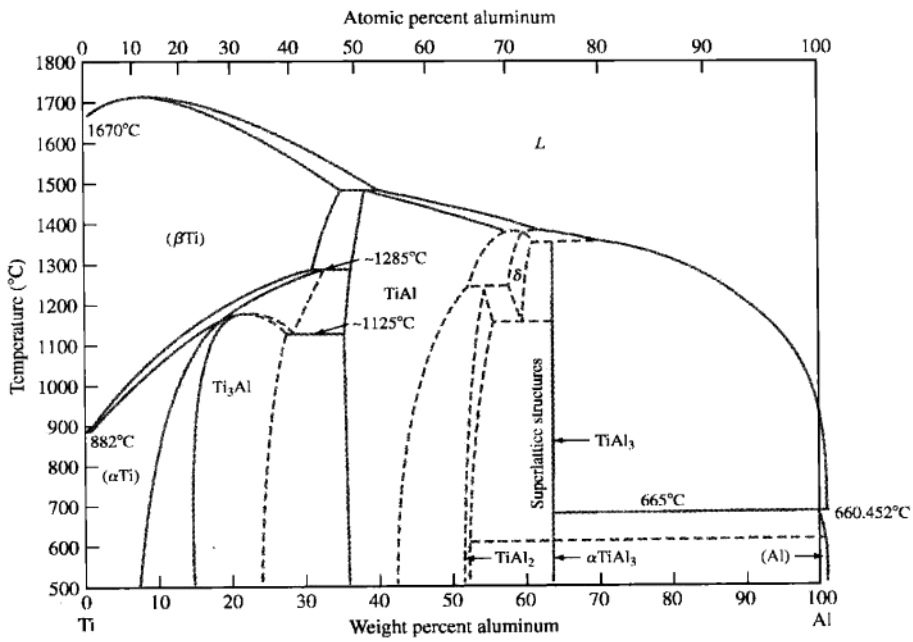

Figure P8.41
Titanium-aluminum phase diagram
(From "Binary Phase Diagrams," ASM Int, 1986, p 142 Used by permission of ASM International)

Synthesis and Evaluation Problems

***8.43** In Fig. 8.12, determine the degree of freedom, F, according to Gibbs rule at the following points:

(*a*) At the melting point of pure tin.
(*b*) Inside the α region.
(*c*) Inside the α + liquid region
(*d*) Inside the $\alpha + \beta$ region
(*e*) At the eutectic point

8.44 In the Pb-Sn phase diagram (Fig. 8.12) answer the following questions:

(*a*) What is α (explain in detail including atomic structure? What is β?
(*b*) What the maximum solubility of Sn in α? At what temperature?
(*c*) What happens to the α in part (*b*) if it is cooled to room temperature?
(*d*) What is the maximum solubility of Sn in liquid metal at the lowest possible temperature? What is that temperature?
(*e*) What is the solubility limit of Sn in α when liquid is present? (This will be a range.)

8.45 Based on the Cu – Ag phase diagram in Fig. P8.22, draw the approximate cooling curve for the following alloys with approximate temperatures and explanations:
(*i*) Pure Cu, (*ii*) Cu – 10wt% Ag (*iii*) Cu – 71.9 wt% Ag (*iv*) Cu – 91.2 wt% Ag

8.46 Based on the Pd – Ag phase diagram in Fig. EP 8.3, draw the approximate cooling curve for the following alloys with approximate temperatures and explanations:
(*i*) Pure Pd, (*ii*) Pd – 30wt% Ag (*iii*) Pd – 70 wt% Ag (*iv*) Pure Ag

8.47 A number of elements along with their crystal structures and atomic radii are listed in the following table. Which pairs might be expected to have complete solid solubility in each other?

	Crystal structure	Atomic radius (nm)		Crystal structure	Atomic radius (nm)
Silver	FCC	0.144	Lead	FCC	0.175
Palladium	FCC	0.137	Tungsten	BCC	0.137
Copper	FCC	0.128	Rhodium	FCC	0.134
Gold	FCC	0.144	Platinum	FCC	0.138
Nickel	FCC	0.125	Tantalum	BCC	0.143
Aluminum	FCC	0.143	Potassium	BCC	0.231
Sodium	BCC	0.185	Molybdenum	BCC	0.136

8.48 Derive the lever rule for the amount in weight percent of each phase in two-phase regions of a binary phase diagram. Use a phase diagram in which two elements are completely soluble in each other.

8.49 Based on the Al – Ni phase diagram given in Fig. P8.39, how many grams of Ni should be alloyed with 100 grams of Al to synthesize an alloy of liquidus temperature of approximately 640°C?

8.50 An Al-10 wt % Ni alloy, Fig. P8.39, is completely liquid at 800°C. How many grams of Ni can you add to this alloy at 800°C without creating a solid phase?

8.51 Based on the Al_2O_3-SiO_2 phase diagram in Fig. 8.27, the wt% of phases present for Al_2O_3 – 55 wt% SiO_2 over the 1900 to 1500°C temperature range (use 100°C increments).

8.52 (*a*) Design a Cu-Ni alloy that will be completely solid at 1200°C (use Fig. 8.5). (*b*) Design a Cu-Ni alloy that will exist at a completely molten state at 1300°C and becomes completely solid at 1200°C.

8.53 (*a*) Design a Pb-Sn alloy that will have a 50-50 solid and liquid phase fraction at 184°C. (*b*) How many grams of each component should you use to produce 100 grams of the overall alloy? (Use Fig. 8.12.)

8.54 Given that Pb and Sn have similar tensile strengths, design a Pb-Sn alloy that when cast would be the strongest alloy (use Fig. 8.12). Explain your reasons for your choice.

***8.55** Consider the sugar-water phase diagram shown in Fig. P8.55. (*a*) What wt% sugar can you dissolve in water at room temperature? (*b*) What wt% sugar can you dissolve in water at 100°C? (*c*) What would you call the solid curve?

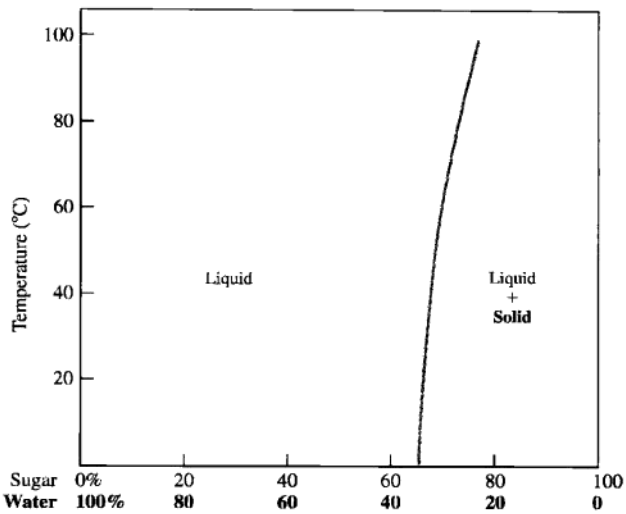

Figure P8.55

8.56 In Fig. P8.55, if 60 grams of water and 140 grams of sugar are mixed and stirred at a temperature of 80°C, (*a*) will this result in a single phase solution or a mixture? (*b*) What will happen if the solution/mixture in part (*a*) is slowly cooled to room temperature?

8.57 In Fig. P8.55, if 30 grams of water and 170 grams of sugar are mixed and stirred at a temperature of 30°C, (*a*) will this result in a single phase solution or a mixture? (*b*) If it's a mixture, how many grams of solid sugar will exist in the mixture? (*c*) How many grams of sugar (solid and dissolved) will exist in the mixture?

8.58 At 80°C, if the wt% of sugar is 80%, (*a*) what phases exist? (*b*) What is the weight fraction of each phase? (*c*) What is the wt% of water?

8.59 (*a*) Based on the phase diagram in Fig. P8.59, explain why city workers throw rock salt on icy roads. (*b*) Based on the same diagram, suggest a process that would produce almost pure water from seawater (3wt% salt).

***8.60** Referring to Fig. P8.59, explain what happens as 5wt% salt solution is cooled from room temperature to −30°C. Give information regarding phases available and the compositional changes in each phase.

8.61 Referring to Fig. P8.59, (*a*) explain what happens as 23wt% salt solution is cooled from room temperature to −30°C. Give information regarding phases available and the compositional changes in each phase. (*b*) What would you call this reaction? Can you write a transformation equation for this reaction?

8.62 Using Fig. P8.39, explain what the phase diagram is showing when the overall alloy composition is Al – 43wt% Ni (below 854°C)? Why is there a vertical line at that point in the phase diagram? Verify that the formula for the compound is Al_3Ni. What do you call such a compound?

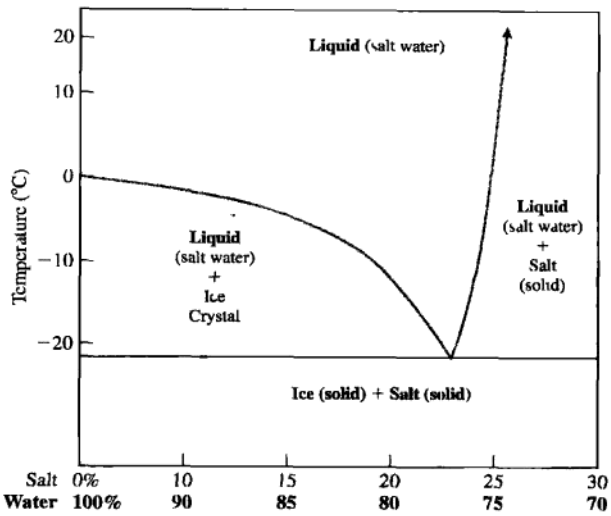

Figure P8.59

8.63 Using Fig. P8.39, explain why, according to the diagram, the intermetallic Al_3Ni is represented by a single vertical line while intermetallics Al_3Ni_2 and Al_3Ni_5 are represented by a region.

8.64 (*a*) In the Ti-Al phase diagram, Fig. P8.41, what phases are available at an overall alloy composition of Ti – 63 wt% Al at temperatures below 1300°C? (*b*) What is the significance of the vertical line at that alloy composition? (*c*) Verify the formula next to the vertical line. (*d*) Compare the melt temperature of this compound to that of Ti and Al. What is your conclusion?

CHAPTER

9 Engineering Alloys

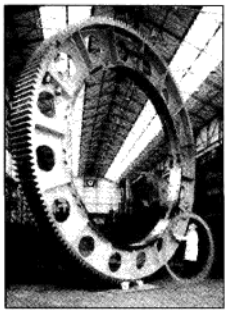
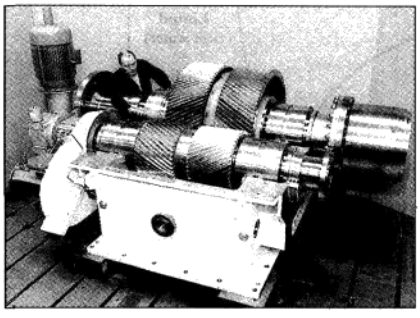


(© *Textron Power Transmission.*)

A variety of metal alloys such as plain-carbon steels, alloy steels, stainless steels, cast iron, and copper alloys are used in manufacturing various gears. For example, chromium steels are used for automobile transmission gears, chromium-molybdenum steels are used for aircraft gas turbine gears, nickel-molybdenum steels are used for earth moving equipment, and some copper alloys are used to manufacture gears for low load levels. The choice of the gear metal and its manufacturing depends on size, stresses involved, power requirements, and the environment in which they will operate. The chapter-opening photos show gears of various sizes used in various industries.[1] ■

[1] http://www.textronpt.com/cgi-bin/products.cgi?prod=highspeed&group=spcl

LEARNING OBJECTIVES

By the end of this chapter, students will be able to . . .

1. Describe steelmaking and processing of steel components, differentiate between plain carbon steel, alloy steel, cast iron, and stainless steel.
2. Reconstruct the iron-carbon phase diagram indicating all key phases, reactions, and microstructures.
3. Describe what pearlite and marteniste are, their mechanical property differences, their microstructural differences, and how they are produced.
4. Define isothermal and continuous cooling transformations.
5. Describe annealing, normalizing, quenching, tempering, martempering, and austempering processes.
6. Describe the classification of plain carbon and alloy steels, and explain the effect of various alloying elements on properties of steel.
7. Describe the classification, heat-treatability, microstructure, and general properties of aluminum alloys, copper alloys, stainless steels, and cast irons.
8. Explain the importance and applications of intermetallics, shape memory, and amorphous alloys.
9. Describe the advantages and disadvantages of alloys that are used in biomedical applications.

Metals and alloys have many useful engineering properties and so have widespread application in engineering designs. Iron and its alloys (principally steel) account for about 90 percent of the world's production of metals mainly because of their combination of good strength, toughness, and ductility at a relatively low cost. Each metal has special properties for engineering designs and is used after a comparative cost analysis with other metals and materials (see Table 9.1).

Alloys based on iron are called *ferrous alloys,* and those based on the other metals are called *nonferrous alloys.* In this chapter, we shall discuss some aspects of the

Table 9.1 Approximate prices ($/lb) of some metals as of May 2001*

Steel†	0.27	Nickel	2.74
Aluminum	0.67	Tin	2.30
Copper	0.76	Titanium‡	3.85
Magnesium	3.29	Gold	3108.00
Zinc	0.45	Silver	52.00
Lead	0.22		

*Prices of metals vary with time.
†Hot-rolled plain-carbon steel sheet.
‡Titanium sponge. Prices for large quantity.

processing, structure, and properties of some of the important ferrous and nonferrous alloys. The last two sections of this chapter are devoted to advanced alloys and their application to various fields, including the biomedical field.

9.1 PRODUCTION OF IRON AND STEEL

9.1.1 Production of Pig Iron in a Blast Furnace

Most iron is extracted from iron ores in large blast furnaces (Fig. 9.1). In the blast furnace coke (carbon) acts as a reducing agent to reduce iron oxides (mainly Fe_2O_3) to produce raw pig iron, which contains about 4 percent carbon along with some other impurities according to the typical reaction

$$Fe_2O_3 + 3CO \longrightarrow 2Fe + 3CO_2$$

The pig iron from the blast furnace is usually transferred in the liquid state to a steelmaking furnace.

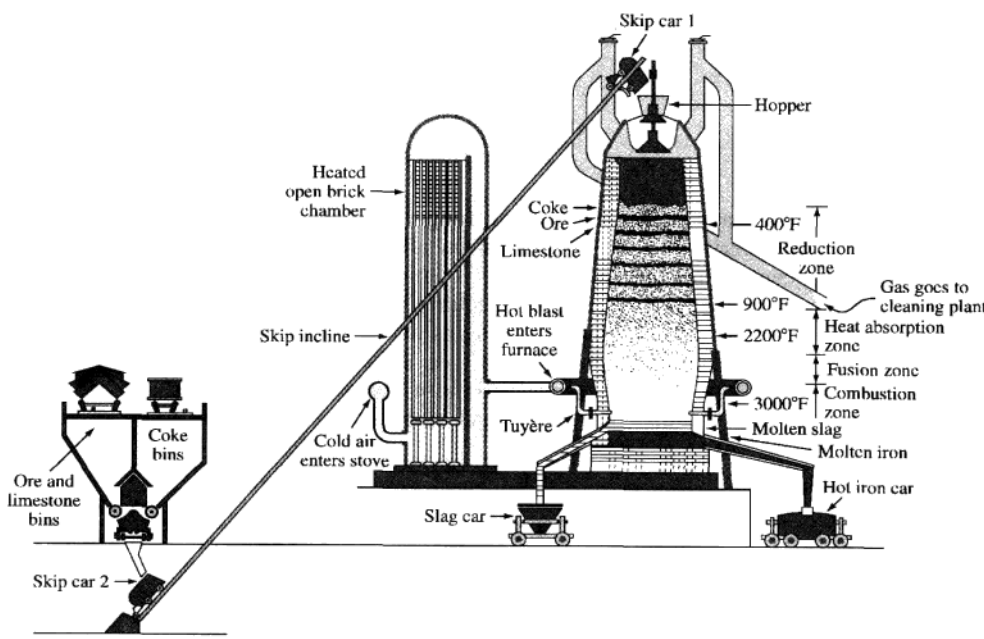

Figure 9.1
Cross section of the general operation of a modern blast furnace.
Animation *(After A.G. Guy, "Elements of Physical Metallurgy," 2d ed., © 1959, Addison-Wesley, Fig. 2-5, p. 21.)*

9.1.2 Steelmaking and Processing of Major Steel Product Forms

Plain-carbon steels are essentially alloys of iron and carbon with up to about 1.2 percent carbon. However, the majority of steels contain less than 0.5 percent carbon. Most steel is made by oxidizing the carbon and other impurities in the pig iron until the carbon content of the iron is reduced to the required level.

The most commonly used process for converting pig iron into steel is the basic-oxygen process. In this process pig iron and up to about 30 percent steel scrap are charged into a barrel-shaped refractory-lined converter into which an oxygen lance is inserted (Fig. 9.2). Pure oxygen from the lance reacts with the liquid bath to form iron oxide. Carbon in the steel then reacts with the iron oxide to form carbon monoxide:

$$FeO + C \longrightarrow Fe + CO$$

Immediately before the oxygen reaction starts, slag-forming fluxes (chiefly lime) are added in controlled amounts. In this process, the carbon content of the steel can be drastically lowered in about 22 min along with a reduction in the concentration of impurities such as sulfur and phosphorus (Fig. 9.3).

The molten steel from the converter is either cast in stationary molds or continuously cast into long slabs from which long sections are periodically cut off. Today approximately 96 percent of the steel is cast continuously, with about 4000 ingots still being cast individually. However, about one-half of the raw steel is produced by recycling old steel, such as junk cars and old appliances.[2]

After being cast, the ingots are heated in a soaking pit (Fig. 9.4) and hot-rolled into slabs, billets, or blooms. The slabs are subsequently hot- and cold-rolled into

[2]Table 23, pp. 73–75 of the *Annual Statistical Report of the AI&SI.*

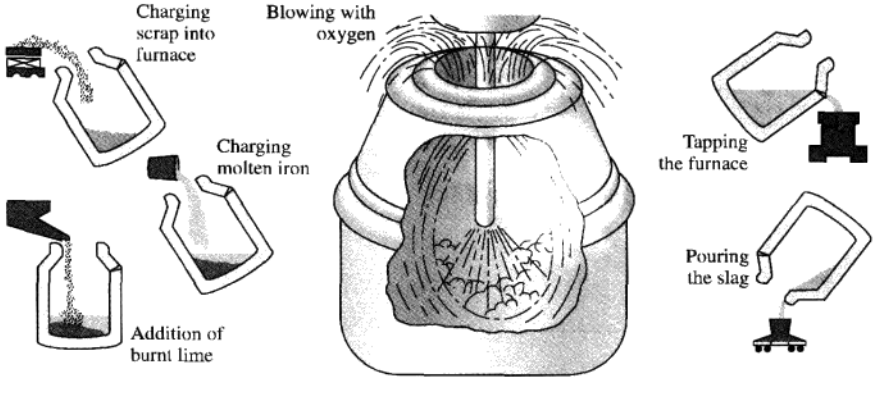

Figure 9.2
Steelmaking in a basic-oxygen furnace.
(*Courtesy of Inland Steel.*)

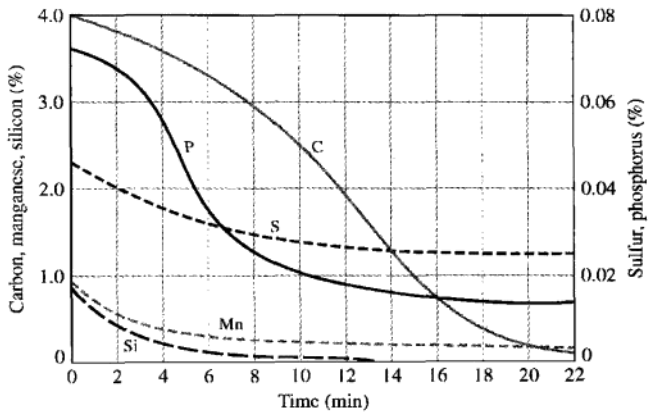

Figure 9.3
Schematic representation of progress of refining in a top-blown basic-lined vessel.
[*From H.E. McGannon (ed.), "The Making, Shaping, and Treating of Steel," 9th ed., United States Steel, 1971, p. 494. Courtesy of United States Steel Corporation.*]

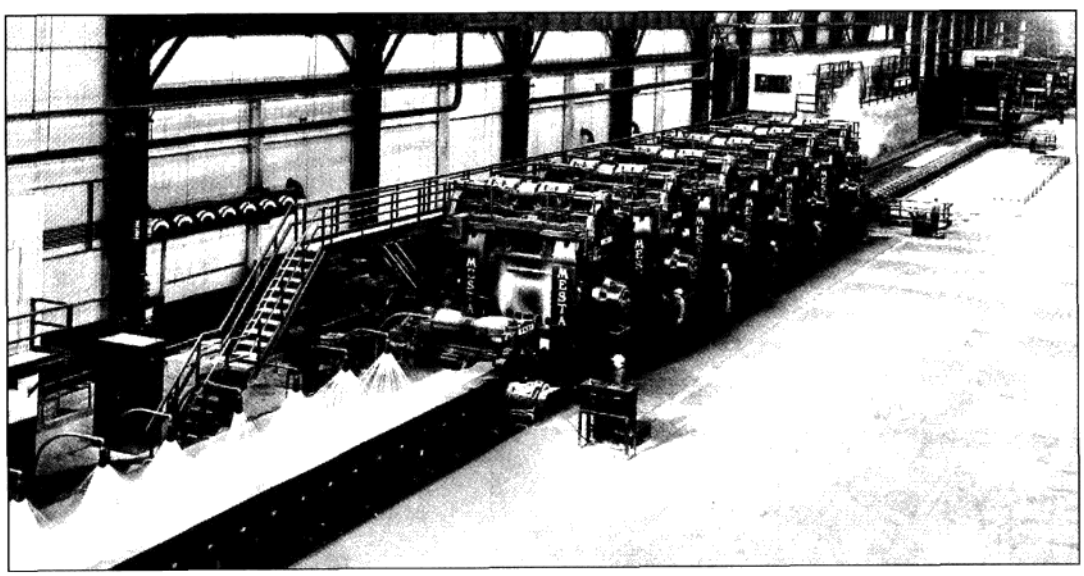

Figure 9.4
Hot rolling of steel strip. This picture shows the roughing hot-rolling mills in the background and six finishing hot-rolling mills in the foreground. A strip of steel is exiting the last finishing stand and is being water-quenched.
(*Courtesy of United States Steel Corporation.*)